

Tidal Phenomena in the Scheldt Estuary, part 2

1204410-000

Title

Tidal Phenomena in the Scheldt Estuary, part 2

Project

1204410-000

Reference

1204410-000-ZKS-0001

Pages

73

Keywords

Tidal wave propagation; Tidal dynamics; Scheldt estuary

Summary




The Scheldt estuary is a large-scale estuary in the south-west part of the Netherlands. The estuary is connected to the Scheldt river, which originates in the north-west of France. The total length of the Scheldt river including the estuary is about 350 km; the tide penetrates up to the city of Gent in Belgium (about 180 km from the mouth). The length of the estuary is about 60 km (up to Bath). The cross-sections of the estuary show two to three deeper channels with shoals in between and tidal flats close to the banks. The width of the mouth at Westkapelle (The Netherlands) is about 20 to 25 km and gradually decreases to about 0.8 km at Antwerp.

Analytical and numerical models have been used to study the effects of water depth, planform, abrupt changes of the cross-section and tidal storage on the tidal range along the Scheldt estuary.

Finally, the relative importance of the terms of the equations of continuity and momentum of the linearized analytical model for a converging tidal channel as applied to the Scheldt estuary has been studied. The numerical model (DELFT2DH-model) results of water levels and depth-averaged velocities in the Scheldt estuary have been analyzed to estimate the contribution of the slope term and the frictional term in various channel sections.

References

LTV Zandhuishouding Schelde Estuarium 2010

Version	Date	Author	Initials	Review	Initials	Approval	Initials
	Oct. 2011	prof. dr. ir. L.C. van Rijn		ir. K. Kuijper		ir. T. Schilperoort	

State

final

Contents

1 Introduction	1
2 Description of Western Scheldt estuary	3
2.1 General characteristics	3
2.2 Channels, shoals and cells	6
3 Tidal computations	11
3.1 Basic tidal phenomena in Scheldt estuary	11
3.2 Analytical and numerical simulations of tidal flow in converging channels	18
3.2.1 Numerical and analytical models	18
3.2.2 Effect of water depth on tidal range	19
3.2.3 Effect of planform schematizations on tidal range	25
3.2.4 Effect of abrupt changes of cross-section on tidal range	30
3.2.5 Effect of tidal flats on tidal range	41
3.2.6 Effect of tidal storage on tidal range	47
4 Scale analysis and relative importance of basic tidal processes	49
4.1 Introduction	49
4.2 Analytical model for exponential planform	49
4.2.1 Basic equations	49
4.2.2 Analytical model results	50
4.3 Numerical model results	56
4.3.1 Model run conditions Scheldt Estuary	58
4.3.2 Scale analysis of force terms	66
5 Summary and conclusions	67
6 References	73
 Appendices	
A Cross-sections of Scheldt Estuary	A-1

1 Introduction

The Scheldt estuary is a large-scale estuary in the south-west part of the Netherlands. The estuary is connected to the Scheldt river, which originates in the north-west of France. The total length of the Scheldt river including the estuary is about 350 km; the tide penetrates up to the city of Gent in Belgium (about 180 km from the mouth). The length of the estuary is about 60 km (up to Bath). The cross-sections of the estuary show two to three deeper channels with shoals in between and tidal flats close to the banks. The width of the mouth at Westkapelle (The Netherlands) is about 20 to 25 km and gradually decreases to about 0.8 km at Antwerp.

The shape of the Scheldt estuary is very similar to that of other large-scale alluvial estuaries in the world. The width and the area of the cross-section reduce in upstream (landward) direction with a river outlet at the end of the estuary resulting in a converging (funnel-shape) channel system. The bottom of the tide-dominated section generally is fairly horizontal. Tidal flats are present along the estuary (deltas).

The tidal range in estuaries is affected by four dominant processes:

- inertia related to acceleration and deceleration effects;
- amplification due to the decrease of the width and depth (convergence) in landward direction;
- damping due to bottom friction and
- partial reflection at abrupt changes of the cross-section and full reflection at the landward end of the estuary (in the absence of a river).

The Scheldt estuary has important environmental and commercial qualities. It is the main shipping route to the Port of Antwerp in Belgium. The depth of the navigation channel to the Port of Antwerp in Belgium is a problematic issue between The Netherlands and Belgium because of conflicting interests (commercial versus environmental). Large vessels require a deep tidal channel to Antwerp, which enhances tidal amplification with negative environmental consequences. Since 1900, the main shipping channel has been deepened (by dredging and dumping activities) by a few metres. Furthermore, sand mining activities have been done regularly. Both types of dredging works may have affected the tidal range along the estuary. The tidal range at the mouth (Westkapelle and Vlissingen) has been approximately constant over the last century, but the tidal range inside the estuary has gone up by about 1 m (**Pieters, 2002**). Particularly, the high water levels have gone up considerably. The low water levels have gone down slightly at some locations (about 0.2 m at Antwerp) despite sea level rise of about 0.2 m per century.

To be able to evaluate the consequences of the (ongoing) channel deepening on the tidal range, it is of prime importance to understand the basic characteristics of the tidal wave propagation in the Scheldt estuary.

The basic questions addressed in this report are:

- what is the role of the shape and dimensions of the tidal channels (both in planform and in the cross-section) on tidal wave propagation?
- what is the role of bottom friction in relation to the depth of the main channels?
- what is the role of (partial) reflection of the tidal wave due to *abrupt* width and depth changes of the cross-section?
- what is the relative importance of the various force terms of the momentum balance describing tidal wave propagation?

These questions have been addressed (by Prof. Dr. L.C. van Rijn; Deltares and University of Utrecht) using an analytical model and a 1D numerical model. The analytical model is based on the linearized equations of continuity and momentum for constant depth and an exponential planform. The 1D numerical model includes all terms and takes quadratic friction into account. The present study is a continuation of an earlier study on tidal wave propagation in the Scheldt estuary (**Van Rijn, 2011a**).

The analytical and numerical models have been used to identify the most important processes and parameters (sensitivity computations) for schematic cases with boundary conditions as present in the Scheldt estuary.

This approach generates basal information and knowledge of the tidal propagation in the Scheldt estuary.

K. Kuijper of Deltares is gratefully acknowledged for his detailed comments.

2 Description of Western Scheldt estuary

2.1 General characteristics

The Scheldt estuary in the south-west part of the Netherlands and in the north-west part of Belgium (see **Figures 2.1.1, 2.1.2 and 2.1.3**) is connected to the Scheldt river, which originates in the north-west of France. The total length of the Scheldt river including the estuary is about 350 km; the tide penetrates up to the city of Gent in Belgium (about 180 km from the mouth). The length of the estuary is about 60 km between Vlissingen and Bath. The cross-sections of the estuary show two to three deeper channels with shoals in between and tidal flats close to the banks. The width of the mouth at Westkapelle (The Netherlands) is about 20 to 25 km and gradually decreases to about 0.8 km at Antwerp, see **Table 2.1.1**. The width-averaged water depth (h_0) to MSL at the mouth between Vlissingen and Hansweert is about 12 m. The width-averaged water depth (h_0) to MSL between Hansweert and Bath is about 11 m. The width-averaged bottom is almost horizontal up to $x = 80$ km from the mouth. Since 1900, the main shipping channel has been deepened (by dredging and dumping activities) various times affecting the tidal range along the estuary. The tidal range at the mouth (Westkapelle and Vlissingen) has slightly increased over the last century, but the tidal range inside the estuary has gone up by about 0.5 to 1 m due to various channel deepening (Pieters, 2002), see **Table 2.1.2**. Particularly, the high water levels have gone up considerably. The low water levels have gone down slightly at some locations (about 0.2 m at Antwerp) despite sea level rise of about 0.2 m per century. A detailed description of the historical developments is given by Pieters (2002).

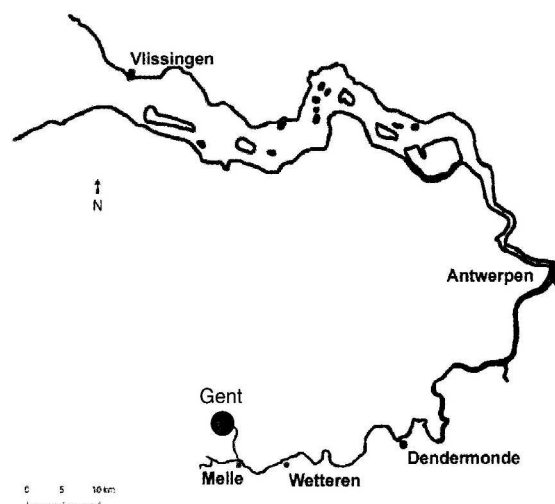


Figure 2.1.1 Scheldt estuary, The Netherlands

Table 2.1.1 Tidal data (annual mean spring tide) of Scheldt estuary around 2000

Stations	Distance x (km)	Width b (km)	Tidal range H (m)	H/H ₀ (measured)
Westkapelle (mouth)	0	25	4.2 (= H ₀)	1
Vlissingen	12	6	4.5	1.07
Terneuzen	30	6	4.8	1.14
Hansweert	45	6	5.0	1.19
Bath	63	3	5.5	1.31
Antwerpen	95	0.8	5.85	1.39
Rupelmonde	110	<0.5	5.95	1.42
Temse	115	<0.5	5.85	1.39
Dendermonde	130	<0.5	4.2	1.0
Gent	160	<0.5	2.34	0.55

Table 2.1.2 Tidal data of Scheldt estuary in 1900 and 2010 (annual mean tide)

Location	1900			2010		
	LW (m to NAP)	HW (m to NAP)	Tidal range (m)	LW (m to NAP)	HW (m to NAP)	Tidal range (m)
Vlissingen	- 1.9	+ 1.7	3.6	- 1.8	+ 2.0	3.8
Bath	- 2.3	+ 2.2	4.5	- 2.2	+ 2.8	5.0
Antwerpen	- 2.1	+ 2.3	4.4	- 2.3	+ 3.0	5.3

The two most important tidal constituents are the M₂ and the S₂-components. The tidal curve at the mouth (Westkapelle) has a very regular (almost sinusoidal) pattern. The tidal range increases in landward direction up to Rupelmonde (upstream of Antwerp), see **Table 2.1.1** and decreases from there in landward direction (based on De **Kramer, 2002**).

The tide is semi-diurnal with a tidal range (H₀) at the mouth (Westkapelle) varying in the range of 2.4 m at neap tide to 4.2 m at spring tide. Historical tidal data at various stations in the Scheldt estuary are shown in **Table 2.1.2** (based on **Pieters, 2002**).

The maximum peak tidal velocity at mouth (\hat{u}_0) varies in the range of 0.8 to 1.2 m/s.

The tidal volume (ebb+flood volume) is of the order of $2.2 \cdot 10^9 \text{ m}^3$ near Vlissingen and $0.2 \cdot 10^9 \text{ m}^3$ near the Dutch-Belgian border.

The discharge of the Scheldt river varies in the range of 50 to 200 m³/s. The mean annual discharge is about 120 m³/s. The highest discharge is about 600 m³/s. Given the relatively small river discharge, the estuary is a well-mixed flow system with a constant fluid density over the water depth.

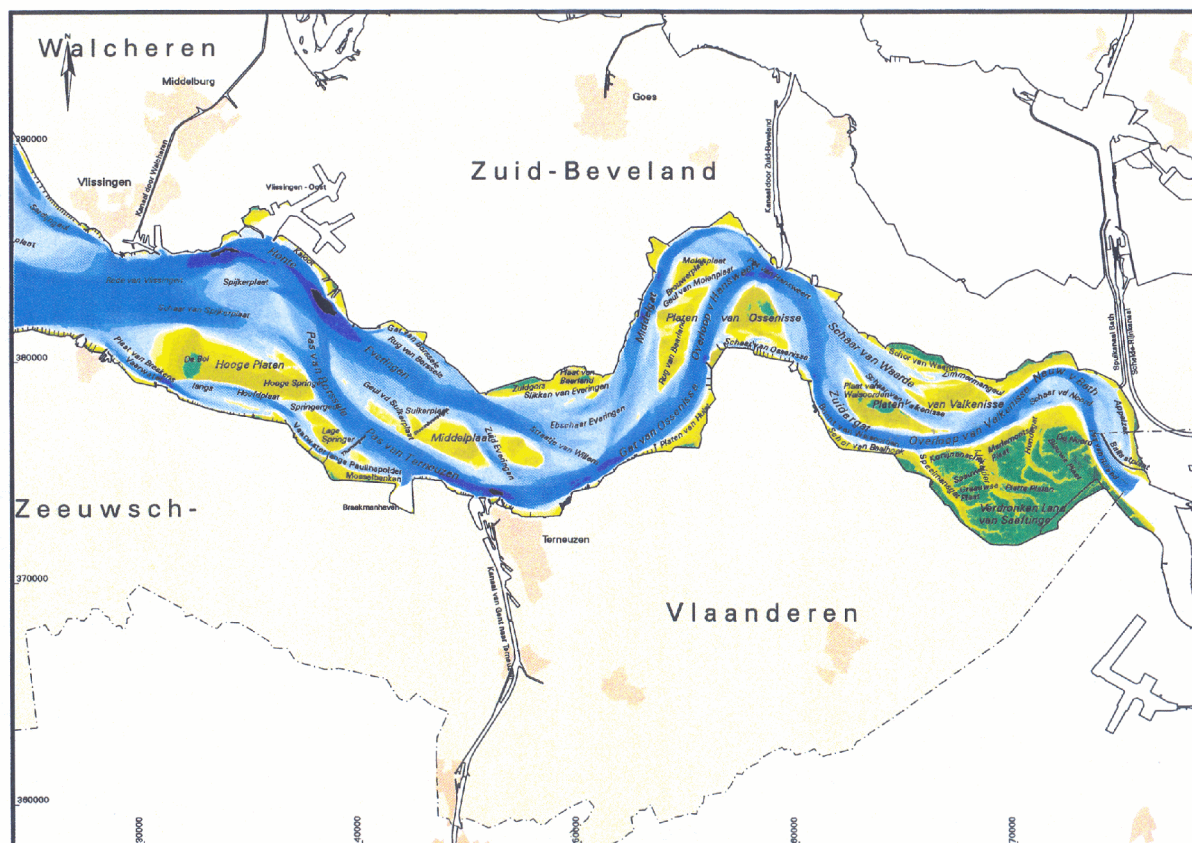


Figure 2.1.2 *Morphological patterns of Western Scheldt estuary*

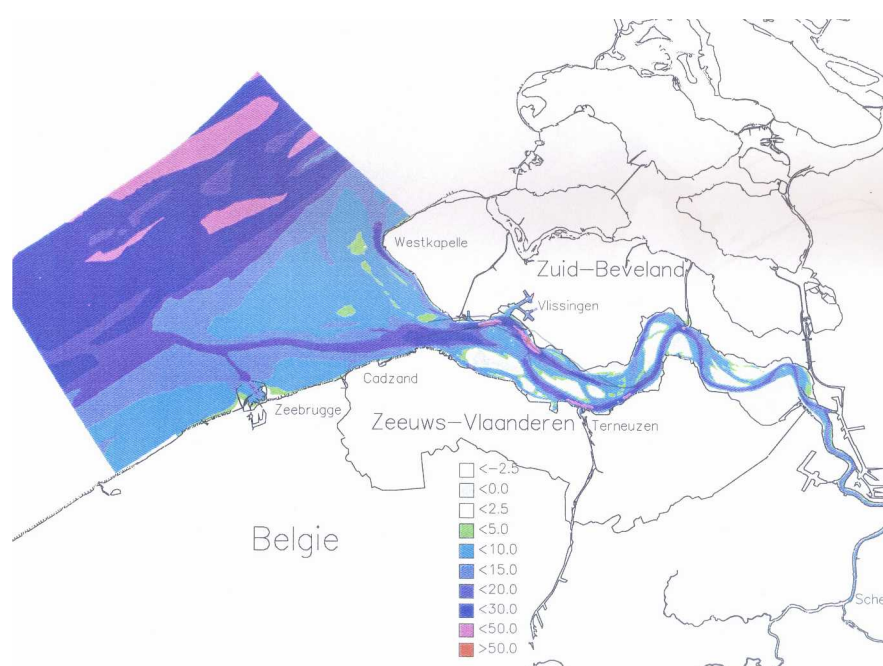


Figure 2.1.3 *Bathymetry of 2001 of Western scheldt estuary including mouth area*

2.2 Channels, shoals and cells

The Scheldt estuary can be subdivided into a series of macro-cells (**Deltares, 2011**). Each cell consists of meandering tidal channels with decreasing dimensions in landward direction. The lateral boundaries are formed by dikes. The tidal channels show a regular pattern of main flood and main ebb channels (primary and secondary channels).

The type of tidal flow (flood-dominated or ebb-dominated) is presented in **Table 2.2.1**. The maximum flow velocities during flood and ebb tide (mean tide) are taken from the DELFT3D-model for Scheldt estuary (see **Section 4.3**). Generally, the flood tide enters through the more shallow channels (mean depths of 10 to 15 m) and leaves through the deeper channels (mean depths of 15 to 20 m with respect to MSL). The main ebb channels are deepest and form the navigation route to the Port of Antwerp. The main flood channels generally are shallower than the main ebb channels. Shallow areas (sills) are found at the seaward side of the ebb channels and at the landward side of the flood channels. Along the banks smaller, former main, channels can be found (marginal channels). Various connecting (tertiary) channels are present between the parallel main flood and ebb channels.

The sediment in the Scheldt estuary mainly consists of medium fine sand in the channels (0.2 to 0.4 mm sand) and fine sand on the shoals (0.05 to 0.2 mm sand). The percentage of mud (< 0.03 mm) is rather small (< 10%) in the main channels. Alongside the estuarine margins, at the intertidal areas and salt marshes, the percentage of mud is much larger.

The Scheldt estuary can be subdivided into a series of macro-cells (**Deltares, 2011**), as follows (see **Figure 2.2.1**):

1. macro-cell 1+2 with channels around tidal flats Hooge Platen;
2. macro-cell 3 with channels around tidal flat Middelgat;
3. macro-cell 4 with channels around tidal flats Platen van Ossensisse;
4. macro-cell 5 with channels around tidal flats Platen van Valkenisse;
5. macro-cell 6+7 with channels north of Verdonken land van Saeftinge.

Both the total area of intertidal shoals (roughly above -2 m NAP) and the subtidal zone (roughly between -5 m and -2 m NAP) have decreased substantially (about 20% to 30%) over the period 1950 to 2000 in the western part of the estuary.

Substantial dredging at the sill locations is required to maintain the required depth of the main navigation route to Antwerp (Belgium). Mean annual dredging volumes have gradually increased from about 4 to 5 Mm³ per year in the 1960's to about 10 Mm³ per year around 2000 to accomodate the passage of larger vessels to the Port of Antwerp (**Deltares, 2004**).

The sills were deepened again in the period 1997-1998 (second deepening campaign). Recent morphological changes after the second deepening of the navigation route (1997-1998) have been reported by **Rijkswaterstaat 2006** (MOVE final report, RIKZ, Rijkswaterstaat).

The initial dredging volume in the period 1997-1998 was about 7.5 million m³ over a total area of 7.5 km² (about 7% of the total tidal channel area (about 100 km²) of the Scheldt estuary between Vlissingen and Bath). The total deepening was about 1 m (3 feet).

The dredged material was dumped in the secondary channels of the western part and in the middle part of the estuary.

Analysis of the morphological data in the period 1998 to 2005 (after the second deepening campaign) shows:

- the total dredging volume east of Vlissingen is about 11 Mm³ per year between 1999 and 2002 which decreases to about 7.5 Mm³ per year in 2005, which is less than the dredging volume before the second deepening campaign (about 9.5 Mm³ per year); sill dredging is reduced from about 6.5 Mm³ per year before the second deepening campaign 1997 to about 5 Mm³ per year after the second deepening campaign 1998 (opposite to the estimated increase of the sill dredging volume);
- the area and volume of the main channels have increased;
- the area and volume of the secondary channels have decreased substantially in the western part of the estuary;
- the total surface area of shallow water (subtidal zone) between -5 m and -2 m NAP has not changed;
- the surface area and volume of the shoals (intertidal zone above low water -2 m NAP) have decreased in the western and in the middle part of the estuary;
- the total sand mining volume was about 2 Mm³ per year (within allowed limits).

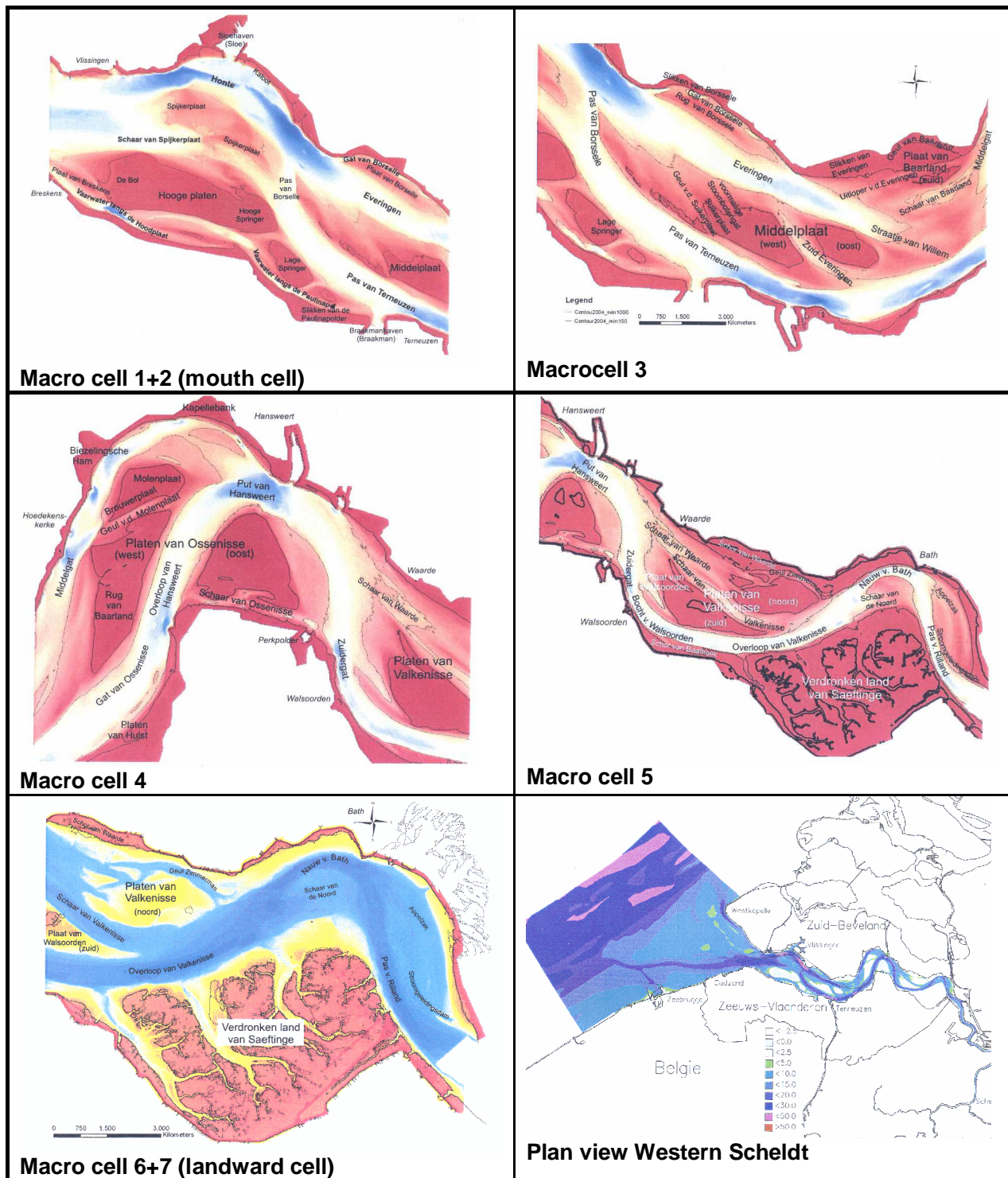


Figure 2.2.1 Macro cells of the Scheldt estuary

Table 2.2.1 *Dimensions of Channels, Scheldt estuary*
(depth values based on bathymetry 1998; velocities based on DELFT-model)

Cell	Channel	Type of channel	Width	Length	Mean depth below NAP	Maximum flow vel. Flood	Maximum flow vel. Ebb
			B (m)	L (m)	h (m)	\bar{u} (m/s)	\bar{u} (m/s)
1	Oostgat	ebb-dom.	500	3000	15-20	0.7-0.9	0.8-1.0
	Wielingen	flood-dom.	2000	6000	15-30	1.1-1.3	1.0-1.2
2	Honte	ebb-dom.	700	6000	20-40	1.2-1.4	1.2-1.4
	Schaar Spijkerplaat	flood-dom.	500	3000	10-20	1.0-1.2	0.8-1.0
	Geul zuid Hoofdplaat	flood-dom.	200	6000	10-20	0.9-1.1	0.7-0.9
	Drempel Borssele	ebb-dom.	300	2000	15-20	0.8-1.0	0.7-0.9
3	Everingen	flood-dom.	700	6000	20-30	1.2-1.4	1.2-1.4
	Drempel Baarland	flood-dom.	300	2000	10-15	1.0-1.2	1.0-1.2
	Zuid-Everingen	ebb-dom.	300	3000	10-15	0.7-0.9	0.8-1.0
	Straatje Willem	flood-dom.	300	2000	7-10	0.9-1.1	0.8-1.0
	Pas van Terneuzen	ebb-dom.	700	6000	20-35	1.2-1.4	1.2-1.4
4	Middelgat	ebb-dom.	500	7000	20-30	1.0-1.2	1.0-1.2
	Put van Hansweert	ebb-dom.	500	2000	20-40	1.2-1.4	1.2-1.4
	Gat van Ossenis	flood-dom.	700	4000	20-25	1.2-1.4	1.2-1.4
	Overloop Hansweert	flood-dom.	500	4000	15-25	1.2-1.4	1.2-1.4
	Schaar Ossenis	flood-dom.	200	3000	7-10	0.7-0.9	0.7-0.9
	Zuidergat	ebb-dom.	500	6000	15-25	1.2-1.4	1.2-1.4
	Drempel Hansweert	ebb-dom.	300	2000	15-20	0.8-1.0	0.8-1.0
5	Schaar van Waarde	flood-dom.	300	2000	10-15	0.9-1.1	0.7-0.9
	Schaar Valkenisse	flood-dom.	300	3000	10-15	1.0-1.2	0.8-1.0
	Bocht Walsoorden	ebb-dom.	400	3000	15-20	1.0-1.2	1.0-1.2
6+7	Nauw van Bath	ebb-dom.	300	3000	15-20	1.2-1.4	1.2-1.4
	Overloop Valkenisse	ebb-dom.	700	5000	15-20	1.2-1.4	1.0-1.2
	Pas Rilland	ebb-dom.	400	4000	15-20	1.2-1.4	1.2-1.4
	Drempel Bath	ebb-dom.	300	1500	15-20	1.0-1.2	1.0-1.2
	Drempel Valkenisse	ebb-dom.	300	1500	15-20	1.0-1.2	1.0-1.2
	Rilland-Liefkenshoek	ebb-dom.	300	7000	10-15	0.9-1.1	0.9-1.1

Figure 2.2.2 shows the widths (B) and the width-averaged depths (h) below MSL and the areas (A) of the cross-sections based on **Savenije (2005)**. The cross-sectional areas (A) follow a very regular decreasing exponential curve with a converging length scale of about $L_A = 28$ km. The width reduction in landward direction shows more variability. The width-averaged depth below MSL fluctuates around a constant value of about 10.5 m up to Antwerp at 110 km from the mouth (sea boundary). The depths are larger at locations where the widths are smaller.

Figure 2.2.3 shows the widths (B) and the width-averaged depths (h) below MSL and the areas (A) of the cross-sections based on the bathymetry of 1998 as used in the Delft2DH-model of DELTARES. The locations of the cross-sections and the cross-section profiles are shown in **Appendix A**.

The results of **Figure 2.2.3** are similar to those of **Figure 2.2.2**. The width represents the total width of the channel (width of shoals and flats above MSL has been subtracted from total width). The converging length scale of the cross-sectional area over 100 km is about 26 km and that of the width is about 28 km. The width-averaged depth (to MSL) fluctuates around the value of 10 m up to Antwerp (Belgium).

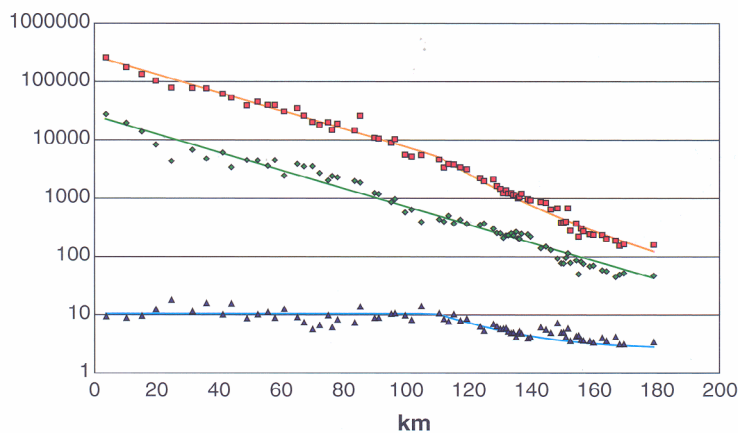


Figure 2.2.2 Width-averaged depth (h), width (B) and cross-sectional area (A) as function of distance to the sea boundary (west of Vlissingen), Scheldt estuary (Savenije, 2005)

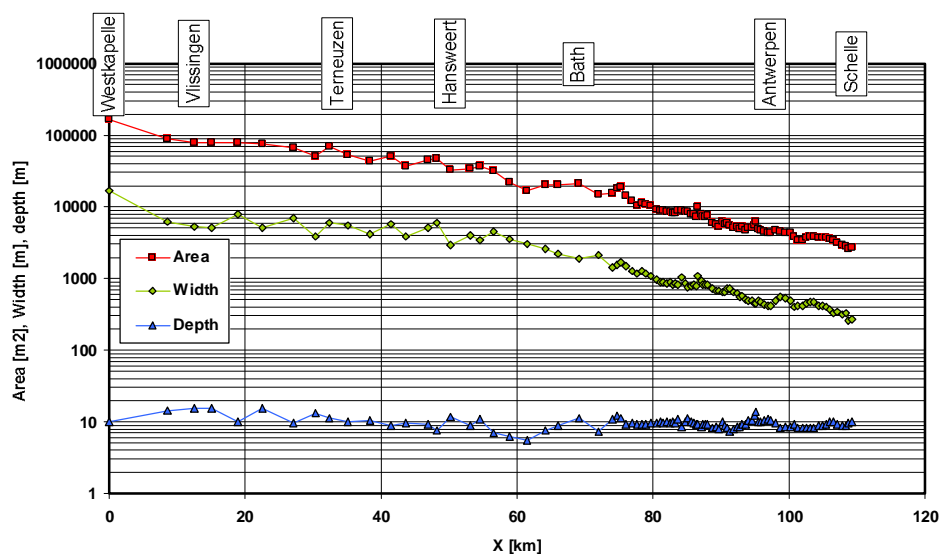


Figure 2.2.3 Width-averaged depth, width and cross-sectional area as function of distance to the sea boundary (Westkapelle), Scheldt estuary (Deltares 2011)

3 Tidal computations

3.1 Basic tidal phenomena in Scheldt estuary

The fluid motion in a tidal wave is governed by external forces (water surface slope, wind forces, Coriolis forces), internal forces (boundary friction) and inertial forces (acceleration and deceleration). Basically, inertial forces are apparent forces defined as the product of mass and acceleration and can be seen as the apparent resistance of the fluid mass against temporal changes in movement.

In deep, unbound water a tidal wave will propagate as a single progressive harmonic wave (forward moving wave without phase shift between water levels and velocities). Near coasts the propagation of the tidal wave is affected by the following processes:

- reflection,
- amplification (funneling and shoaling),
- deformation,
- damping.

The tidal wave in the Scheldt estuary includes all of these basic phenomena.

Figure 3.1.1 shows instantaneous water surface profiles during mean tidal conditions at various times after HW in Vlissingen (**Pieters, 2002**). The HW and LW contour curves of spring, mean and neap tides are also shown.

The tidal ranges at Vlissingen are approximately:	3.0 m	during neap tide
	3.7 m	during mean tide,
	4.5 m	during springtide.
The tidal ranges at Antwerp are approximately:	4.5 m	during neap tide,
	5.3 m	during mean tide,
	6.0 m	during springtide.

The water surface profiles along the Scheldt estuary show the basic features of a single progressive wave. The tidal wave propagates landward while amplifying and deforming. The tidal wave is amplified between Vlissingen and Antwerp (increase of tidal range) and is damped landward of Antwerp where the water depth decreases rapidly (rapid increase of boundary friction). The tidal wave also deforms (steepening of the wave front) due to larger water depths under the crest.

The tidal wave in the Scheldt estuary is not a **single** progressive wave (which has no phase shift between horizontal and vertical tide). The horizontal tide (velocity) runs ahead of the vertical tide by about 2 hours. As a standing wave system has a phase shift of 3 hours, this may suggest that reflection plays a significant role in the Scheldt estuary. **Jay (1991)** and **Van Rijn (2011b,c)** have shown that a progressive tidal wave in a converging channel (funnel-type channel) may mimic a standing wave by having a phase difference close to 3 hours between the tidal velocities and the tidal elevations and a very large wave speed. This behaviour is enforced by the very gradual, but systematic reduction of the flow width in landward direction (flow convergence) causing continuous reflection. As such the tidal signal in a convergent estuary will always consist of an incoming and an outgoing wave.

Figures 3.1.2 and 3.1.3 show the historical development of the HW, LW lines and the tidal range along the Scheldt estuary (based on **Pieters, 2002**). The amplification of the tidal range landward of Hansweert (40 km) increases systematically since 1950. The maximum value increases from about 1.2 to 1.4 (15% increase). The location of maximum amplification has shifted landwards from 60 km to 95 km.

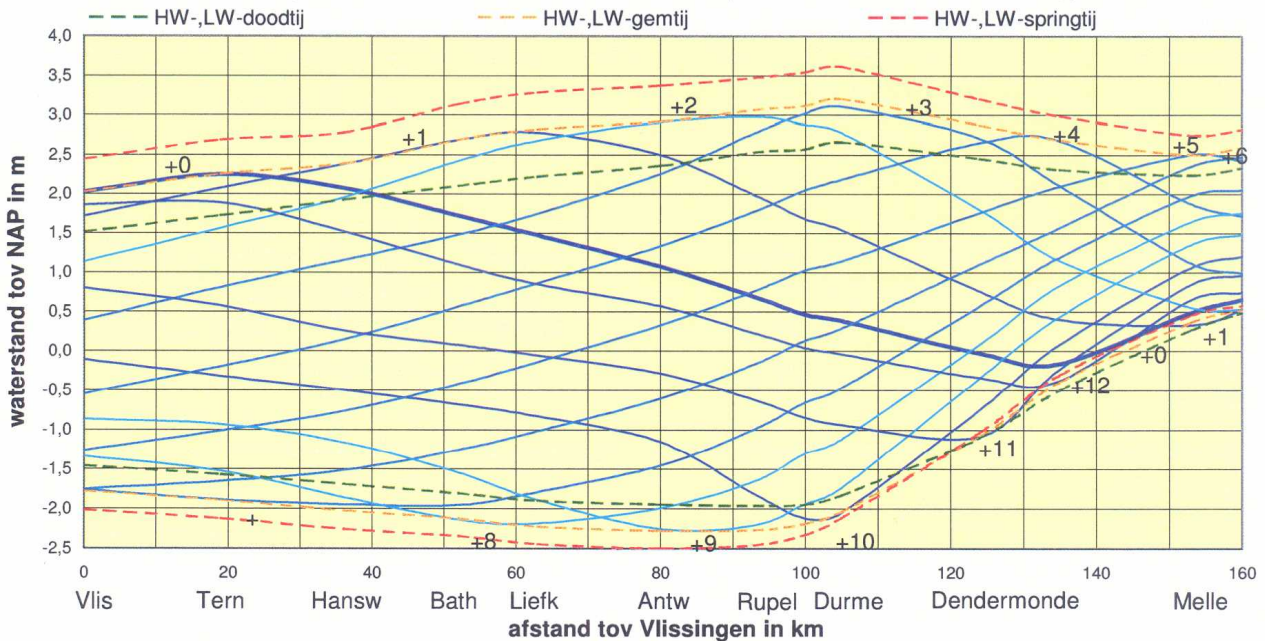


Figure 3.1.1 Water surface profiles in Scheldt estuary and Scheldt river (Pieters, 2002) (+0= HW in Vlissingen; +1= 1 hour after HW in Vlissingen near mouth) (vertical: water level to NAP \approx MSL; horizontal: distance to Vlissingen)

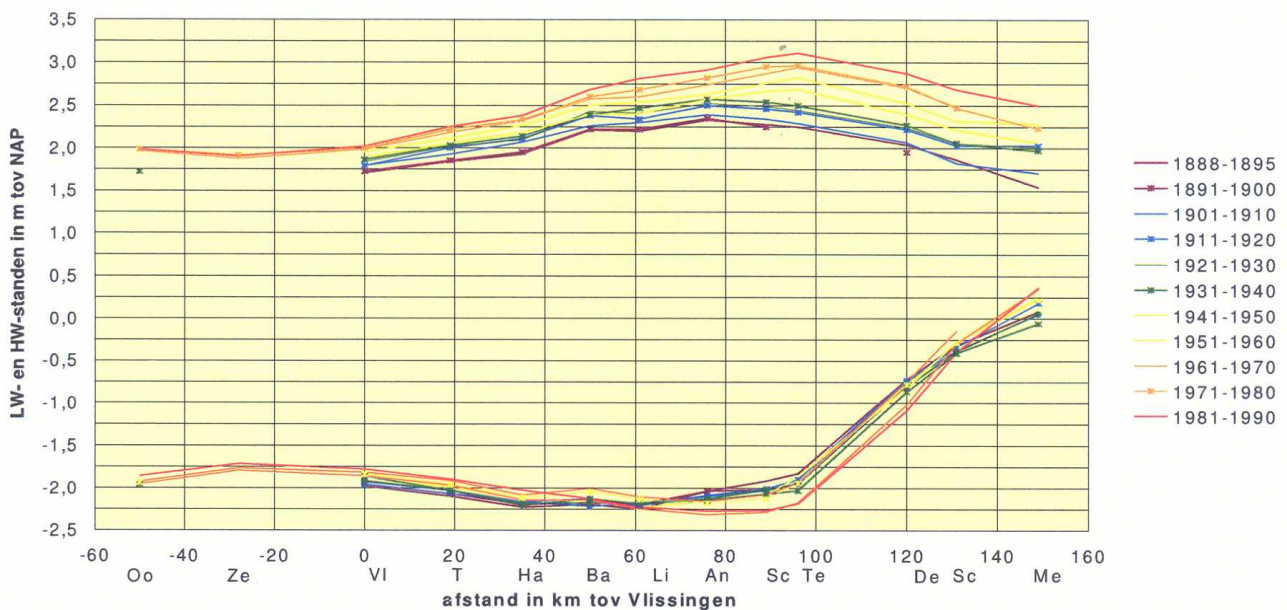


Figure 3.1.2 HW and LW lines along Scheldt estuary; 1888 to 1990 (Pieters, 2002)

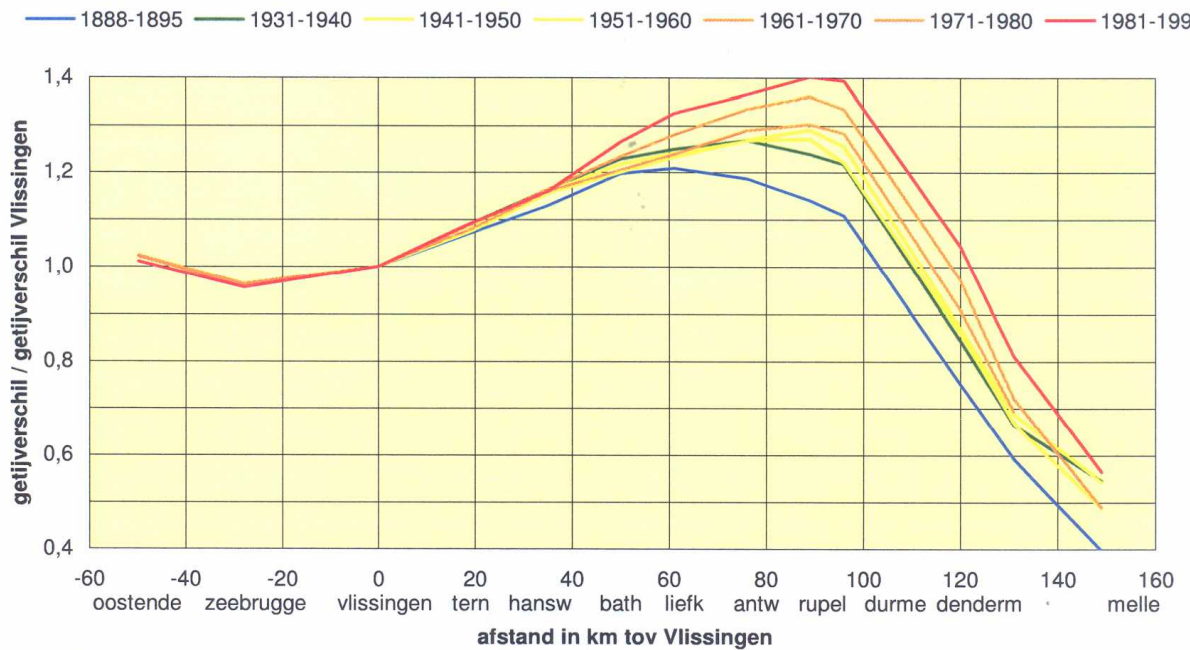


Figure 3.1.3 Ratio of tidal range and tidal range of Vlissingen along Scheldt estuary; 1888 to 1990 (based on Pieters, 2002)

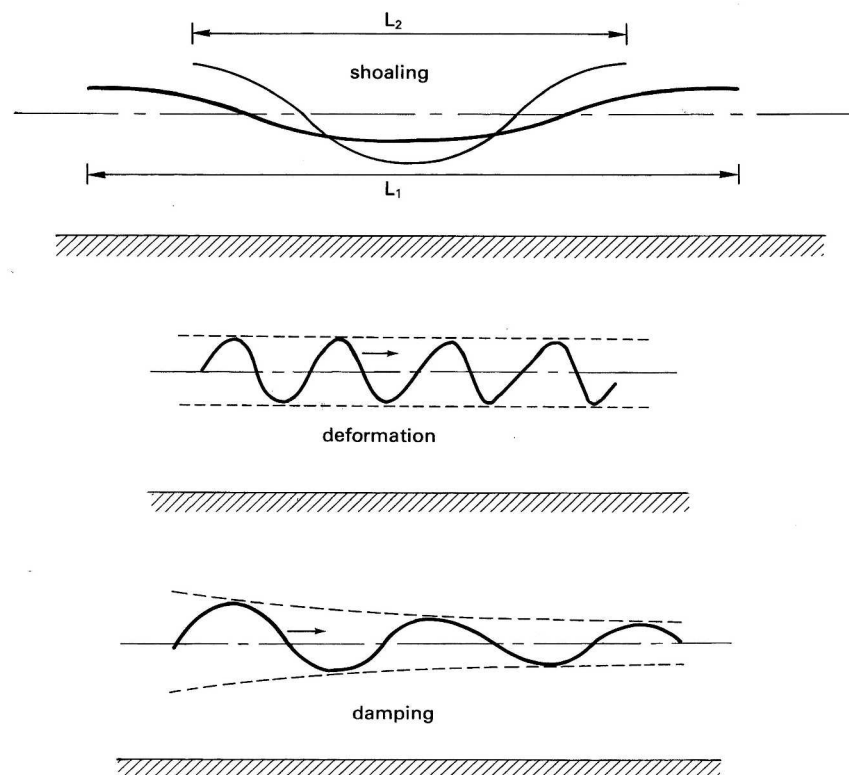


Figure 3.1.4 Amplification (funnelling; shoaling), deformation and damping of tidal waves

1. Reflection

Reflection is herein defined as wave propagation opposite to the incoming wave motion due to the presence of a change of the depth and/or width. **Reflection** is one of the most important wave phenomena near coasts and in estuaries. Full reflection will occur in a closed-end channel.

Partial reflection will occur if the depth and width of the cross-section become smaller abruptly (narrowing of the cross-section). If a local sill (relatively shallow section) and/or a local constriction are present, the water level upstream of this location (seaward during flood and landward during ebb) will build up to overcome the extra flow resistance at this location. This backwater effect will propagate upstream (seaward during flood), which can be interpreted as partial reflection of the tidal wave.

A long wave is partly reflected when it propagates abruptly from a wide and deep prismatic section (b_1 and h_1) into a narrow and shallow prismatic section (b_2 and h_2). The transmitted wave length $L_2 = c_2 T$ is reduced in the narrow and shallow section, because c_2 is reduced (T remains constant). Thus, $L_2 < L_1$. The reflected wave interferes with the incoming wave resulting in a composite wave. The transmitted wave in the shallow section has a shorter length but a larger height than the incident wave (known as **shoaling**).

The reflection factor for a sudden change of the cross-section can be crudely expressed as:

$\gamma = (b_2 c_2 \cos \varphi_2) / (b_1 c_1 \cos \varphi_1)$ with b = flow width, c = wave speed, φ = phase shift between horizontal and vertical tide (**Van Rijn, 2011b, Pieters, 2002**).

The ratio of the reflected wave height and the original incoming wave height in prismatic channels is crudely given by: $H_r/H_i = (1-\gamma)/(1+\gamma)$.

Using $h_1 \cong h_2$ and $b_2/b_1 \cong 0.5$, this yields: $H_r/H_i = (1-\gamma)/(1+\gamma) \cong 0.3$.

Thus, if the width of the narrow prismatic section is 50% of the width of the wide prismatic section, the reflected wave height is about 30% of the incoming wave height. Hence, the composite (incoming plus reflected) wave height increases considerably.

Standing waves are generated in the case of total reflection against a vertical boundary. Resonance may occur if the channel length is of the same order of magnitude as a quarter of the tidal wave length ($L_{\text{channel}} \cong 0.25 L_{\text{wave}}$).

Pieters (2002) stresses the importance of partial reflection of the tidal wave due to **abrupt** local changes of cross-sections of the Scheldt estuary. According to **Pieters (2002)**, the reflection effects amount to about 20% to 30% of the tidal range at Vlissingen.

Pieters (2002) makes the following remarks:

- an abrupt change of the cross-section (abrupt depth and width changes) influences the tidal wave propagation on the incoming side of the wave; the reflected wave interferes with the incoming wave resulting in a larger wave height (positive reflection) on both sides of the cross-section involved (pages p 28, 33, 24);
- the discharge is about 75° degrees ahead of the water surface level elevation (page 67), which means that the tidal wave strongly deviates from a progressive tidal wave and that substantial reflection occurs (phase lead is 90° in standing wave system);
- dredging of the Overloop van Hansweert-channel has resulted in larger depths and smaller local flow velocities which both lead to reduced flow resistance and less damping of the tide (page 72);
- over the length of the Scheldt estuary and the Lower Scheldt river (Beneden-Schelde), the phase difference between the tidal velocity and the tidal water level elevation has increased in the period 1965 to 1995, suggesting a further shift towards a standing wave system which is consistent with the increase of the tide.

Various dredging campaigns have been executed in the last 30 years to widen and deepen the navigation channel to Antwerp. During this period the tidal range has increased substantially, see **Figures 3.1.2 and 3.1.3** (based on **Pieters, 2002**).

In the perception of **Pieters** the widening and deepening effects will result in less partial reflection effects and hence a smaller tidal range. On the other hand the widening and deepening will also result in less damping (less friction). Given the observed increase of the tidal range in the Scheldt estuary, the reduced frictional effects seem to be dominant.

2. Amplification (funneling and shoaling)

Funneling is herein defined as the increase of the wave height due to the gradual decrease of the width of the system.

Shoaling is herein defined as the increase of the wave height due to the gradual decrease of the depth of the system.

Both processes lead to landward amplification of the wave height (tidal range) in convergent channels (decreasing width and depth in landward direction) and is an important phenomenon in estuaries where the depth and the width are gradually decreasing.

The principle of tidal wave amplification can be easily understood by considering the wave energy flux equation, which is known as **Green's law (1837)**. The total energy of a sinusoidal tidal wave per unit length is equal to $E = 0.125 \rho g b H^2$ with b = width of channel, H = wave height. The propagation velocity of a sinusoidal wave is given by: $c_0 = (gh_0)^{0.5}$ with h_0 = water depth. Assuming that there is no reflection and no loss of energy (due to bottom friction), the energy flux is constant resulting in: $E_0 c_0 = E_x c_x$ or $H_x/H_0 = (b_x/b_0)^{-0.5} (h_x/h_0)^{-0.25}$.

Thus, the tidal wave height H_x increases for decreasing width and depth.

The wave length $L = c_0 T$ will decrease if c_0 decreases for decreasing depth resulting in a shorter and higher wave (**Figure 3.1.4**).

A strongly converging channel will lead to a large phase shift (70° to 85°) between the velocity curve and the water surface curve (**Van Rijn, 2011a,b,c**). The apparent wave speed will also increase. In the case of a standing wave system the phase shift is 90° and the apparent wave speed is infinite.

The sinusoidal water level curve and the velocity curve of the tidal wave at any location within a converging channel can be subdivided (splitted) into an ingoing (landward) progressive tidal wave and an outgoing (seaward) progressive tidal wave. Both the ingoing and outgoing progressive (frictionless) waves are assumed to travel with wave speed $c_0 = (gh)^{0.5}$.

$$\text{It is valid that:} \quad q = q_{in} + q_{out} \quad (3.1)$$

$$\eta = \eta_{in} + \eta_{out} \quad (3.2)$$

$$\text{It is also valid:} \quad q_{in} = c_0 \eta_{in} \quad \text{and} \quad q_{out} = -c_0 \eta_{out} \quad (3.3)$$

$$\text{This yields:} \quad q = c_0 \eta_{in} - c_0 \eta_{out} \quad (3.4)$$

$$\eta_{in} = q/c_0 + \eta_{out} \quad \text{and} \quad \eta_{out} = -q/c_0 + \eta_{in} \quad (3.5)$$

$$\text{Thus:} \quad \eta = (q/c_0 + \eta_{out}) + \eta_{out} = q/c_0 + 2\eta_{out} \quad \text{or} \quad \eta_{out} = 0.5 (\eta - q/c_0) \quad (3.6)$$

$$\eta = \eta_{in} + (-q/c_0 + \eta_{in}) = -q/c_0 + 2\eta_{in} \quad \text{or} \quad \eta_{in} = 0.5 (\eta + q/c_0) \quad (3.7)$$

with: η = tidal water level elevation and q = tidal discharge per unit width.

If the values of q ($=\bar{u}h$) and η are known as function of time, the values of η_{in} and η_{out} can be determined as function of time from q ($=\bar{u}h$) and η .

Using the linearized momentum equations, an analytical solution of q ($=\bar{u}h$) and η can be derived for a converging tidal channel with an exponential planform and constant depth (**Van Rijn, 2011a,b,c**).

Figures 3.1.5A,B show the velocity and water level curve at $x=100$ km and at the mouth ($x=0$ km) in a channel with exponentially decreasing width (length= 180 km, width at mouth $b_o=25$ km, converging length scale $L_b=25$ km, with depth of $h=10$ m) based on the analytical model for an exponential planform. The computed phase lead of the velocity curve (dashed black curve) with respect to the water level curve (black curve) is 76° or 2.6 hours.

Using Equations (3.6) and (3.7), the water level curve (black curve) at $x=100$ km is splitted into an ingoing tidal wave (blue curve) with amplitude $\hat{\eta}_{in}=1.8$ m and an outgoing tidal wave (red curve) with amplitude $\hat{\eta}_{out}=1.53$ m ($\approx 85\%$ of amplitude of incoming wave), both travelling with c_o .

The water level curve (black curve) at $x=0$ km is splitted into an ingoing tidal wave (blue curve) with amplitude $\hat{\eta}_{in}=1.2$ m and an outgoing tidal wave (red curve) with amplitude $\hat{\eta}_{out}=1.05$ m ($\approx 85\%$ of amplitude of incoming wave), both travelling with c_o . Thus, at the seaward boundary the tidal wave also consists of a reflected wave.

Using this analysis method, the outgoing wave can be seen as a reflected wave produced by the converging planform of the estuary.

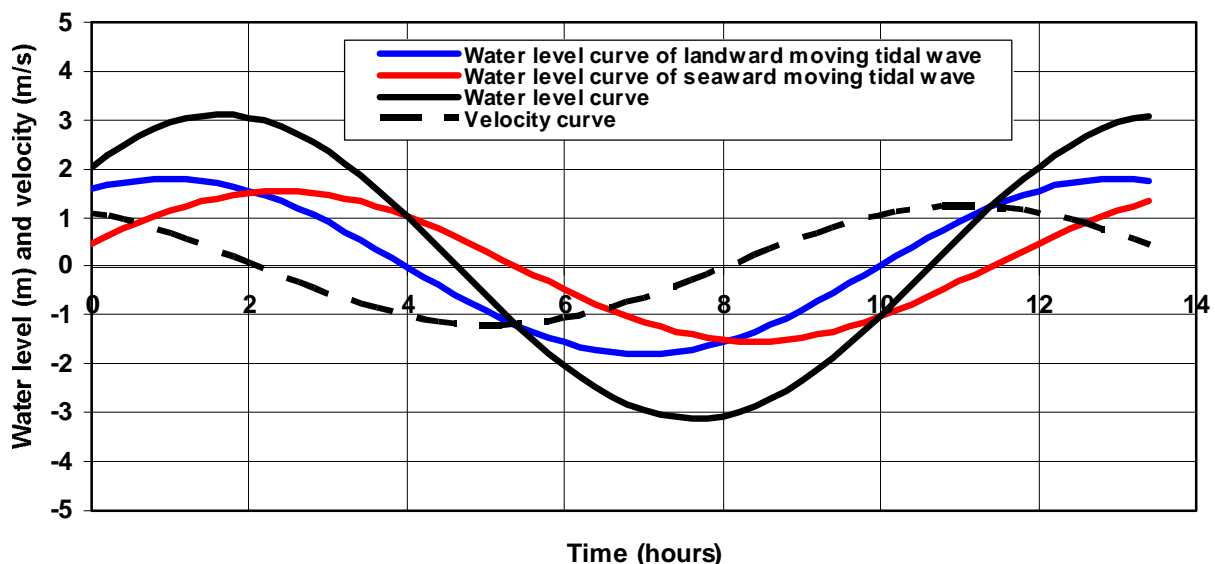


Figure 3.1.5A Water level and velocity in converging channel; ingoing and outgoing water level curves, at $x=100$ km from mouth

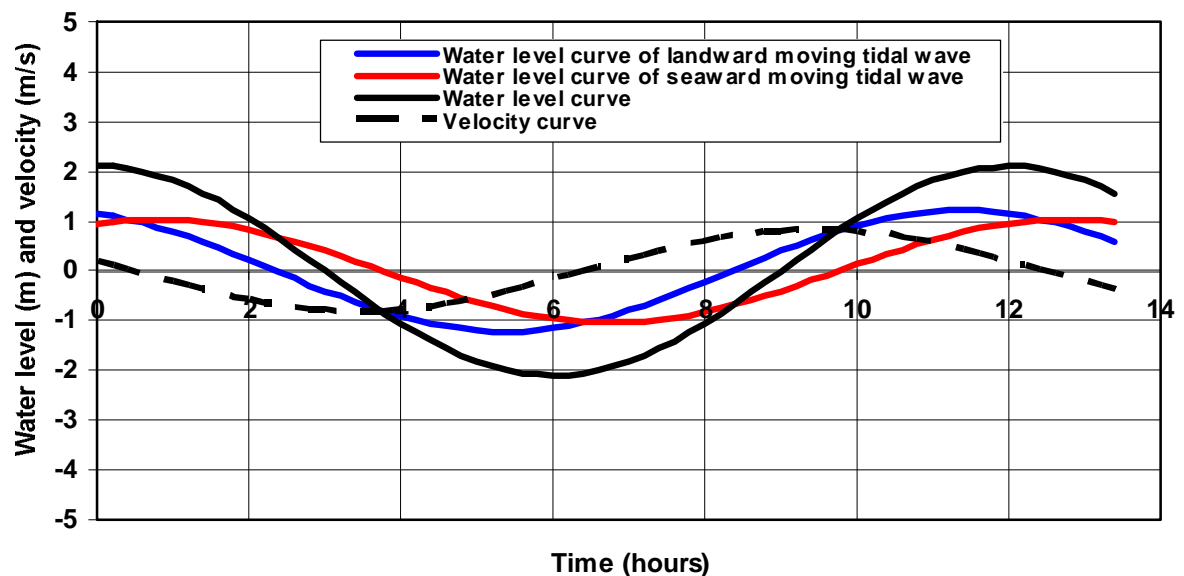


Figure 3.1.5B *Water level and velocity in converging channel; ingoing and outgoing water level curves, at mouth $x=0$ km*

3. Deformation

A harmonic wave propagating from deep water to shallow water cannot remain harmonic (sinusoidal) due to the decreasing water depth. Furthermore, the water depth (h) varies along the wave profile. The water depth is largest under the wave crest and smallest under the wave trough. As the propagation velocity is proportional to $h^{0.5}$, the wave crest will propagate faster than the wave trough, and the wave shape will change which is known as **deformation** (Figure 3.1.4). The wave is then no longer a smooth sinusoidal wave; the tidal high water becomes a sharply peaked event and low water is a long flat event. The deformed wave profile (wave skewness) can be described by additional sinusoidal components known as **higher harmonics** of the basic wave. Bottom friction and shoaling will also lead to wave deformation. Bore-type asymmetric waves can only be described by higher harmonics if a phase shift is introduced between the base wave and the higher harmonic wave.

4. Damping

Friction between the flowing water and the bottom causes a loss of energy and as a result the wave height will be reduced (energy $\propto H^2L$). These effects may be relatively important in the landward part of the estuary where the channels are smaller and relatively shallow. Small changes of the channel width and depth may have relatively large effects on the tidal wave propagation in this part of the estuary (see also **Pieters, 2002**). Dredging of channels in this eastern part of the estuary will have a different effect on tidal wave propagation than dredging of channels in the mouth region.

Generally, frictional losses are quadratically related to the mean velocity. Using quadratic (non-linear) friction, the equations of motion and continuity can only be solved numerically. Using linear friction, analytical solutions can be obtained. According to the energy principle of **Lorentz**, the total energy dissipation in a tidal cycle is the same for both linearized and quadratic friction.

Using linear friction and a constant water depth, the wave height (tidal range) will decrease exponentially during propagation in a prismatic channel (**Figure 3.1.4**).

Non-linearity of the friction term (bottom friction $\approx \bar{u}^2$ or $\bar{u}|\bar{u}|$) generates higher frequency components than the basic frequency ω of a tidal wave ($\omega = 2\pi/T$).

3.2 Analytical and numerical simulations of tidal flow in converging channels

3.2.1 Numerical and analytical models

In this study both numerical and analytical models have been used.

The 1D numerical model can simulate the real pattern of width and depth variations taking all terms of the momentum equation and quadratic friction into account, but lateral flows and 3D effects are excluded.

Analytical models can be derived by neglecting the convective acceleration term and assuming linear properties of the momentum equation, linear friction, constant depth (to MSL) and a prismatic or exponential planform of the estuary.

In an earlier study **Van Rijn (2011a,b,c)** has shown that the tidal range in the Scheldt estuary can be simulated by an analytical solution method for converging channels neglecting wave reflection at the closed channel end. Using this analytical approach, the (funnel-type) planform of the estuary is represented by an exponential curve based on $b = b_o \exp(x/L_b)$ with b = width of estuary, b_o = width at mouth and L_b = converging length scale, x = longitudinal coordinate (negative in landward direction). The cross-sections of the Scheldt estuary have been schematized into rectangular profiles with constant depth h_o .

It may be argued whether the rather irregular pattern of the tidal channels can be represented sufficiently accurate by using a 1D model approach, as bend effects are not taken into account. Basically, this requires a 3D model approach which is beyond the present scope of research. However, in essence the Scheldt estuary consists of primary and secondary tidal channels with gradually decreasing dimensions in landward direction. Sills/shoals are present at various locations, but nature deals with these constrictions by flow diversion (lateral flows) from primary to secondary channels.

The analytical model can only deal with exponentially decreasing widths based on rectangular cross-sections. The cross-sectional area of parallel primary and secondary channels should be combined to one channel cross-section. Therefore, this type of model can only represent the basic trends caused by gradual geometrical convergence and frictional damping.

In the case of a **compound** cross-section consisting of a main channel and tidal flats it may be assumed that the flow over the tidal flats is of minor importance and only contributes to the tidal storage. The discharge is conveyed through the main channel. This can to some extent be represented by using $c_o = (g h_{eff})^{0.5}$ with $h_{eff} = A_c/b_s = \alpha_h h_c$ and $\alpha_h = A_c/(b_s h_c) = (b_c/b_s) h_c = (b_c/b_s) h_o$, A_c = area of main channel ($= b_c h_c = b_c h_o$), $h_c = h_o$ = depth of main channel, b_c = width of main channel and b_s = surface width.

The transfer of momentum from the main flow to the flow over the tidal flats can be seen as additional drag exerted on the main flow (by shear stresses in the side planes between the main channel and the tidal flats). This effect can be included crudely by increasing the friction in the main channel.

If the hydraulic radius (R) is used to compute the friction parameters (m and C) and the wave propagation depth ($h_{\text{eff}} = R$), the tidal wave propagation in a compound channel will be similar to that in a rectangular channel with the same cross-section A .

The tidal wave propagation in the Scheldt estuary can also be simulated by using the four-pole method (**Verspuy 1985, Pieters, 2002, Van Rijn, 2011b**). This method is based on a combination of the incoming wave and the reflected wave. Using this approach, the estuary is schematized into series of **prismatic** sections, each with constant width and depth, see **Figure 3.2.1**. The water level and discharge at the end of each section are used as boundary conditions at the entrance of the next section. The computation goes from section to section in landward direction. In each new section a new incoming and reflected wave is computed based on the section parameters. The method has been employed to the Scheldt estuary by **Pieters (2002)**. His results show the generation of a reflected wave with an amplitude of about 1 m in the Scheldt estuary, which is approximately constant along the estuary. The phase shift between the incoming and reflected wave is about 65° at the mouth decreasing to about 30° at the end of the estuary. The phase shift of the velocity and water level curve at the mouth of the estuary is assumed to be 70° (input parameter derived by calibration)

The major drawback of this method is that the convergence (shoaling) process within each prismatic channel section is neglected. The tide will be damped exponentially due to bottom friction along each prismatic section length. To correct for the absence of convergence, an apparent reflected wave has to be introduced. So channel convergence is replaced by wave reflection at each abrupt transition in channel section. Another deficiency is that the phase lead between the vertical and the horizontal tide is not part of the solution, but has to be known (input value) from measured data, otherwise no solution is possible. **Pieters (2002)** has fitted this value to get the best overall results along the estuary. Finally, the method is not really predictive as the phase shift between the vertical and the horizontal tide is unknown for future scenarios with changed channel characteristics (channel depth and width changes).

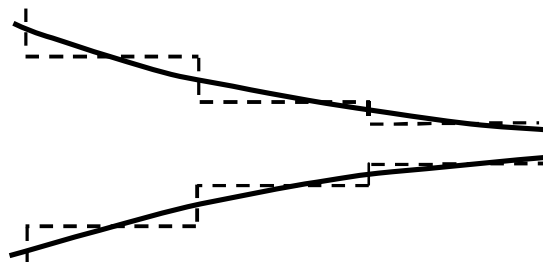


Figure 3.2.1 Schematization of estuary planform in fourpole-method

3.2.2 Effect of water depth on tidal range

To demonstrate the applicability of the analytical model for a converging estuary, the tidal range of spring tide ($H_o = 4.2$ m, $T = 12$ hours) has been computed along a converging estuary (**Figure 3.2.2**) with a length of 180 km, the width at the mouth is $b_o = 25$ km, the converging length scale is $L_b = 25$ km, the width at the end of the channel is $b = 20$ m, the water depth to MSL is $h_o = 10$ m (width-averaged depth), the bed roughness is $k_s = 0.05$ m (Manning coefficient $n \cong 0.024$; **Pieters (2002)** has used $n = 0.025$). The channel is closed at the end ($Q_r = 0$ m³/s). The dimensions of this flow system are broadly similar to those of the Scheldt estuary and Scheldt river (**Van Rijn, 2011a**). The computed tidal range values of the analytical model (neglecting reflection at the closed end) are shown in **Figure 3.2.3**.

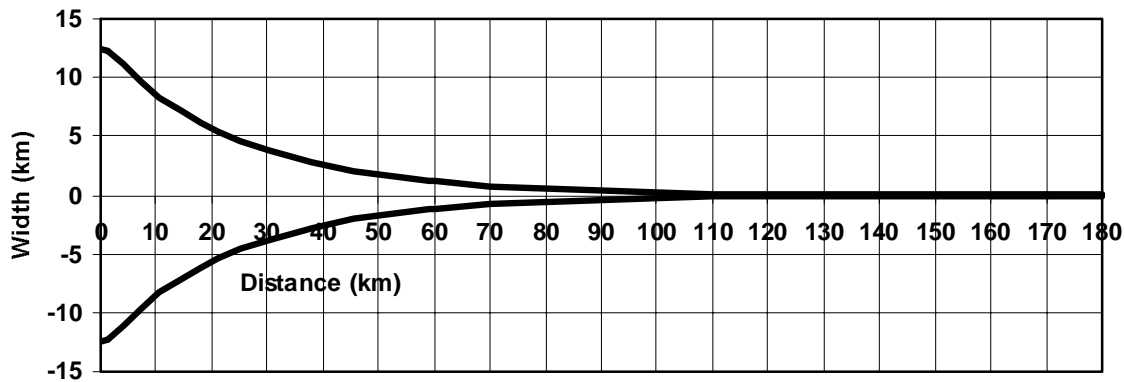


Figure 3.2.2 Planform of estuary; width along estuary
(total length= 180 km, depth=constant)

The results of the numerical 1D model of Deltares (including reflection) are also shown for this case with constant depth. The tidal range values of the numerical 1D model are systematically smaller (10% to 15%) as this model is based on quadratic friction, whereas the analytical model is based on linear friction. Using a larger bed roughness of $k_s = 0.1$ m instead of $k_s = 0.05$ m, the results of the analytical model are in very good agreement with those of the numerical model. Measured tidal range values (springtide) up to Antwerp are in reasonable agreement (within 5% to 10%) with the results of both models. Measured tidal range values landward of Antwerp are not shown as the real water depths in the Scheldt river are much smaller than the constant water depth of 10 m used in this computation.

Figure 3.2.4 shows the ratio of the tidal range at $x = 90$ km and that at the mouth ($x = 0$ km) as a function of the water depth using both models. The water depth values have been varied in the range of 5 to 100 m. The results of the analytical and numerical models are in good agreement.

Tidal damping occurs for water depth values smaller than about 7 m due to the dominant effect of friction.

Tidal amplification occurs for water depths larger than about 7 m due to dominant funneling effect (decrease of width). The amplification effect is maximum for a water depth of about 12 m. The tidal amplification reduces again for water depths larger than 12 m. Tidal amplification approaches 1 for very large depths (> 50 m). In that case the wave speed is very large and the length of the tidal wave is much larger ($L = cT$) than the channel length resulting in an almost horizontal water surface moving up and down, see **Figures 3.2.5 and 3.2.6** showing water surface profiles at HW and LW.

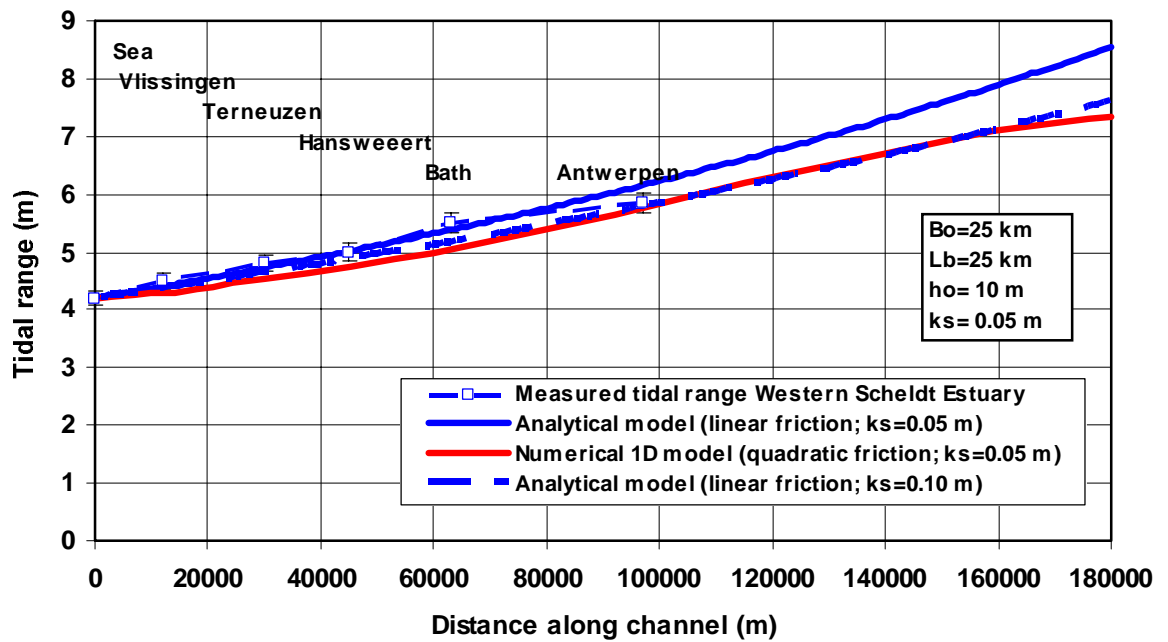


Figure 3.2.3 Tidal range along converging estuary

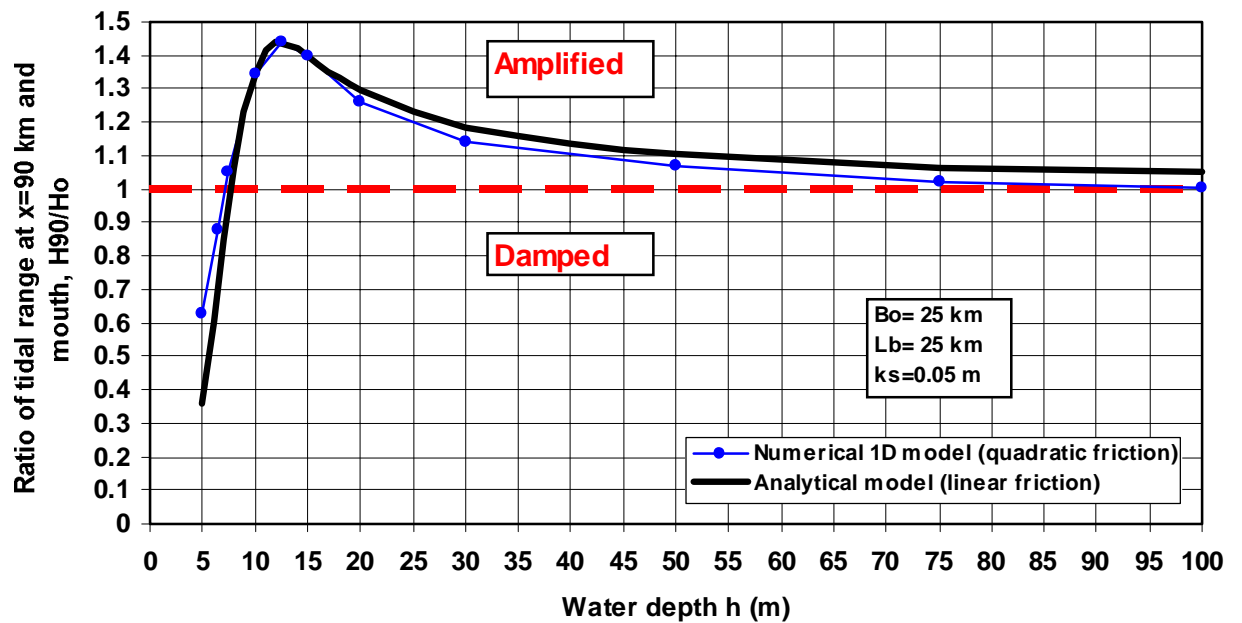


Figure 3.2.4 Ratio H_{90}/H_0 of the tidal range at $x=90$ km and at the mouth $x=0$ km as function of water depth

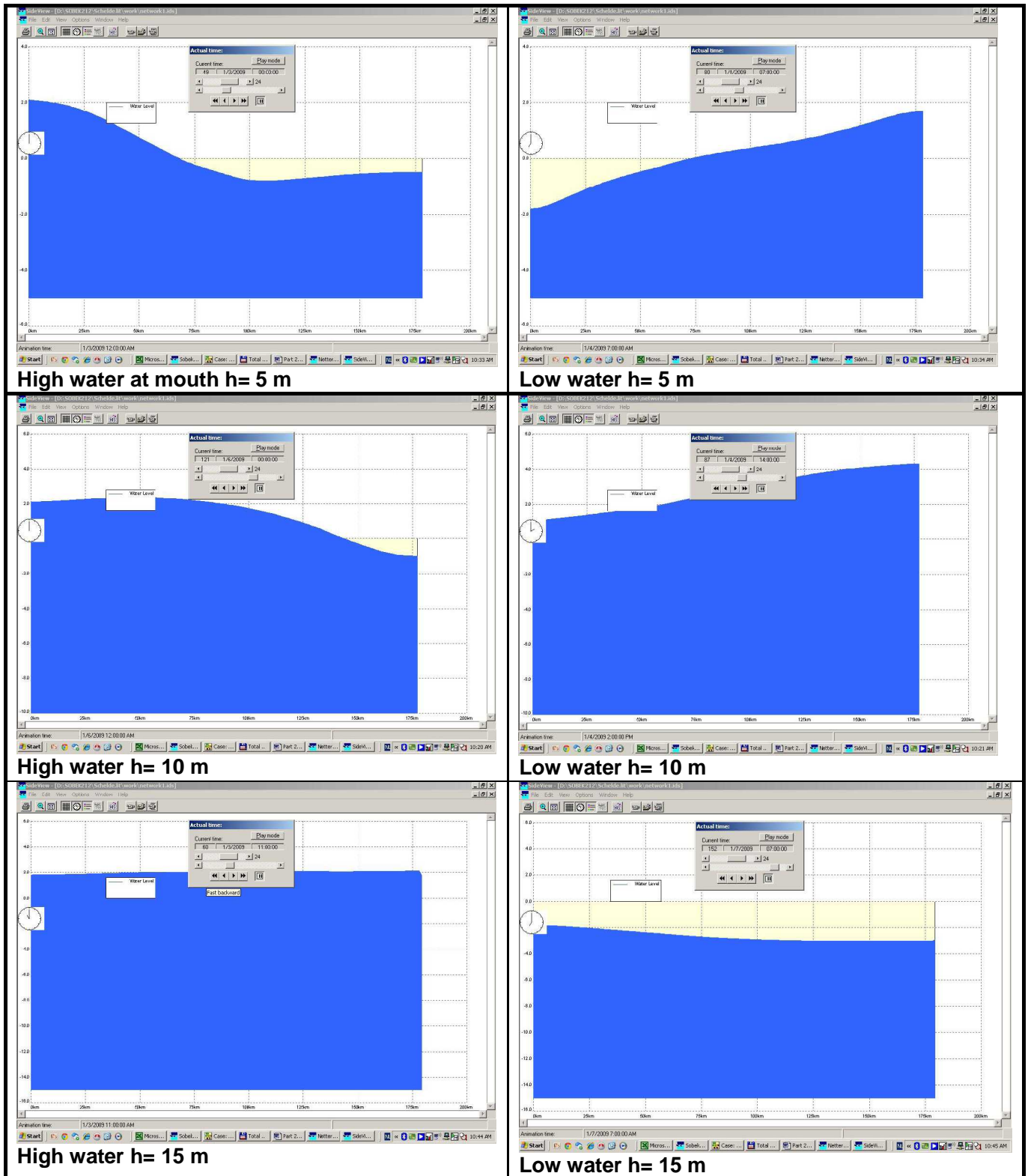


Figure 3.2.5 Water surface profiles at High Water and Low Water (mouth); $h = 5, 10$ and 15 m (yellow colour); length = 180 km

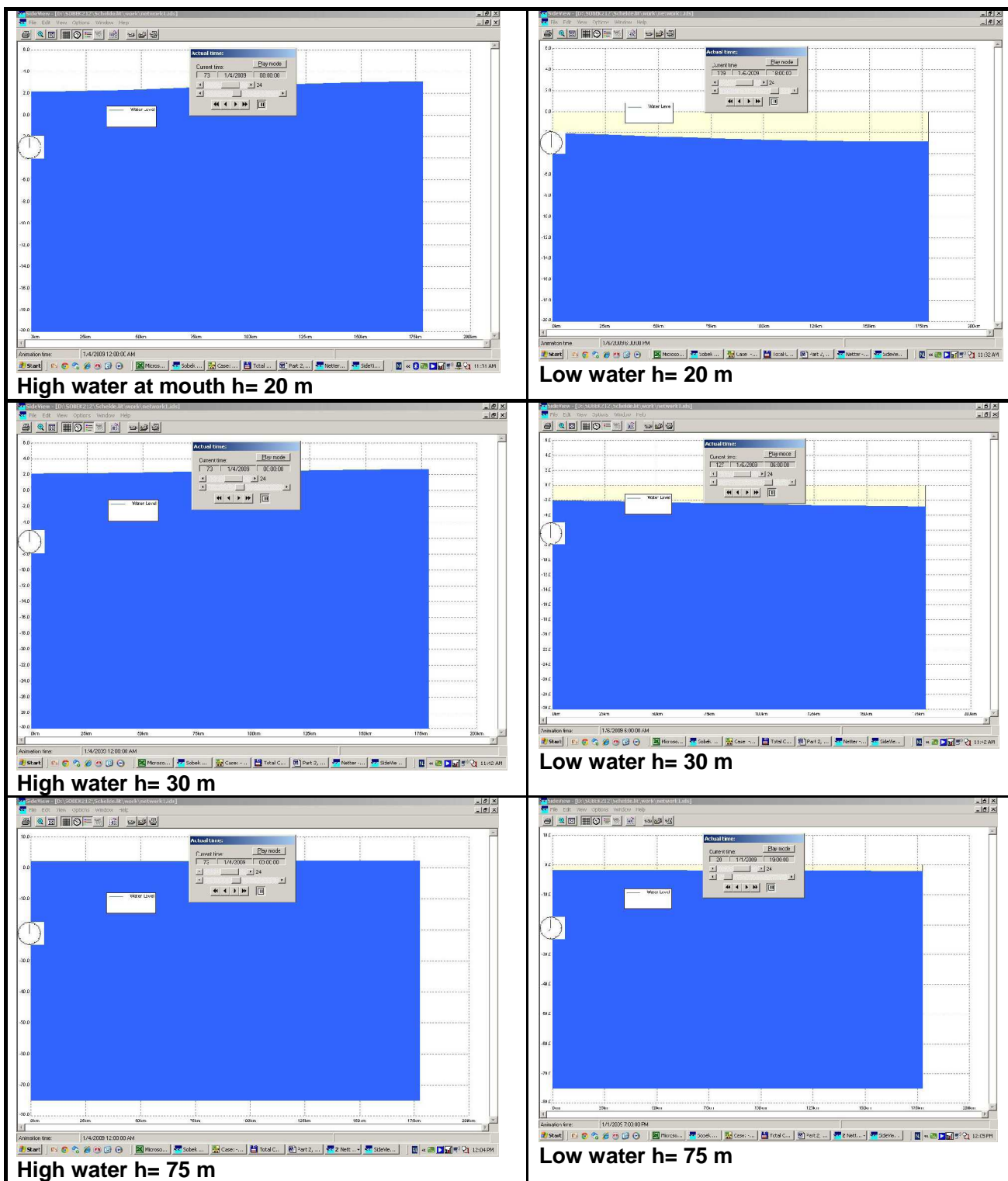


Figure 3.2.6 Water surface profiles at High Water and Low Water (mouth);
h= 20, 30 and 75 m (yellow colour); length= 180 km

According to the analytical model, the tidal range in a converging channel is described by:

$$H_x = H_o [e^{(-0.5\beta + \mu)x}]$$

with: x = longitudinal coordinate (negative in landward direction), $\beta=1/L_b$ = convergence coefficient, L_b = convergence length scale ($\cong 25$ km), $b_o= 25$ km, μ = friction coefficient.

Tidal damping occurs for $(-0.5\beta + \mu) > 0$ or $0.5\beta < \mu$.

Tidal amplification occurs occurs for $(-0.5\beta + \mu) < 0$ or $0.5\beta > \mu$.

The values of 0.5β and μ for water depths in the range of 5 to 100 m are given in **Table 3.2.1**. Both coefficients are about equal for a water depth of about 7 m. Damping dominates for water depths smaller than about 7 m and amplification dominates for water depths in the range of 7 to 25 m. The amplification effect gradually reduces for larger depths. The values of

Table 3.2.1 also show that both coefficients become equal again for very large depths. In the case of a very deep channel the wave propagation velocity is very large and hence a very long wave is present ($L= cT$). The wave length is then much larger than the channel length and the wave will act as a standing wave with a horizontal surface (almost no friction due to large depth and small velocities) moving up and down. This has been verified by a run with the 1D-flow model for a converging channel with a length of about 180 km, width at mouth of 25 km, width at end of about 20 m (converging length scale of about 25 km), see **Figure 3.2.6** ($h= 75$ m). The tidal range in the channel was found to be equal to the tidal range at the mouth at all sections (except in the end section where reflection occurred).

Table 3.2.1 Friction and convergence coefficients ($L_b= 25$ km, $k_s= 0.05$ m)

Water depth h (m)	Coefficient $0.5\beta=0.5/L_b$ (-)	Coefficient μ (-)	Peak tidal velocity at mouth \hat{u} (m/s)
5	$2.0 \cdot 10^{-5}$	$2.89 \cdot 10^{-5}$	1.07
7	$2.0 \cdot 10^{-5}$	$2.04 \cdot 10^{-5}$	0.98
8	$2.0 \cdot 10^{-5}$	$1.82 \cdot 10^{-5}$	0.94
10	$2.0 \cdot 10^{-5}$	$1.60 \cdot 10^{-5}$	0.82
12	$2.0 \cdot 10^{-5}$	$1.57 \cdot 10^{-5}$	0.70
15	$2.0 \cdot 10^{-5}$	$1.62 \cdot 10^{-5}$	0.56
20	$2.0 \cdot 10^{-5}$	$1.71 \cdot 10^{-5}$	0.41
25	$2.0 \cdot 10^{-5}$	$1.77 \cdot 10^{-5}$	0.32
50	$2.0 \cdot 10^{-5}$	$1.89 \cdot 10^{-5}$	0.16
100	$2.0 \cdot 10^{-5}$	$1.95 \cdot 10^{-5}$	0.08

3.2.3 Effect of planform schematizations on tidal range

1. Schematization of landward river section

The numerical 1D-model has been used to analyse the effect of width and depth variations in the most landward section (landward of $x = 90$ km) of the Scheldt estuary and Scheldt river system. The width at the mouth is $b_0 = 25$ km. The convergence length scale is $L_b = 25$ km. The total length is 180 km. The landward end is closed (no river inflow).

Four schematizations have been applied (see **Figure 3.2.7**):

- Schematization A: exponential width variation between mouth at $x = 0$ km and $x = 180$ km (width at end = 20 m based on $L_b = 25$ km; **Figure 3.2.2**); water depth = 10 m;
- Schematization B: exponential width variation between mouth and $x = 90$ km (width at 90 km = 630 m based on $L_b = 25$ km); constant width = 630 m between 90 and 180 km; water depth = 10 m;
- Schematization C: exponential width variation between mouth and $x = 90$ km (width at 90 km = 630 m based on $L_b = 25$ km); width reduction from 630 m to 100 m between $x = 90$ km and $x = 115$ km; constant width = 100 m between 115 and 180 km; constant water depth = 10 m;
- Schematization D: exponential width variation between mouth and $x = 90$ km (width at 90 km = 630 m based on $L_b = 25$ km), water depth = 10 m; width reduction from 630 m to 100 m between $x = 90$ km and $x = 115$ km; constant width = 100 m between 115 and 180 km; water depth = 5 m between 115 and 180 km.

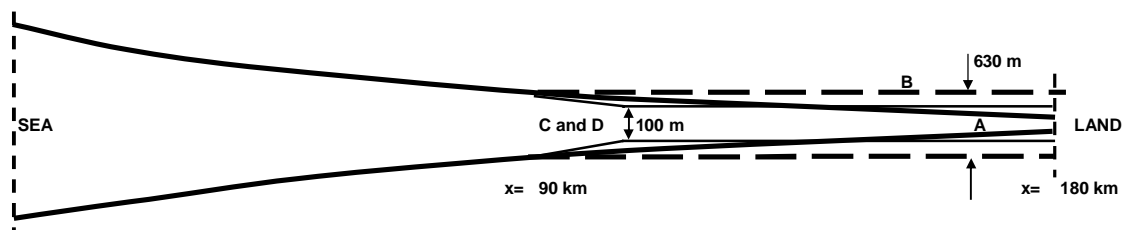


Figure 3.2.7 Schematizations

Figure 3.2.8 shows the computed tidal range values of springtide conditions (mouth: $H_0 = 4.2$ m, $T = 12$ hours). Measured tidal range values up to Melle in Belgium are also shown.

The convergence effect is maximum in Schematization A with an exponential width decrease up to the end of the flow system. The tidal range values up to station Bath based on the numerical model results are slightly too small compared to measured data. In this part of the estuary the widths according to the exponential planform are somewhat too small. The channel near Bath (Nauw van Bath) is relatively narrow. If the width is kept constant to $b_{90} = 630$ m after 90 km (schematization B), the tidal range drops considerably due to the bottom friction effects up to 160 km. Landward of 160 km the tidal range increases again due to reflection against the closed land boundary.

If the width is reduced between 90 and 115 km from 630 m tot 100 m and kept constant at 100 m beyond 115 km (schematization C), the tidal range drops much less. Reflection effects can be seen over the last 20 km.

If the water depth is reduced from 10 m between 0 and 90 km to 5 m between 115 and 180 km (Schematization D), the tidal range decreases to realistic values, as measured in Stations Wichelen and Melle due to the effect of increased bottom friction. More accurate simulations of the tidal wave propagation requires detailed representation of the geometry of the estuary, which is beyond the scope of the present study.

These results clearly show the importance of the width convergence resulting in a significant increase of the tidal range if the width is reduced. A constant width landward of a converging section leads to decrease of the tidal range in the constant-width section but also in the more seaward converging section (schematization B).

The results also show that the tidal range in the seaward half of the estuary ($x < 90$ km) is only affected by schematization B.

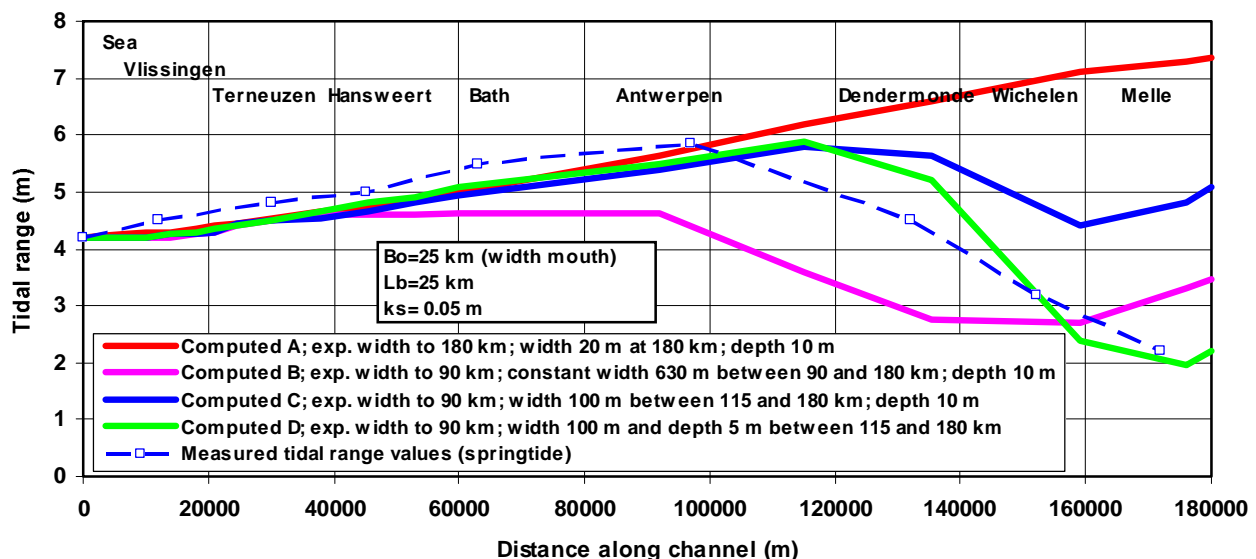


Figure 3.2.8 Measured and computed tidal ranges along Scheldt estuary and river

2. Schematization of flood and ebb channels of Scheldt estuary

The tidal range of the Scheldt estuary can be simulated quite well by the analytical model using the dimensions of the flood and ebb channels only.

Figure 3.2.9 shows the schematized flow system of the Scheldt estuary. In essence, the flow system is a two-channel system with primary and secondary channels between the mouth and section 10 (west of Bath); landward of that section only one dominant channel is present. Generally, shallow sills/shoals are present at the transitions from primary to secondary channels, see **Figure 3.2.9**. Large vessels sail up to Antwerp through the primary navigation channel.

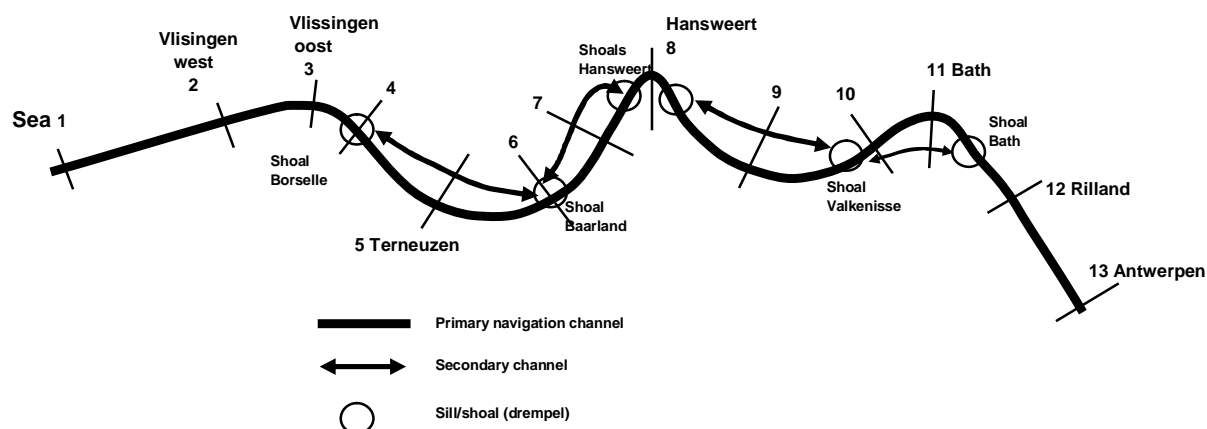


Figure 3.2.9 Schematized primary and secondary channels of Scheldt estuary

Table 3.2.2 Dimensions of schematized primary and secondary channels of Scheldt estuary

Cross-section	Dis tance	Schematization E			Schematization F		
		Primary channel width	Primary channel depth to NAP	Primary channel area	Prim. and sec. channel width	Prim. and sec. channel depth to NAP	Prim. and sec. channel area
	(km)	(m)	(m)	(m ²)	(m)	(m)	(m ²)
1 Sea	0	2500	15	37500	5000	10-15	50000
2 Vlissingen-West	12	1500	25	22500	3000	10-25	30000
3 Vlissingen-Oost	19	700	30	21000	1500	10-30	15000
4 Drempel Borssele	25	400	15-30	6000	1000	10-30	10000
5 Terneuzen	34	500	30	15000	1000	10-30	10000
6 Gat Ossenissee	42	500	25	12500	1000	10-25	10000
7 Middelgat	47	400	25	10000	1000	10-25	10000
8 Hansweert	54	400	25	10000	800	10-25	10000
9 Zuidergat-Schaar Valkenisse	60	300	20	6000	600	10-20	6000
10 Overloop Valkenisse	66	300	20	6000	500	10-20	5000
11 Bath	71	200	20	4000	400	10-20	4000
12 Rilland	77	200	20	4000	300	10-20	3000
13 Antwerpen	97	150	15	2250	200	10-15	2000

Two funnel-type channel schematizations have been applied to represent this flow system by the analytical model (see **Table 3.2.2**), as follows:

- Schematization E: primary channel
with $b_o = 2.5$ km, $L_b = 30$ km, $h_o = 12$ and 15 m, $k_s = 0.05$ m,
- Schematization F1: primary and secondary channel
with $b_o = 5$ km, $L_b = 30$ km, $h_o = 12$ and 15 m, $k_s = 0.05$ m
(cross-sections of parallel channels between Vlissingen and Bath have been combined into one rectangular cross-section)
- Schematization F2: primary and secondary channel
with $b_o = 5$ km, $L_b = 40$ km, $h_o = 12$ and 15 m, $k_s = 0.05$ m
(cross-sections of parallel channels between Vlissingen and Bath have been combined into one rectangular cross-section)

Figure 3.2.10 shows measured and computed areas of the cross-sections of **Table 3.2.2**. The 'measured' values are estimates (with accuracy of 30%) of the areas of the cross-sections of the main tidal channels, see **Appendix A**. The areas are gradually decreasing in landward direction and can be represented by exponential functions ($A = A_o \exp(-x/L_A)$) with $A = bh =$ area of cross-section, $A_o =$ area at mouth, $L_A = L_b =$ convergence length scale $\cong 30$ to 40 km, $h =$ water depth to MSL=constant).

Schematization E focusing on the primary (navigation) channel includes several narrow cross-sections at Stations 4, 6, 8, 10 and 11 with minimum depths of about 15 m below NAP (\cong MSL). Shoals/sills are present at these locations. The water depth at these sills is kept at about 15 m below MSL by dredging. The water depths of the tidal channels on the seaward and landward sides of the sills are much larger up to 30 m (see **Table 3.2.2**). For example, the local width at the Borssele sill (Station 4) is about 400 m yielding a cross-sectional area of about 6000 m^2 , which is much smaller than the available areas just upstream (about 20000 m^2 at Station 3) and downstream (about 15000 m^2 at Station 5) of the sill location (Station 4). Hence, this sill location may easily give rise to some (partial) reflection of the tidal wave. However, part of the flow will be diverted through the secondary channel (Everingen) between Stations 4 and 6 compensating the reflection effect.

Schematization F includes both the primary and secondary channels. Cross-sections of the parallel primary and secondary channels between Vlissingen and Bath have been combined into one rectangular cross-section. The primary channel refers to the main navigation channel.

Figure 3.2.11 shows measured and computed tidal range values between the mouth (sea boundary) and Antwerp. The results of Schematization F1 are not shown as they are almost identical to those of E. Thus, an increase of the width only (keeping the depth and convergence length the same) has not much effect on the results. All schematizations yield amplification of the tidal range. The simulations E and F1 yield amplification of the tidal range in landward direction in reasonable agreement with the measured values due to the convergence (funneling) effect. The results of schematization F2 show a smaller amplification effect for a smaller water depth of 12 m and a larger convergence length of 40 km. The effect of the water depth is much larger for a convergence length of 40 km than for a convergence length of 30 km.

Similar computations have been made for the Section Hansweert-Antwerpen only with length of about 45 km using the tidal range, peak tidal velocity and flow width computed at Hansweert as new boundary conditions (based on Schematization E; primary channel and boundary conditions at sea). The computed tidal range at Antwerpen was found to be within 3% of that for Schematization E with boundary conditions at sea (both for a depth of 12 m and 15 m; $L_b = 30$ km; the width at sea is 2500 m; the width reduces from 550 m at Hansweert to about 125 m at Antwerpen).

Based on these results, it can be concluded that realistic amplification values are obtained using the dimensions of the dominant tidal channels only (channel width at mouth of 2.5 to 5 km, minimum water depth of 12 to 15 m and convergence length scales of 30 to 40 km). The water depth and the convergence length are most important parameters.

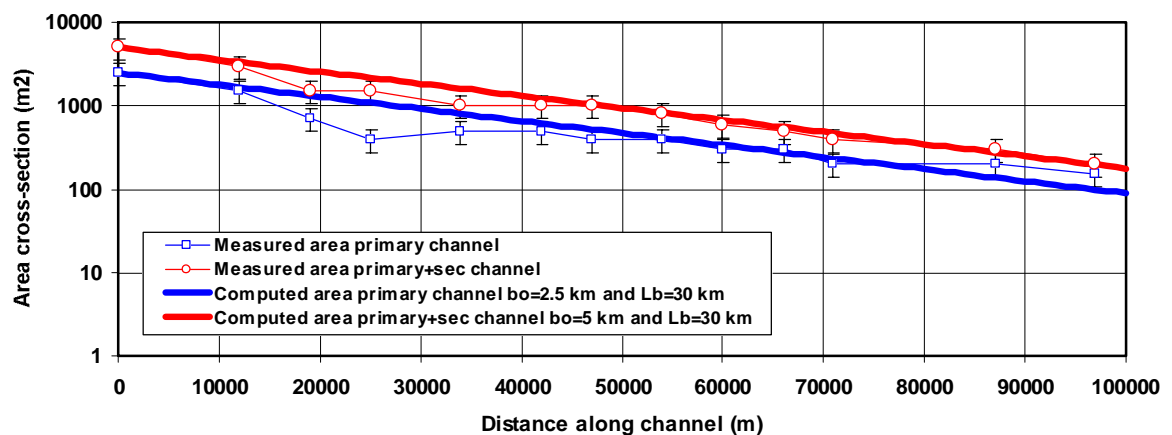


Figure 3.2.10 *Measured and computed areas of cross-sections along channel; Scheldt estuary*

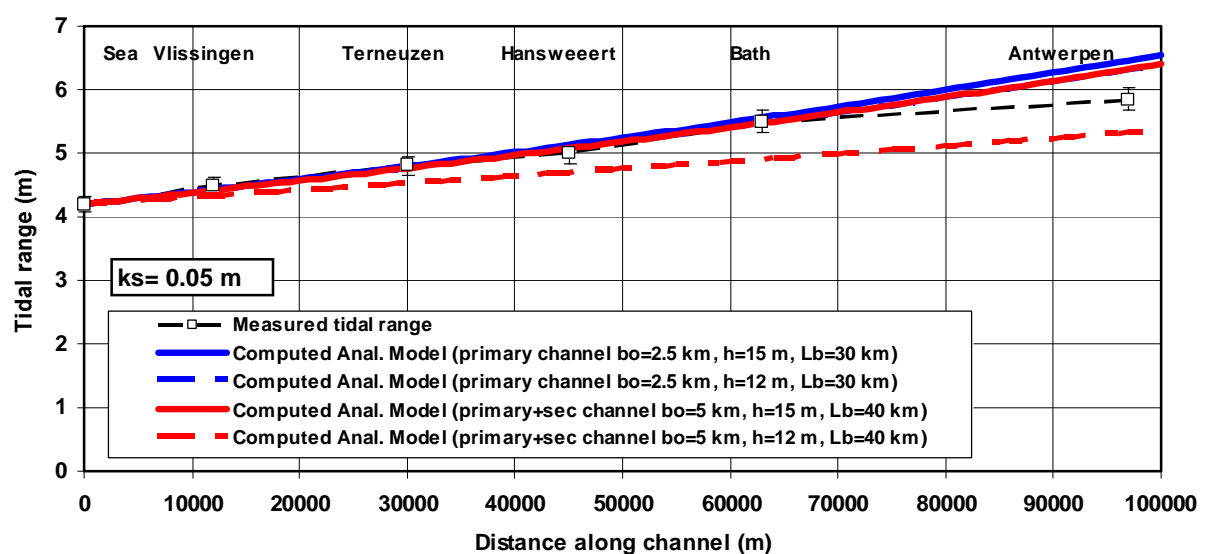


Figure 3.2.11 *Measured and computed tidal range values along tidal channel; Scheldt estuary*

3.2.4 Effect of abrupt changes of cross-section on tidal range

The presence of **abrupt** changes of local cross-sections may cause partial reflection and deformation of the tidal wave resulting in a significant change of the tidal range along the estuary. This can only be studied by using the 1D numerical model.

Two types of estuaries are considered: **prismatic** estuary and **converging** estuary.

Prismatic estuary

The estuary has a length of 180 km and a width (b) of 1 km. The estuary is closed at the end with no river inflow. The depth (h) is 20 m below MSL and the bottom roughness is $k_s = 0.05$ m. The tidal range at the mouth is 4.2 m and the tidal period is $T = 12$ hours.

The following cases are defined (see **Figure 3.2.12**):

- Case A: **straight, prismatic channel** without sills and narrows
- Case B: **two short sills** are present at 35 km and at 70 km from the sea; the horizontal sill bottom is set at -10 m below MSL (cross-section reduction of 50%); the slopes of the sill have a length of 3 km; the horizontal middle section of each sill has a length of 3 km (total length of two sills is 18 km; 10% of total estuary length; total reduction of cross-section is 50%).
- Case C: **two narrow sections** are present at 35 km and at 70 km from the sea; the length of the narrow middle section is 3 km; the length of the inflow and outflow section also is 3 km (total length of two narrows of 18 km; 10% of total length of estuary); the width of the narrow section is set at 50% of the original width over length of 3 km in the middle (total reduction of cross-section is 50%).
- Case D: **two sills and two narrow sections** are present at 35 km and at 70 km from the sea; the horizontal sill bottom is set at respectively at -10 m below MSL (water depth reduction of 50%); the length of the inflow and outflow section also is 3 km; total length of 18 km; 10% of total length of estuary); the width of the narrow section is set at 50% of the original width over length of 3 km in the middle (total reduction of cross-section is 75%).

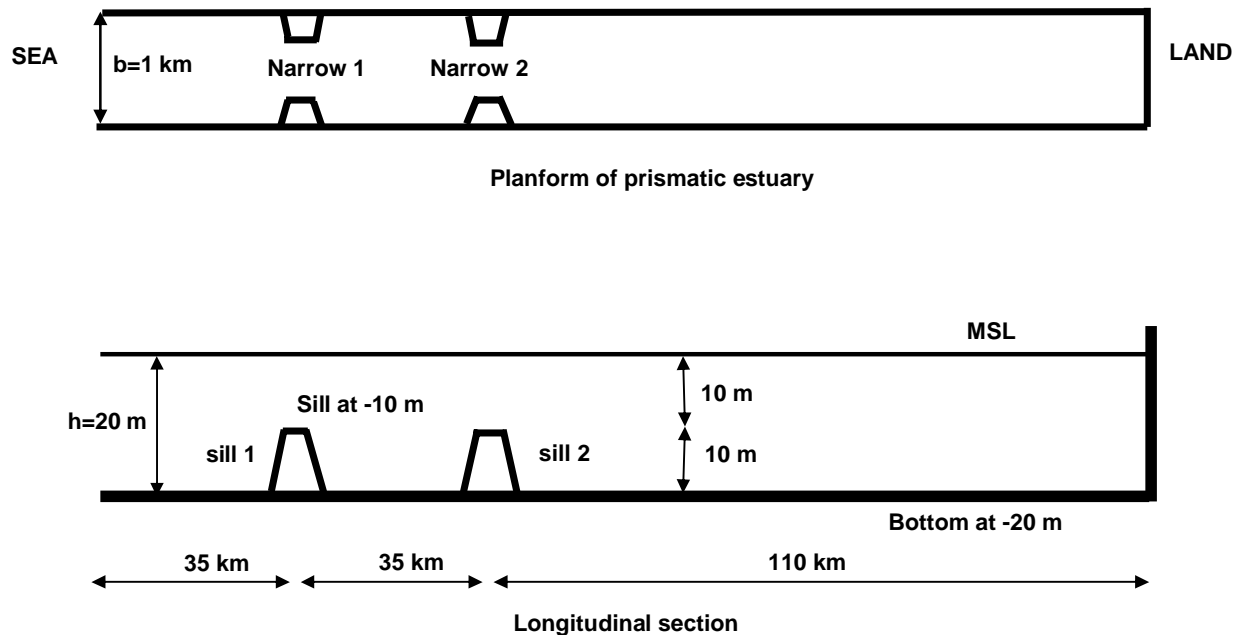


Figure 3.2.12 Upper: planform of prismatic estuary with two narrow sections (Case C)
 Lower: longitudinal section with two short sills (Case B)

Figure 3.2.13 shows the computed HW and LW levels and the tidal range between HW and LW for the situation with and without sills/narrows.

In the **absence** of sills and narrows the tidal range gradually decreases from 4.2 m at the sea to about 2 m at about 50 km from the mouth and increases again between 50 and 180 km due to reflection of the tidal wave at the closed landward boundary.

If two short sills (Case B) or two narrows (Case C) are present, the tidal range increases on the seaward side due to reflection and decreases on the landward side. The increase of the tidal range on the seaward side and the decrease of the tidal range on the landward side are maximum if the sills and the narrows are present simultaneously (Case D) reducing the local cross-section by about 75%. The maximum increase of the tidal range is about 1.2 m at $x=30\text{ km}$ and the maximum decrease is about 2 m at $x=180\text{ km}$ (Case D).

The effect of sills is larger than the effect of narrows as both the wave speed and the flow resistance are affected by a change of the depth (sill cases).

The HW values are higher and the LW are lower on the seaward side of sill/narrow locations. The LW values are gradually shifted upward on the landward side (maximum about 1 m at the end of the estuary) compared with the results of Case A (no sills and narrows).

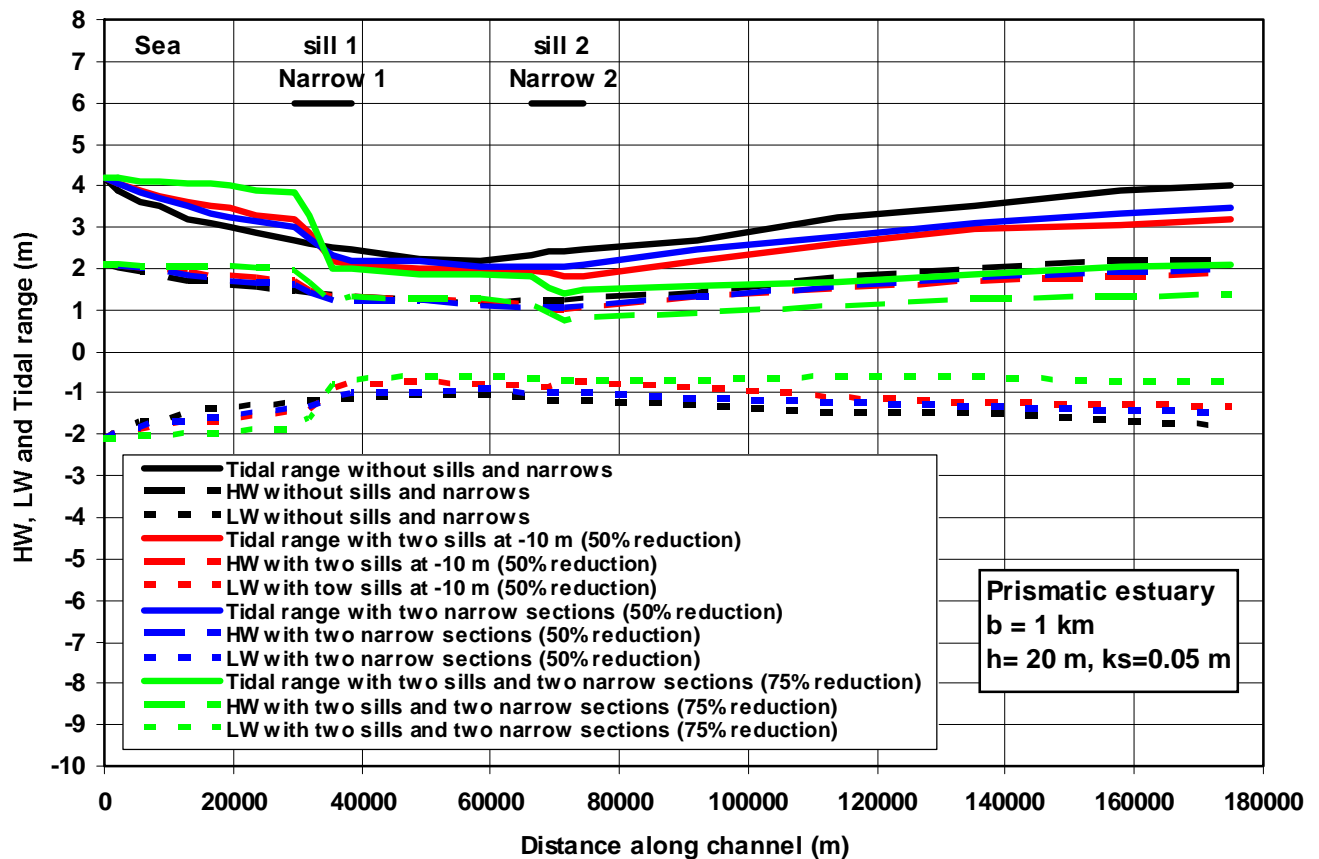


Figure 3.2.13 Effect of abrupt depth changes (sills and narrows) on HW, LW and tidal range along prismatic estuary; Cases A, B, C and D

Converging estuary

The estuary has a length of 180 km and a width (b_0) at the mouth of 25 km. The converging length scale of the exponential planform is $L_b = 25$ km. The estuary is closed at the end with no river inflow. The width at the closed end is about 20 m. The depth (h) is 20 m below MSL and the bottom roughness is $k_s = 0.05$ m. The tidal range at the mouth is 4.2 m and the tidal period is $T = 12$ hours.

Two methods have been applied to represent the exponential planform : method 1 consisting of 10 sections with straight banks between the cross-sections and method 2 consisting of 10 prismatic sections with abrupt changes to reduce the width from section to section, see **Figure 3.2.14**. Method 1 is the default method used.

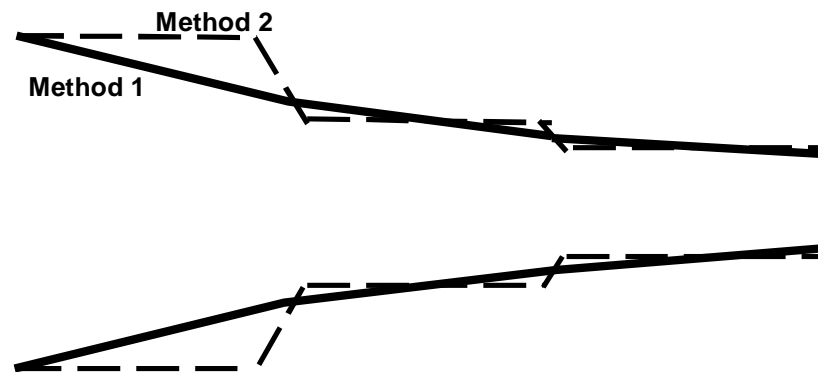


Figure 3.2.14 Numerical representation of exponential planform

The following cases are defined (see **Figure 3.2.15**):

Case E: **converging channel** without sills and narrows.

Case F1: **two short sills** are present at 35 km and at 70 km from the sea; the horizontal sill bottom is set at respectively at -7.5 m (62.5% reduction of cross-section), at -5 m (75% reduction) and at -3 m below MSL (85% reduction); the slopes of the sill have a length of 3 km; the horizontal middle section of each sill has a length of 3 km (total length of two sills is 18 km; 10% of total estuary length).

Case F2: **two short sills** are present at 35 km and at 70 km from the sea; the horizontal sill bottom is at respectively -7.5 m below MSL (62.5% reduction of cross-section); the slopes of the sill have a length of 1 km; the horizontal middle section of each sill has a length of 3 km (total length of two sills is 10 km; 6% of total estuary length).

Case G: **one short sill** is present at 70 km (location 2) from the sea; the horizontal sill bottom is at -7.5 m below MSL (62.5% reduction of cross-section); the slopes of the sill have a length of 3 km; the horizontal middle section of each sill has a length of 3 km (total length of sill is 9 km; 5% of total estuary length).

Case H: **one long sill** is present between 35 and 70 km from the sea; the horizontal sill bottom is at -7.5 m below MSL (62.5% reduction of cross-section); the two slopes of the sill have a length of 3 km; the horizontal middle section of the sill has a length of about 40 km (total length of sill is about 45 km; 25% of total estuary length).

Case I: **two narrow sections** are present at 35 km and at 70 km from the sea; the length of the narrow middle section is 3 km; the length of the inflow and outflow section also is 3 km (total length of two narrow sections is 18 km; 10% of total length of estuary); the width of the narrow section is set at respectively 50% (reduction of 50%), 25% (reduction of 75%) and 10% (reduction of 90%) of the original width over length of 3 km in the middle.

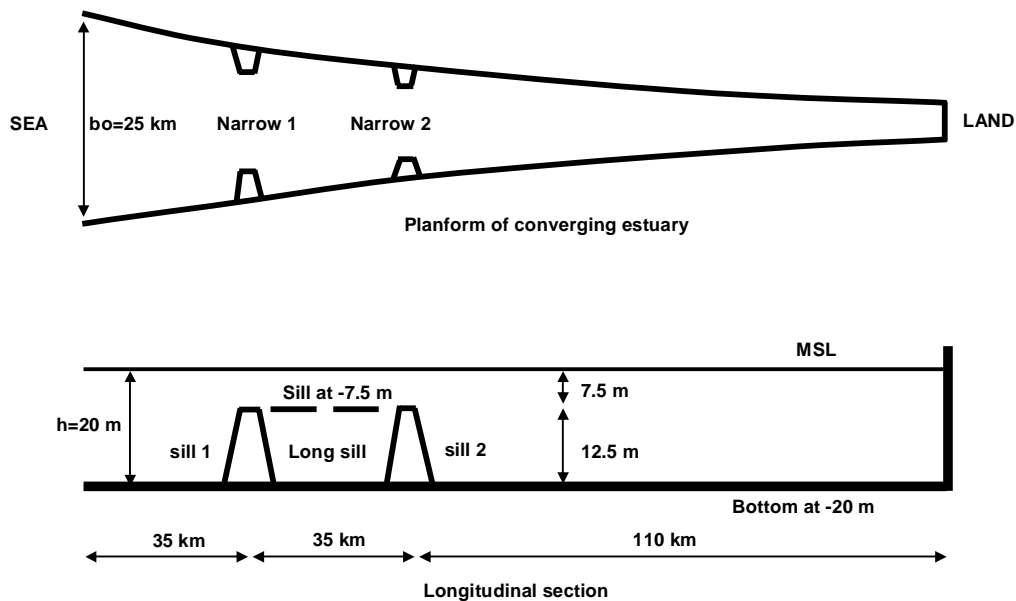


Figure 3.2.15 Upper: planform of converging estuary with two narrow sections (Case I)
 Lower: longitudinal section; two short sills and one long sill (Cases F, G, H)

Figure 3.2.16 shows the computed HW and LW levels and the tidal range between HW and LW for the situation with and without sills. In the **absence** of sills the tidal range gradually increases from 4.2 m at the sea (width of 25000 m) to about 6.5 m at the closed land boundary, where the width is very small (20 m). The amplification of the tide is caused by the landward converging width. Some reflection can be observed at the closed end (between 150 and 180 km). Both schematization methods (1 and 2, see **Figure 3.2.14**) to represent the exponential planform by the numerical model produce almost the same computed tidal range values (within 3%). The results of the default method 1 have been used in all computations. The tidal range is almost the same if two short sills (Case F1) are present. The two sills have a total length of about 18 km which is about 10% of the the total estuary length. This value is somewhat larger than the total dredging area (about 7% of total area) in the Scheldt estuary (see **Section 2.1**). The two sills with the bottom at -7.5 m causing a very abrupt change of the depth from 20 m to 7.5 m locally (62.5% reduction of cross-section), only have a very slight effect on the tidal range (slightly smaller values). The HW and LW lines are almost the same.

Increasing the sill bottom to -5 m below MSL (at both locations) leads to a somewhat larger decrease of about 10% of the tidal range (see **Figure 3.2.16**). The HW and LW lines landward of the sill locations are shifted upward over about 0.5 m, which is caused by tidal asymmetry (shorter wave crest and longer wave trough; flood duration is about 45% and ebb duration is about 55% of the total tidal period). The mean sea level (MSL) is only slightly affected (very small increase).

Increasing the sill bottom to -3 m below MSL (at both locations) leads to a significant decrease (about 20% to 30%) of the tidal range (see **Figure 3.2.16**). The tidal range along the estuary is strongly deformed. The LW lines landward of the sill locations are shifted upward over about 2 m. The HW lines are not so much affected.

The mean sea level (MSL) shows a significant increase of about 0.5 m at the end of the estuary (about 180 km). The tidal water level curve (over time) landward of sill 2 is strongly deformed with a relatively short flood period and a relatively long ebb period..

The tidal range on the seaward side of sill 1 in a converging estuary (in contrast to that in a prismatic estuary) is not much affected in all schematizations.

Figure 3.2.18 shows the water surface profiles in the situation with two short sills (Case F1) at four times (HW, LW, falling tide and rising tide). Small water drops can be observed at the sill locations. At falling tide the seaward water surface drops more quickly than the landward water surface at the sill locations, while at rising tide the seaward water level rises more quickly than the landward water level.

A model run (Case F2) with two short sills but with a shorter length of the sill slopes (slope length of 1 km instead of 3 km; total length of each sill is 5 km instead of 9 km) produced very similar results as presented in **Figure 3.2.16**. Therefore, the results of Case F2 are not shown.

A model run (Case G) with only one short sill (bottom level at -7.5 m) at location 2 produced similar results as with two short sills (Case F1) and are therefore not shown.

The presence of a very long sill covering about 25% of the length of the estuary (Case H) causes damping of the tidal wave (of about 0.2 m) due to increased bottom friction, as shown in **Figure 3.2.17**. The HW and LW are also shifted upwards by about 0.7 m (increase of the mean water level).

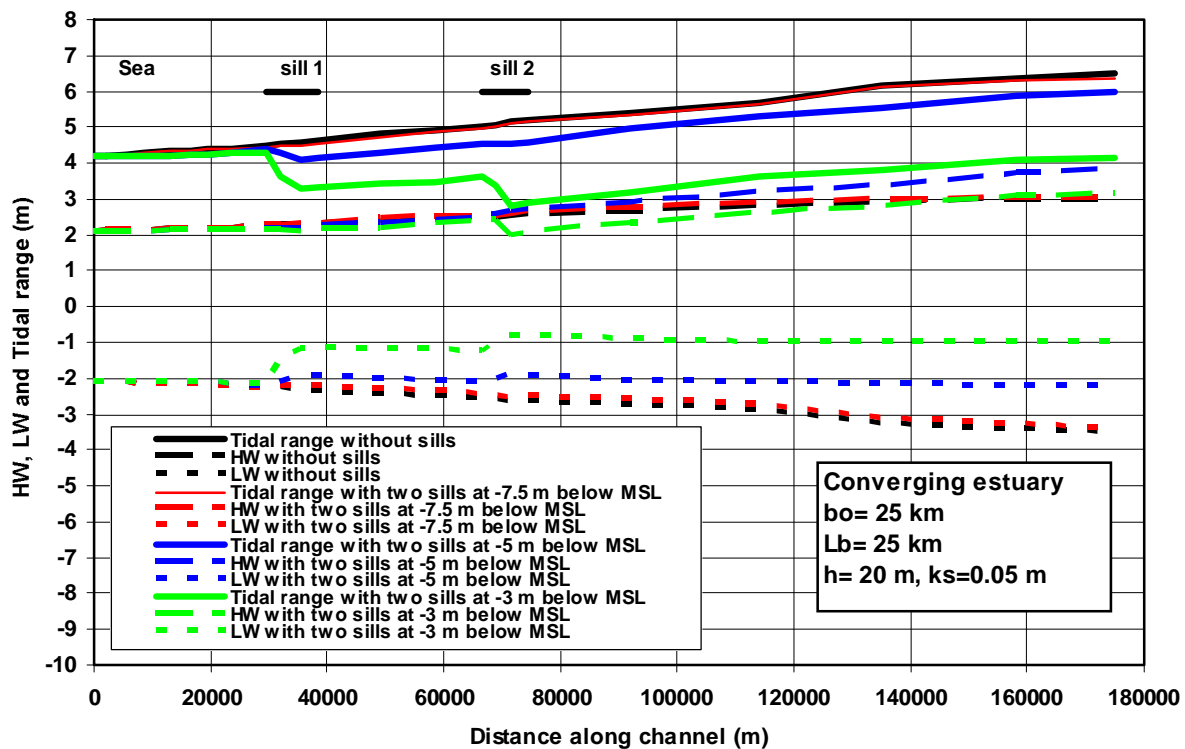


Figure 3.2.16 Effect of abrupt depth changes (short sills) on HW, LW and tidal range along converging estuary; Cases E and F1

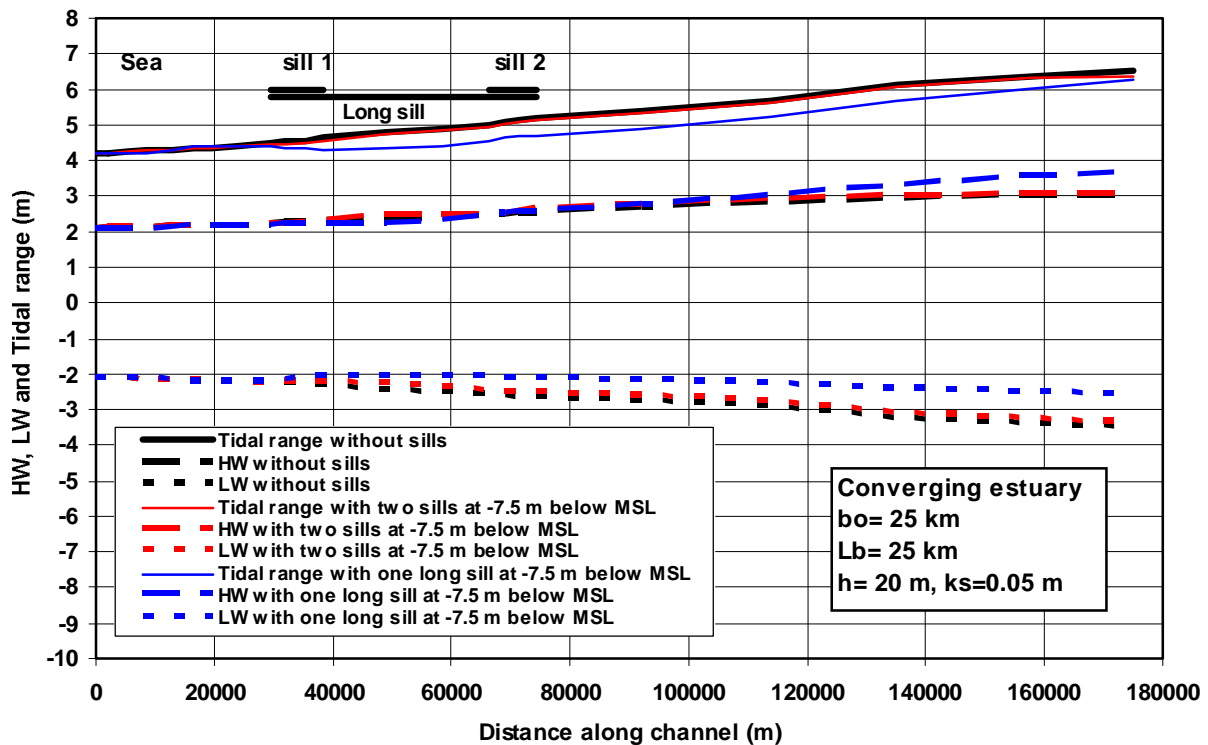


Figure 3.2.17 Effect of abrupt depth changes (short and long sills) on HW, LW and tidal range along converging estuary; Cases E, F1 and H

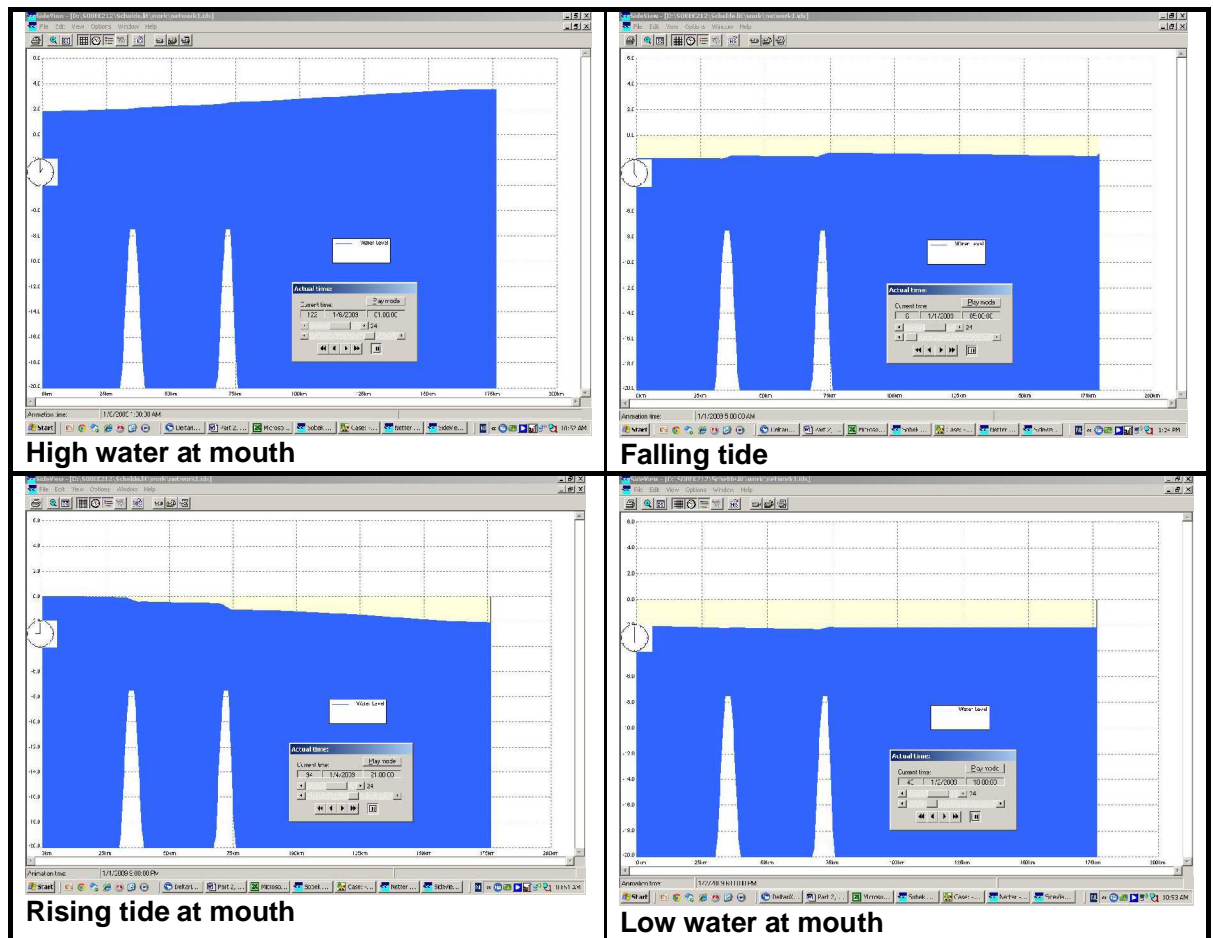


Figure 3.2.18 Water surface profiles along estuary at HW, LW, falling tide and rising tide; two sills with bottom at -7.5 m; original bottom at -20 m; converging estuary; length= 180 km

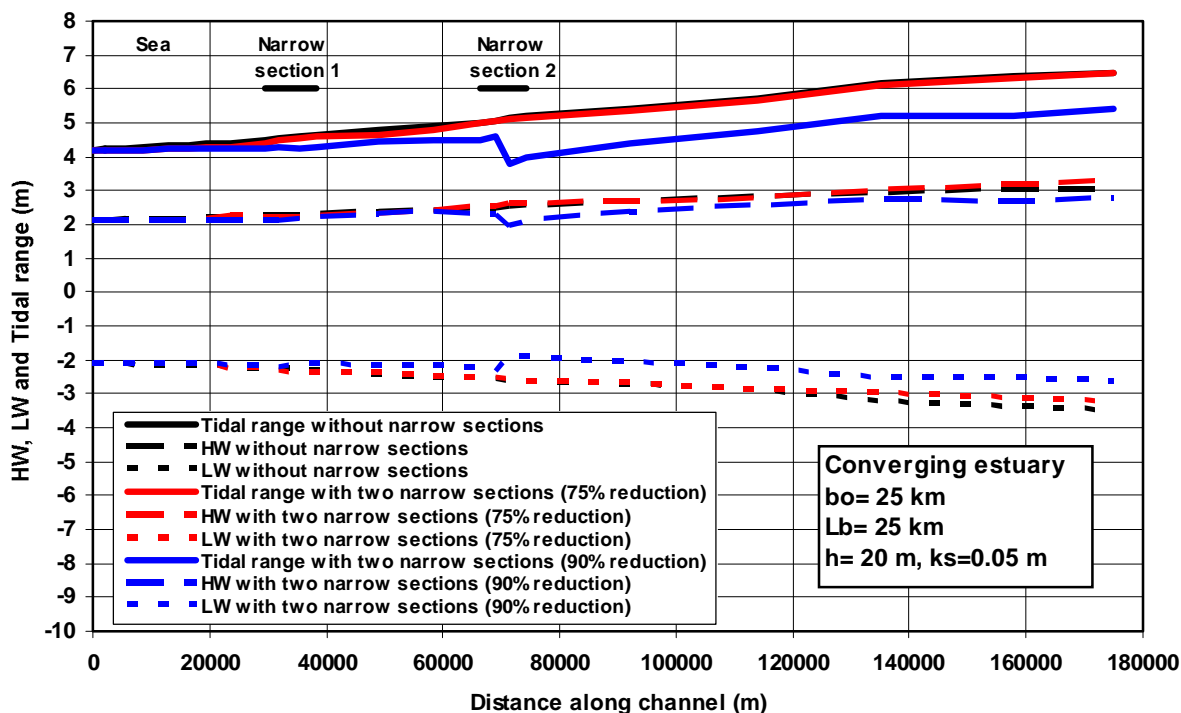


Figure 3.2.19 Effect of abrupt width changes (narrow sections) on HW, LW and tidal range along converging estuary; Cases E and I

Figure 3.2.19 shows the computed HW and LW levels and the tidal range between HW and LW for the situation with and without narrow sections (Case I). In the **absence** of narrow sections the tidal range gradually increases from 4.2 m at the sea (width of 25000 m) to about 6.5 m at the closed land boundary, where the width is very small (20 m). The amplification of the tide is caused by the landward converging width. Some reflection can be observed at the closed end (between 150 and 180 km).

The tidal range and the HW, LW-lines are almost the same if two short narrow sections (with reduction of the width of about 50% and 75%) are present. The narrow sections causing a very abrupt reduction of the width by about 75%, only produce a very slight reduction of the tidal range. The HW and LW lines are shifted up slightly (about 0.1 m).

Increasing the width reduction to 90% leads to a significant decrease of the tidal range (by about 1 m or about 15%) landward of the narrow sections. The HW values are lower and the LW values are higher.

Conclusions related to reduction of abrupt changes of cross-section

Summarizing, it can be concluded that abrupt local changes of the cross-section in a **prismatic** estuary have a significant effect on the tidal range on both sides of the modified cross-section.

Figure 3.2.20 shows the maximum increase (due to reflection effect) of the tidal range on the seaward side as function of the reduction (percentage) of the cross-section in the case of a prismatic estuary.

Figure 3.2.21 shows the maximum decrease of the tidal range on the landward side in the case of a **prismatic** estuary. A 50% reduction of the cross-section yields a 15% to 20% increase/decrease of the tidal range. A 75% reduction of the cross-section yields a 35% to 45% increase/decrease of the tidal range.

In the case of a **converging** estuary the effect of abrupt local changes of the cross-section on the tidal range on both sides of the modified cross-sections is rather insignificant for relatively small changes of the cross-section, see **Figure 3.2.21**. The amplification effect due to the converging planform seems to be dominant over the effects of abrupt changes of the cross-section. Only, very extreme changes (>75%) of the cross-section have a pronounced effect in a **converging** estuary. The reduction of the local depth from 20 m to 7.5 m (local sill; 62.5% reduction of cross-section) yields a very small reduction of the tidal range on the landward side of the sill locations. Similarly, the reduction of the local width by about 75% (local narrows) yields a very slight reduction of the tidal range on the landward side. The increase of the tidal range on the seaward side of the modified cross-section is very marginal (<0.1 m) for all cases studied.

Tidal wave propagation appears to be more sensitive to depth changes (sills) than to width changes (narrows), because the depth affects both the wave speed and the flow resistance. Abrupt depth changes also influence the tidal asymmetry. The tidal curve becomes more peaked with a higher HW and a less low LW.

It is remarked that abrupt changes larger than about 50% are extreme schematizations.

In reality, very abrupt changes of the total cross-sections do not occur.

Figures 2.2.2 and **2.2.3** show a very gradual reduction of the total cross-section. However, the tidal flow system of the Scheldt estuary has local flow constrictions due to the presence of narrow sills. For example, the flood flow from the Honte-channel (cell 1+2) near Vlissingen to the Pas van Terneuzen-channel (see cell 3, **Figure 2.2.1**) is severely constricted by the Borssele sill where the flow area is relatively small (Borssele sill; see **Table 2.2.1**). The tidal flow system with two parallel channels deals with this by creating lateral flows around the sill location (flow diversion) into the less deep Everingen-channel which reduces partial flow reflection effects.

Based on the results of the 1D numerical model runs, it is concluded that local widening and deepening of the navigation channel to Antwerp by dredging will lead to a smaller tidal range on the seaward side and to a larger tidal range on the landward side of the dredging locations. As the increases of the depth and width due to dredging of the navigation channel of the Scheldt estuary are rather small (<10%), the effects on the tidal range will be marginal (<0.1 m).

It is recommended to do 2DH computations focussing on local variation of the width and depth (over a range of conditions from small to large) of the navigation channel to Antwerp.

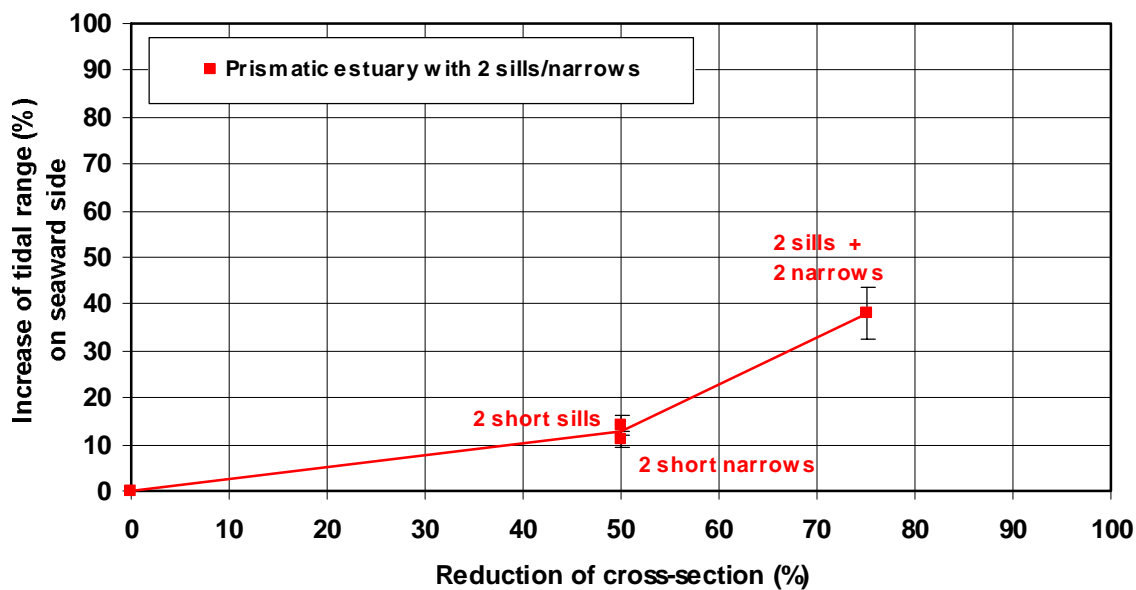


Figure 3.2.20 Increase of tidal range seaward of modified cross-section, prismatic estuary

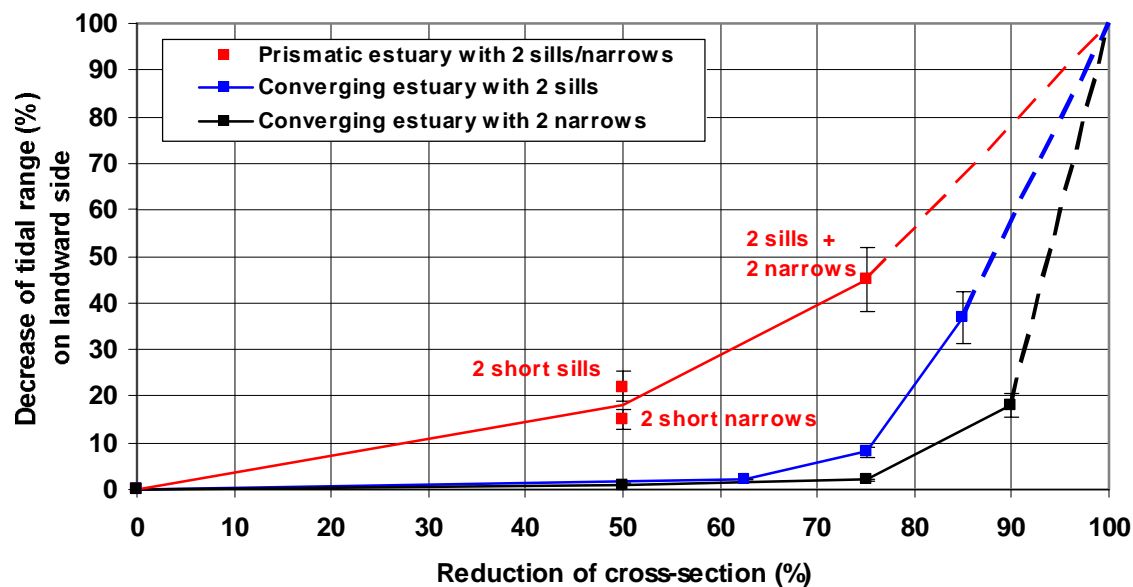


Figure 3.2.21 Decrease of tidal range landward of modified cross-section, prismatic and converging estuary

3.2.5 Effect of tidal flats on tidal range

The analytical models are most valid for a rectangular cross-section. Real tidal channels, however, have a compound cross-section with one or more deeper channels with shallow flats or floods plains in between and along the banks.

The relative importance of the water conveyed through the main channels and above the tidal flats can be obtained from hypsometric curves, which express the horizontal area as a function of depth in a certain channel section (Deltares, 2010). **Figure 3.2.22** shows the hypsometric curve for the section Vlissingen to Bath. The vertical axis shows the depth contour below NAP (about mean sea level, MSL) and the horizontal axis shows the horizontal area at the depth contour. For example, the horizontal area at the -10 m depth contour is $1.1 \cdot 10^8 \text{ m}^2$ between Vlissingen and Bath. The blue area above the curve expresses the total conveyance volume and is about $25 \cdot 10^8 \text{ m}^3$ below NAP. Thus, the total water volume below NAP is about 2500 million m^3 for this section. Given a section length of about 50 km and a mean section width of about 4 km, the mean section depth is about 12.5 m. The total volume above the -2 m depth contour represents the tidal storage volume above the tidal flats (V_{storage}) and is relatively small compared to the total volume in the channels (V_{channel}) below the -2 m NAP depth contour. **Figure 3.2.23** shows the ratio V_{storage} and V_{channel} as a function of time for three channel sections: Vlissingen-Terneuzen, Terneuzen-Hansweert and Hansweert-Bath. The storage volume is about 5% to 15% of the total channel volume and decreases slightly in time between 1955 and 2005. The ratio of V_{storage} and the section length L yields the section-averaged storage width of the cross-section which may be interpreted as an estimate of the width of the tidal flats above the -2 m NAP contour in each section.

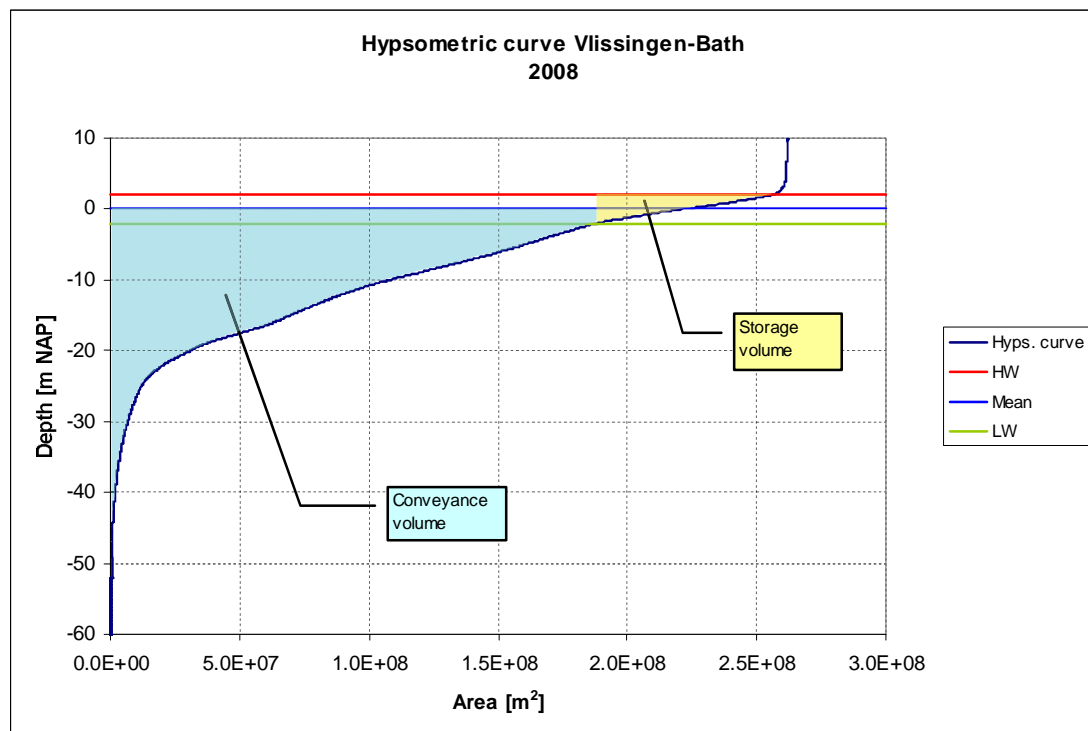


Figure 3.2.22 Hypsometry for the section Vlissingen-Bath in the year 2008 (Deltares, 2010).
 Blue: water volume in channel.
 Yellow: water volume on flats with bounds of $\text{NAP}+2\text{m}$ and $\text{NAP}-2\text{m}$.

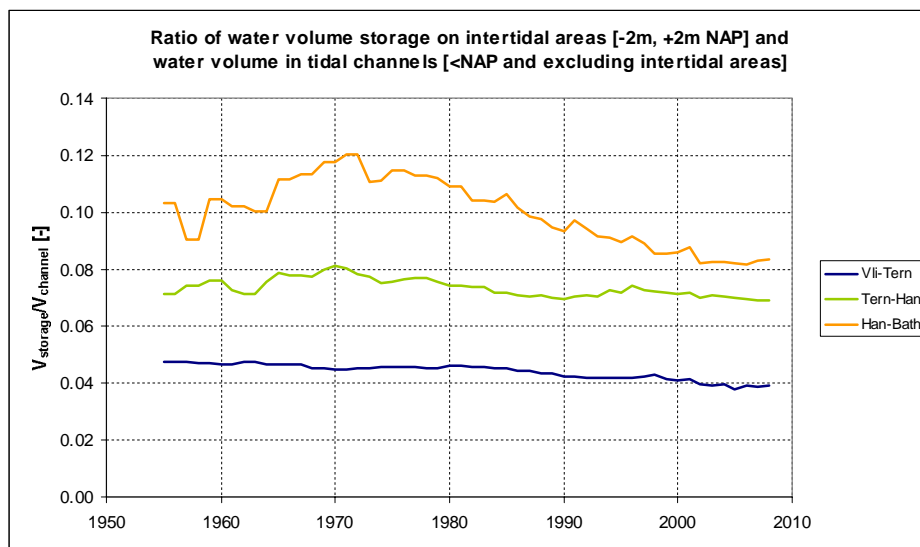


Figure 3.2.23 Ratio of water volume on the intertidal flats and in the channels for the sections Vlissingen-Terneuzen, Terneuzen-Hansweert and Hansweert-Bath

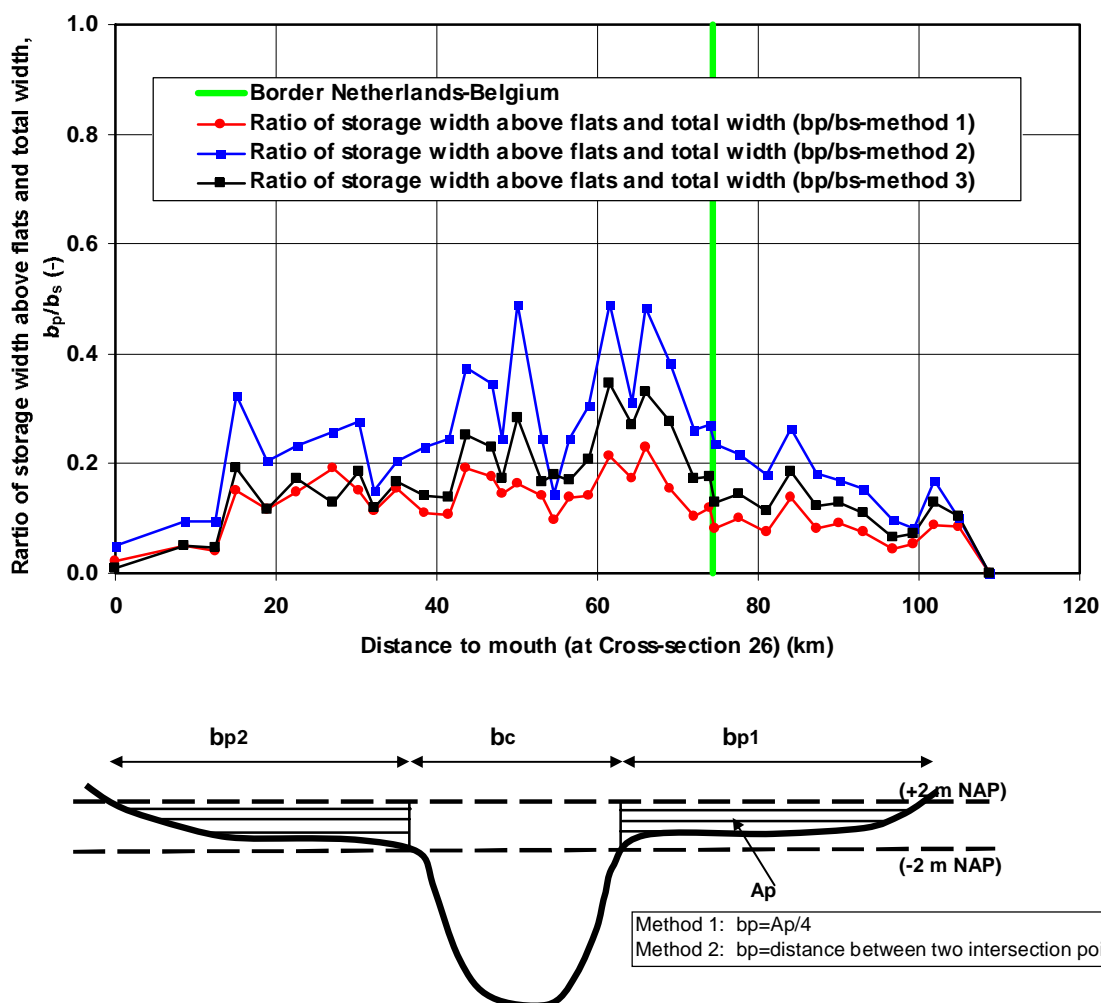


Figure 3.2.24 Ratio of storage width above the intertidal flats and total width; Scheldt estuary.

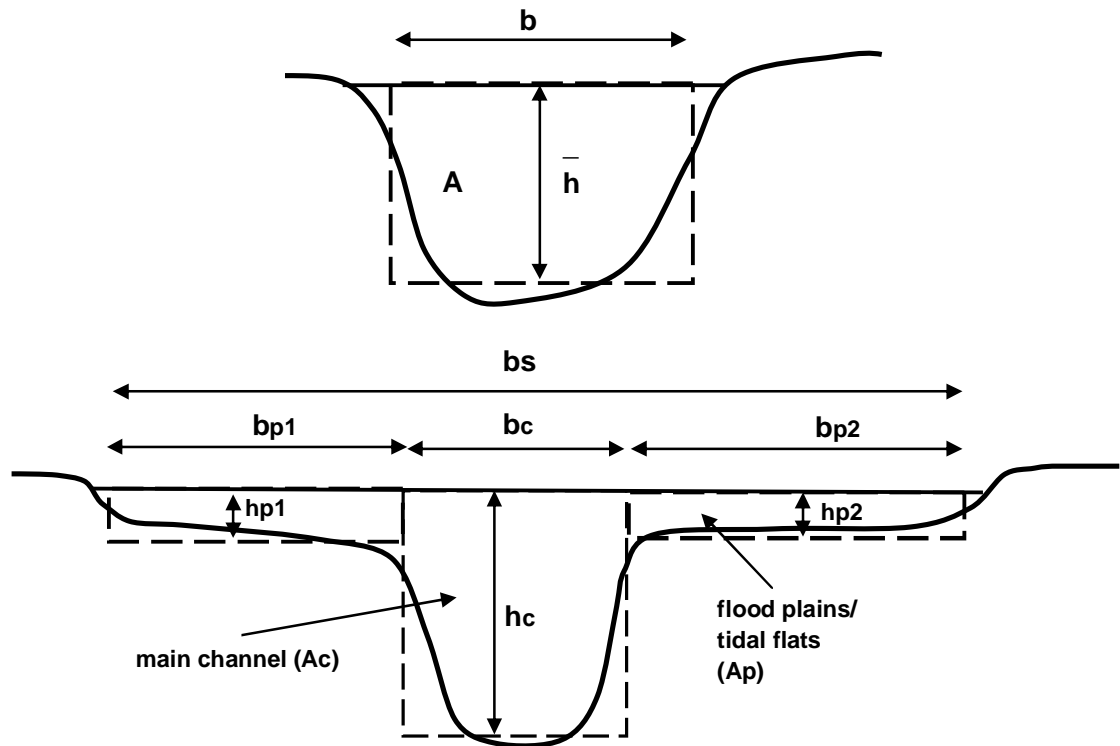


Figure 3.2.25 Regular and compound channels

Figure 3.2.24 shows the ratio storage width above the intertidal flats ($b_p = b_{p1} + b_{p2}$ on both sides of the cross-section) and the total width (b_s) for each cross-section along the Scheldt estuary. The mouth is defined at Cross-section 26, see **Figure A1** of **Appendix A**.

Three methods have been used to determine the storage width above the flats.

Using method 1, the effective storage width (b_p) above the flats is based on the cross-sectional area (A_p) between the +2 m NAP and the surface level of the flats divided by the value of the tidal range (assumed to be 4m). The effective storage width b_p can then be determined as $b_p = A_p / \text{tidal range} = A_p / 4$, see **Figure 3.2.24**. The total width (b_s) is defined as the sum of the channel width (b_c) and the storage width on both sides (b_p).

Using method 2, the storage width above the flats can be determined as the width at +2 m NAP minus the width at -2 m NAP (between intersection points of flats and +2/-2 m NAP lines).

Using method 3, the storage width above the flats is based on the local measured HW and LW values.

Method 3 yields the most realistic values as it is based on the real storage area above the flats between the surface level of the flats and the measured local HW/LW lines. According to method 3, the ratio b_p/b_s is about 5% to 15% in the mouth section (0 to 12 km up to Terneuzen) and varies between 15% and 35% in the section Terneuzen to Bath, where tidal flats and tidal shoals are quite common. The ratio b_p/b_s reduces to almost zero in the river section in Belgium. Method 2 yields much larger values up to 50% in the section near Bath. Averaging along the estuary, the storage width is about 20% of the total width.

Based on these results, it is concluded that the maximum effective storage width related to tidal flats and shoals is not more than about 35% of the total width along the Scheldt estuary and the averaged value along the estuary is about 20%.

To evaluate the effect of the cross-section on the computed water levels, various computations have been made for a compound cross-section consisting of one main channel and tidal flood plains (**Figure 3.2.25**) using the linearized analytical model. The analytical model has been applied to an exponentially converging compound channel with open end (length of 180 km, width at mouth of 25000 m and depth of 10 m, $k_s = 0.05$ m). The effect of the cross-section is taken into account by using the hydraulic radius in the friction term. Two methods have been used to compute the wave speed c_o : based on the hydraulic radius ($R = A/b_s$) and based on the effective wave propagation depth ($h_{eff} = h_c b_c/b_o$). The results are compared to those for a converging channel with a rectangular cross-section.

The compound cross-section is assumed to consist of one main channel and tidal flats; $b_{c,o} = 10000$ m, $b_{p,o} = 15000$ m and $h_{flats} = 3$ m, $b_{s,o} = 25000$ m (see **Figure 3.2.25**).

The depth of the main channel (compound cross-section) is $h_c = h_o$.
The width of the main channel is b_c . The total surface width is b_s .

A compound cross-section with $h_c = h_o = 20$ m, $h_{flat} = 3$ m, $b_s = 25000$ m, $b_c = 10000$ m, $b_p = 15000$ m ($A = 245000$ m²) has a hydraulic radius $R \cong 9.8$ m.

Using this approach, the compound cross-section can be replaced by a rectangular cross-section with $h = 9.8$ m and $b = 25000$ m ($A = 245000$ m²) to give the same tidal range along the channel.

Another approach is to use $h_{eff} = (b_{c,o}/b_{s,o})h_o = 8$ m as the wave propagation depth. This will result in a smaller wave speed $c_o = (g h_{eff})^{0.5}$ and smaller tidal range values.

The width of the cross-section at the mouth is $b_{s,o} = 25000$ m.

The total width of the tidal flats is 15000 m at the mouth (60% of the total width), which is an extreme situation and does not really apply to the Scheldt estuary, see **Figure 3.2.24**. The maximum ratio of the width of the tidal flats and total width is about 35% along the Scheldt estuary and the averaged value along the estuary is about 20%.

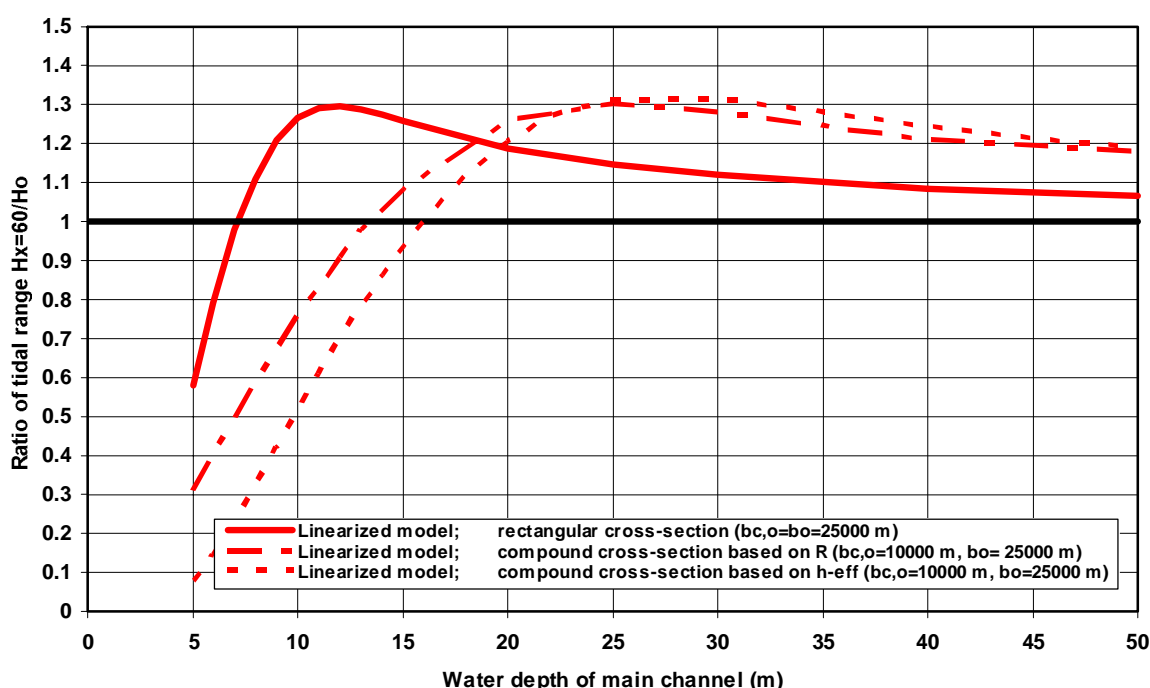


Figure 3.2.26 Ratio $H_{x=60\text{km}}/H_o$ for a converging channel with open end; effect of cross-section (width of tidal flats is 60% of total width)

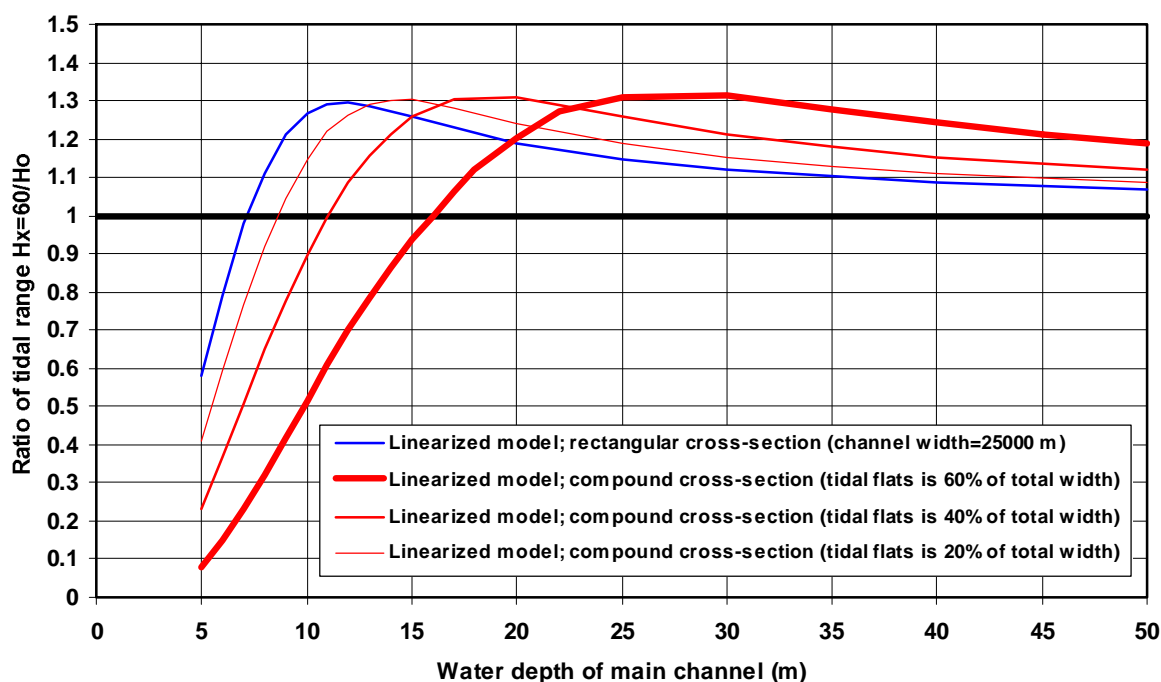


Figure 3.2.27 Ratio $H_{x=60\text{km}}/H_o$ for a converging channel with open end; effect of cross-section for different contributions of tidal flats

Figure 3.2.26 shows the effect of the cross-section on the ratio $H_{x=60\text{km}}/H_o$ based on the analytical model. The analytical results of the linearized model show that significant amplification only occurs in a compound channel when the depth of the main channel is relatively large ($h_o > 15$ m).

For example, a *compound* cross-section with a channel depth of 20 m and an effective depth of 9.8 m (equal to hydraulic radius) has an analytical amplification factor of 1.25 (see **Figure 3.2.26**), which is exactly equal to that of a *rectangular* cross-section with a depth of 9.8 m. This value (amplification= 1.25) is somewhat larger than that (amplification= 1.18) of a rectangular channel with a depth of 20 m. If the main channel depth is larger than about 25 m, the amplification factor based on the analytical results gradually decreases.

It is noted that the representation of a compound channel by using the concept of hydraulic radius to represent the frictional depth and the wave propagation depth is questionable. Based on this concept, the bed-shear stress is distributed evenly along the wet perimeter of the cross-section.

Figure 3.2.27 shows the effect of the tidal flats on the ratio $H_{x=60\text{km}}/H_0$ based on the linearized model for a compound cross-section of a converging tidal channel. The width of the tidal flats at the mouth is varied between 15000 m and 0 m. The latter case refers to a rectangular cross-section. The effect is largest for a relatively large contribution of the tidal flats (60%). The effect is relatively small for a small contribution of the tidal flats (20%).

Figure 3.2.27 clearly shows that the effect of the tidal flats depends on the depth of the main channel and the relative width of the tidal flats (20%, 40% and 60%). Focussing on the Scheldt estuary (thin red curve: tidal flats smaller than about 20% of total width and a main channel depth in the range of 10 to 15 m), the amplification factor defined as H_{60}/H_0 reduces from about 1.25 to 1.15 for a compound channel with depth of 10 m (compared with a prismatic channel) and the amplification factor increases from 1.25 to 1.3 for a compound channel with a depth of 15 m (compared with a prismatic channel). The effects are larger for wider tidal flats (40% and 60%). Thus, for depths in the range of 10 to 12 m, the amplification effect can be reduced by increasing the width of the tidal flats significantly.

It is noted that the assumption of tidal flats with a total width of 15000 m at the mouth (60% of total width at mouth and at all other sections of the analytical model) is an extreme case which does not apply to the Scheldt estuary, where the maximum contribution of the tidal flats is not more than about 35% and the averaged value along the estuary is about 20% (see **Figure 3.2.24**).

Overall, it can be concluded that the effect of the tidal flats on the amplification of the tidal range is found to be marginal for the Scheldt estuary and thus the cross-section can be reasonably well represented by a rectangular cross-section.

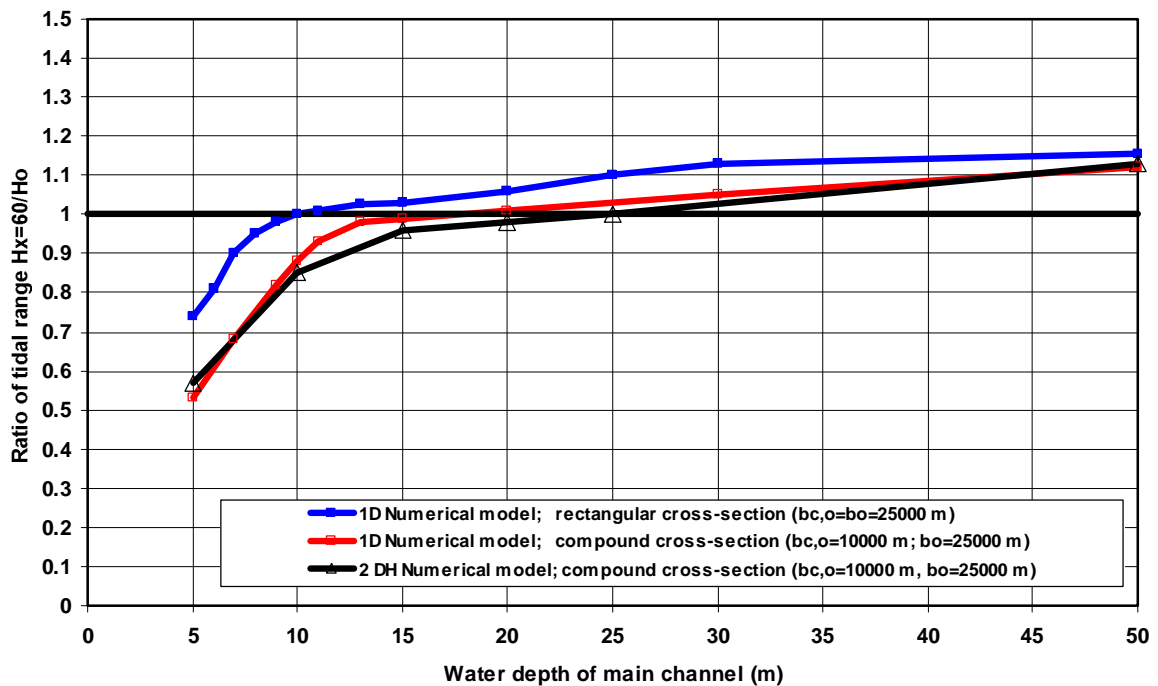


Figure 3.2.28 Ratio $H_{x=60\text{km}}/H_o$ for a converging-prismatic channel; effect of cross-section (width of tidal flats is 60% of total width)

Figure 3.2.28 shows the results of numerical models (1D and 2DH) for a converging-prismatic channel (exponentially converging channel with length of 60 km; prismatic channel with length of 120 km; total length of 180 km; width at mouth of 25000 m; width at 60 km of 2000 m and width at end 180 km of 2000 m; channel depth of 10 m; bed roughness of 0.05 m; closed end). The compound cross-section is assumed to consist of one main channel and tidal flats; $b_{c,o}=10000$ m (channel width at mouth), $b_{p,o}=15000$ m (width of flats at mouth) and $h_{\text{flats}}=3$ m, $b_{s,o}=25000$ m (surface width at mouth). The depth of the main channel (compound cross-section) is $h_c=h_o$. The width of the flats is 60% of the total width.

As reflection generated at the closed end of the prismatic section is involved, the tidal range (H_{60}) has been estimated from the computed water levels at $x=45$ km and $x=60$ km to minimize the contribution of reflection.

The numerical model results show tidal damping for water depths smaller than about 10 m, both for a rectangular and a compound cross-section. The tidal damping is largest for a compound channel. The differences are largest for smaller depths. The numerical model results only show slight amplification for larger water depths (maximum 1.15). The maximum amplification effect in a converging-prismatic channel is somewhat smaller than in a fully converging channel (compare **Figures 3.2.28** and **3.2.26**). The results of the 1D and 2DH numerical models show, however, reasonably good agreement for a channel with a compound cross-section, which puts some confidence on the more simple 1D concepts.

3.2.6 Effect of tidal storage on tidal range

To evaluate the effect of a local tidal storage variation on the computed tidal range values, various computations (using numerical model for compound cross-section only) have been made for a converging-prismatic channel (exponentially converging channel with length of 60 km; prismatic channel with length of 120 km; total length of 180 km; width at mouth of 25000 m;

width at 60 km of 2000 m and width at end 180 km of 2000 m; main channel depth of 10 m; bed roughness of 0.05 m; closed end). The width of the tidal flats has been increased/decreased over a length of about 5 km between $x=20$ and $x=25$ km from the mouth. This simulates a local variation of the storage (local inundation) by increasing/decreasing the local surface area and hence the local storage volume (storage volume is surface area times tidal range). Three runs have been made: decrease of the surface area of about 15 km^2 and an increase of 30 km^2 and 90 km^2 between $x=20$ and $x=25$ km. The total surface area of the converging tidal channel between the mouth (Westkapelle) and the end of the Scheldt estuary (Bath) is about 450 km^2 .

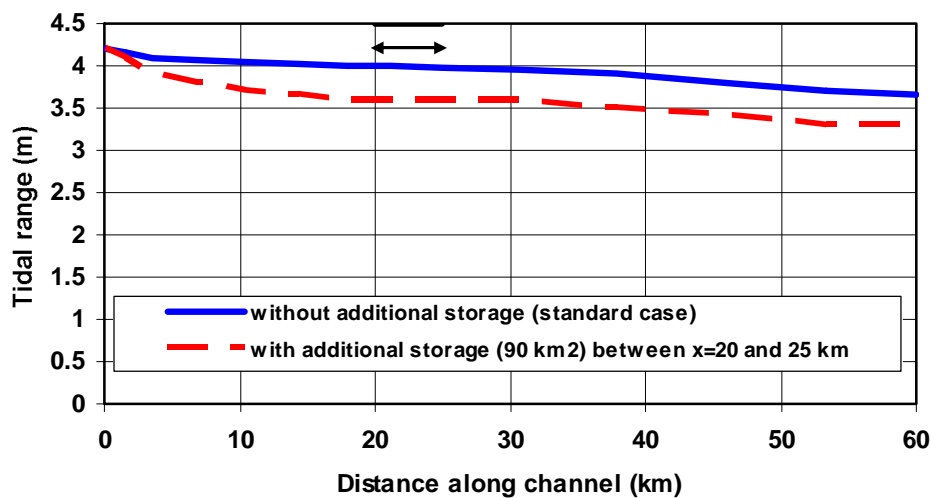


Figure 3.2.29 Tidal range values along converging-prismatic channel (1D numerical model); effect of larger tidal storage

A reduction of the surface area by about 15 km^2 (3%) results in computed tidal range values, which are slightly larger (within 0.05 m). An increase of the surface area leads to smaller tidal range values by about 0.1 m for an increase of 30 km^2 (7%) and by about 0.3 to 0.4 m for an increase of about 90 km^2 (20%), see **Figure 3.2.29**. The effect seems to be weakly non-linear; increasing the storage area by a factor 3 (from 30 to 90 km^2) leads to a decrease of the tidal range from order 0.1 m to about 0.4 m (factor 4). Additional numerical computations are required to reveal this effect more clearly. Furthermore, it is interesting to study the storage volume effects of smaller but higher tidal flats and wider but lower tidal flats (in relative sense) on the tidal range in the Scheldt estuary.

4 Scale analysis and relative importance of basic tidal processes

4.1 Introduction

This section focusses on the relative importance of the terms of the equations of continuity and momentum of the linearized analytical model for a converging tidal channel as applied to the Scheldt estuary. Furthermore, the numerical model (DELFT2DH-model) results of water levels and depth-averaged velocities in the Scheldt estuary are analyzed to estimate the contribution of the slope term and the frictional term in various channel sections.

4.2 Analytical model for exponential planform

4.2.1 Basic equations

The momentum equation of the analytical model reads as (Van Rijn, 2011a,b,c):

$$\frac{\partial \bar{u}}{\partial t} + \frac{g}{\partial x} \frac{\partial \eta}{\partial x} + m \bar{u} = 0 \quad (4.1)$$

with: η = water surface level to MSL, \bar{u} = cross-section-averaged velocity, $m = nA = n b h_o = (8g |\hat{u}|)/(3\pi C^2 R) \cong (8g |\hat{u}|)/(3\pi C^2 h_o) = \text{Lorentz-friction parameter (unit 1/s)}$, \hat{u} = characteristic peak velocity (average value over traject), A = cross-section area, b = width, h_o = water depth to MSL, C = Chézy = coefficient, R = hydraulic radius, x = longitudinal coordinate (negative in landward direction; flood velocity in landward direction is negative).

The convective acceleration ($\bar{u} \partial \bar{u} / \partial x$) being an order of magnitude less, has been neglected.

The detailed solution for a channel of infinite length (Van Rijn, 2011a,b,c):

$$\eta = \hat{\eta}_o e^{(-0.5\beta + \mu)x} \cos(\omega t + kx) \quad (4.2)$$

$$\hat{\eta}_o = -h_o \hat{u}_o (k/\omega)(1/\cos\varphi) \quad (4.3)$$

$$\bar{u} = \hat{u}_o e^{(-0.5\beta + \mu)x} \cos(\omega t + kx + \varphi) \quad (4.4)$$

$$\hat{u}_o = -(\hat{\eta}_o/h_o)(c) \cos\varphi \quad (4.5)$$

$$c = \omega/k$$

$$\mu = \text{friction parameter (Van Rijn, 2011)}$$

$$k = \text{wave number (Van Rijn, 2011)}$$

$$\varphi = \text{phase lead of velocity to water surface level (Van Rijn, 2011)}$$

The three force terms (with unit m/s^2) of the momentum equation can be determined analytically, yielding:

$$\text{Inertial term:} \quad \partial \bar{u} / \partial t = -\omega \hat{u}_0 [e^{(-0.5\beta+\mu)x}] \sin(\omega t+kx+\varphi) \quad (4.6)$$

$$\text{Surface slope term:} \quad g \partial \eta / \partial x = g \hat{\eta}_0 [e^{(-0.5\beta+\mu)x}] [(-0.5\beta+\mu) \cos(\omega t+kx) - k \sin(\omega t+kx)] \quad (4.7)$$

$$\text{Frictional term:} \quad m \bar{u} = m \hat{u}_0 e^{(-0.5\beta+\mu)x} \cos(\omega t+kx+\varphi) \quad (4.8)$$

Analysis of these force terms shows (see also **Figures 4.2.2 to 4.2.5**):

- At slack tide ($\bar{u} \cong 0$): inertial force opposes the surface slope force.
- At maximum flow ($\bar{u} \cong \hat{u}_0$ and $\partial \bar{u} / \partial t \cong 0$): frictional force opposes the surface slope force.
- At horizontal water surface just before HW ($\partial \eta / \partial x \cong 0$): inertial force opposes frictional force.

During most of the rising tide, the slope force is slightly larger (in absolute sense) than the frictional force and thus the flow is accelerated. The surface slope term is maximum just before maximum flow.

During most of the falling tide, the slope force is slightly smaller than the frictional force and the flow is decelerated.

4.2.2 Analytical model results

The analytical model has been applied to two converging channels with an exponential planform and the following characteristics representing the planform of the Scheldt estuary:

- length= 180 km, $\beta = 1/L_b = 0.00004$
- width at mouth $b_0 = 25$ km,
- converging length scale $L_b = 25$ km,
- depth h_0 to MSL= 10 m and 5 m,
- bed roughness $k_s = 0.05$ m,
- tidal amplitude at mouth $\hat{\eta}_0 = 2.1$ m and tidal period $T = 43200$ s= 12 hours,
- no river inflow $Q_r = 0$ m³/s (open boundary without river inflow).

Convergence effect

The convergence effect of the exponential planform is expressed by the coefficient $(\mu-0.5\beta)$, see Equation 4.2. The μ -parameter expresses the frictional damping effect and the β -parameter expresses the amplifying convergence effect of the exponential planform $b = b_0 e^{\beta x}$ with b = width, b_0 = width at mouth, $\beta = 1/L_b$ = convergence coefficient, L_b = convergence length scale, x = longitudinal coordinate (negative in landward direction).

Figure 4.2.1 shows the coefficient $(\mu-0.5\beta)$ as function of the water depth for the geometry of the Scheldt estuary with $\beta = 0.00004$.

If friction dominates, then $\mu > 0.5\beta$ and the tide will be damped,

If convergence dominates, then $\mu < 0.5\beta$ and the tide will be amplified.

If the water depth is very large the μ -value will approach to 0.5β and thus $(\mu-0.5\beta) \rightarrow 0$, which means that the tidal range will become constant and equal to the tidal range at the mouth.

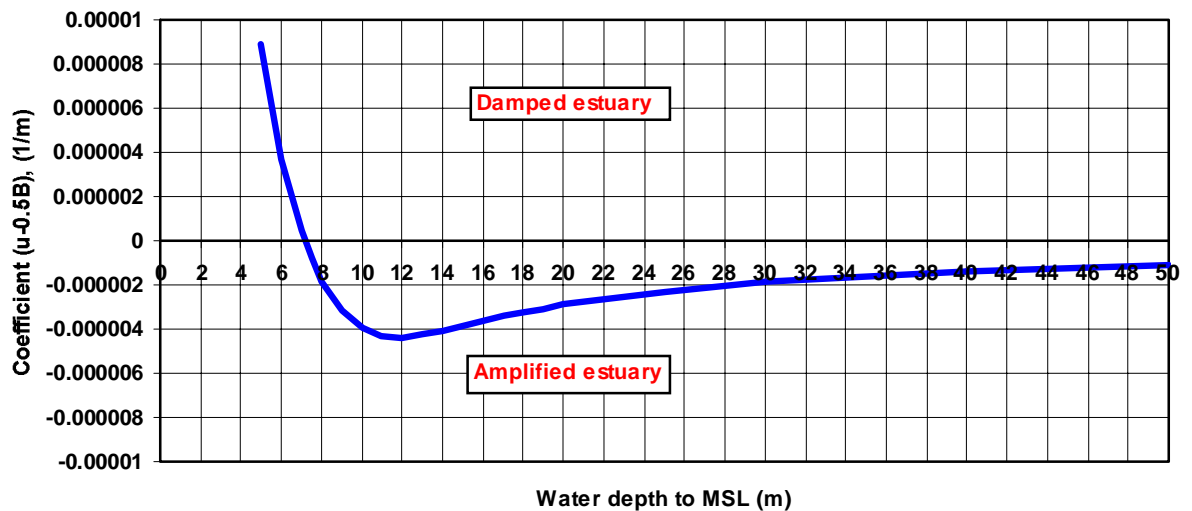


Figure 4.2.1 *Damping-amplification coefficient as function of water depth*

Force terms

Figures 4.2.2 to 4.2.5 show the three force terms of the momentum equation at the mouth $x=0$, at $x= 90$ km and at $x= 120$ km for a depth of $h_0= 5$ m (damped tidal range) and 10 m (amplified tidal range).

The basic parameters and results are presented in **Table 4.2.1**.

The surface slope term and the frictional term always have opposing values. The maximum values of the slope term and the frictional terms are much larger in a damped estuary than in an amplified estuary. The maximum value of the inertial term is much smaller than the other terms in a damped estuary and slightly smaller in an amplified estuary.

The water surface slope is maximum just before maximum flow (velocity lags behind).

The inertial term is maximum around slack tide; the inertial term is minimum around maximum flow, when the surface slope term and the frictional term are dominant.

The force terms of the momentum equations have very similar values (in range of 0.0001 to 0.0003 m/s^2) in the middle of the estuary ($x= 90$ km) for both cases, (damped and amplified) although the local tidal range and peak velocity values are quite different.

Model results for larger depth values of 10 m (amplified cases) show smaller values of the three terms of the momentum equation than for a depth of 5 m (damped cases).

Table 4.2.1 Characteristic data of analytical model for **converging** estuary
(depth of 5 and 10 m)

Depth	Parameters	Location	Remarks
$h_0 = 5$ m	$\hat{u}_0 = 1.07$ m/s $\varphi = 1.96$ hours $m = 0.000581$ m/s $k = 2.96 \cdot 10^{-5}$ $\mu = 2.91 \cdot 10^{-5}$ $c = 4.91$ m/s $c_0 = 7.0$ m/s	$x = 0$ km	maximum values of slope term is about 0.0006 m/s^2 maximum values of frictional term is about 0.0006 m/s^2 maximum value of inertial term is about 0.0002 m/s^2
$h_0 = 5$ m	$\hat{\eta} = 0.47$ m $\hat{u} = 0.47$ m/s	$x = 90$ km	maximum values of slope term is about 0.0003 m/s^2 maximum values of frictional term is about 0.0003 m/s^2 maximum value of inertial term is about 0.00008 m/s^2
$h_0 = 10$ m	$\hat{u}_0 = 0.82$ m/s $\varphi = 2.56$ hours $m = 0.000185$ m/s $k = 0.853 \cdot 10^{-5}$ $\mu = 1.60 \cdot 10^{-5}$ $c = 17.04$ m/s $c_0 = 9.9$ m/s	$x = 0$ km	maximum values of slope term is about 0.0002 m/s^2 maximum values of frictional term is about 0.0002 m/s^2 maximum value of inertial term is about 0.0001 m/s^2
$h_0 = 10$ m	$\hat{\eta} = 3.0$ m $\hat{u} = 1.18$ m/s	$x = 90$ km	maximum values of slope term is about 0.0003 m/s^2 maximum values of frictional term is about 0.0003 m/s^2 maximum value of inertial term is about 0.00015 m/s^2

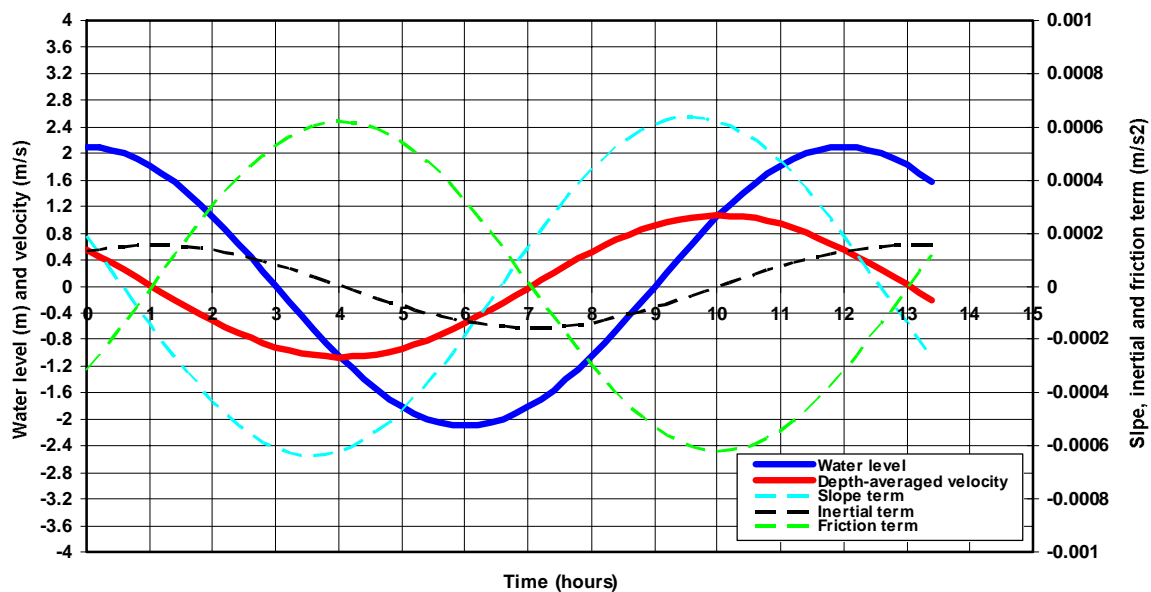


Figure 4.2.2 Water surface and depth-averaged velocity and three force terms of momentum equation over tidal cycle at $x = 0$ km (mouth), depth = 5 m

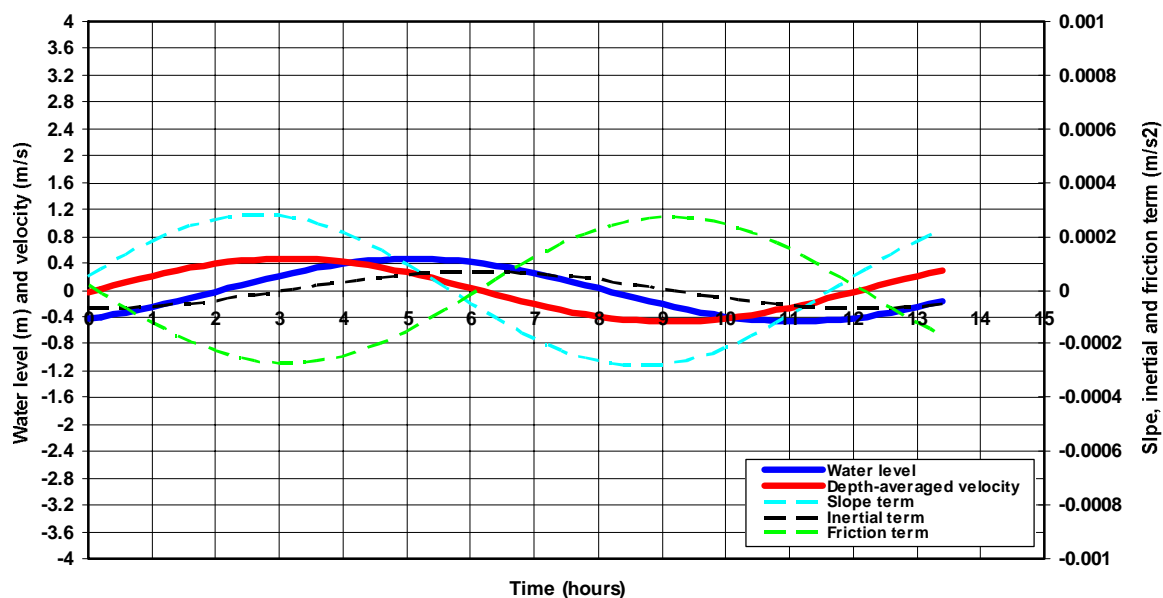


Figure 4.2.3 Water surface and depth-averaged velocity and three force terms of momentum equation over tidal cycle at $x=90$ km (mid-channel); depth = 5 m

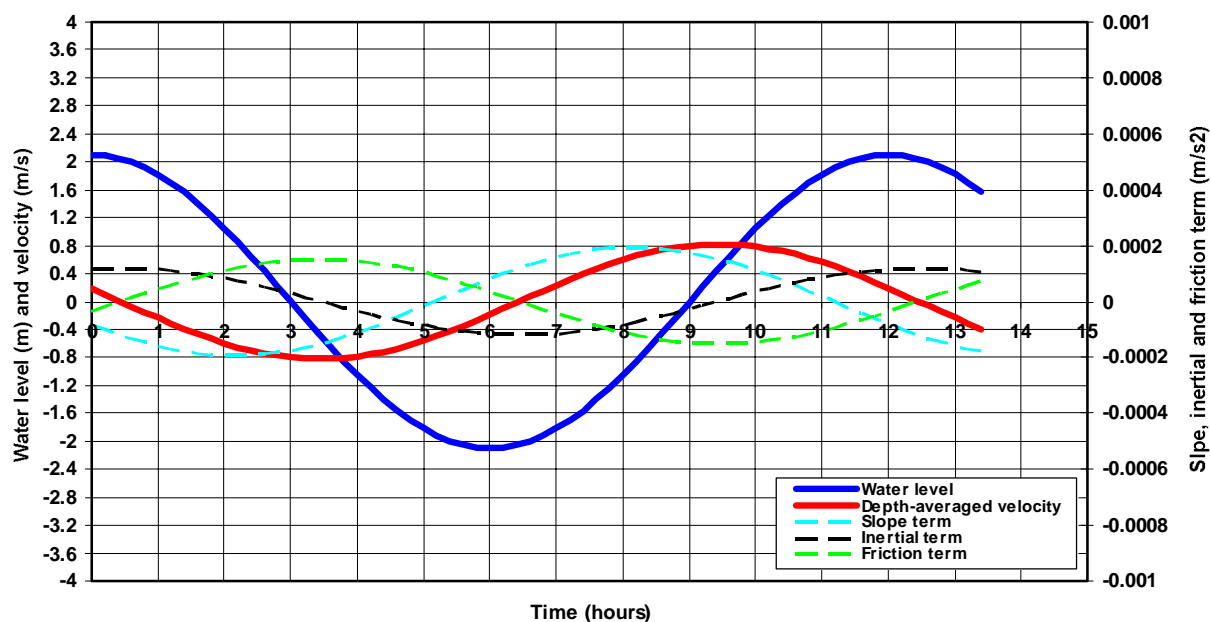


Figure 4.2.4 Water surface and depth-averaged velocity and three force terms of momentum equation over tidal cycle at $x=0$ km (mouth); depth = 10 m

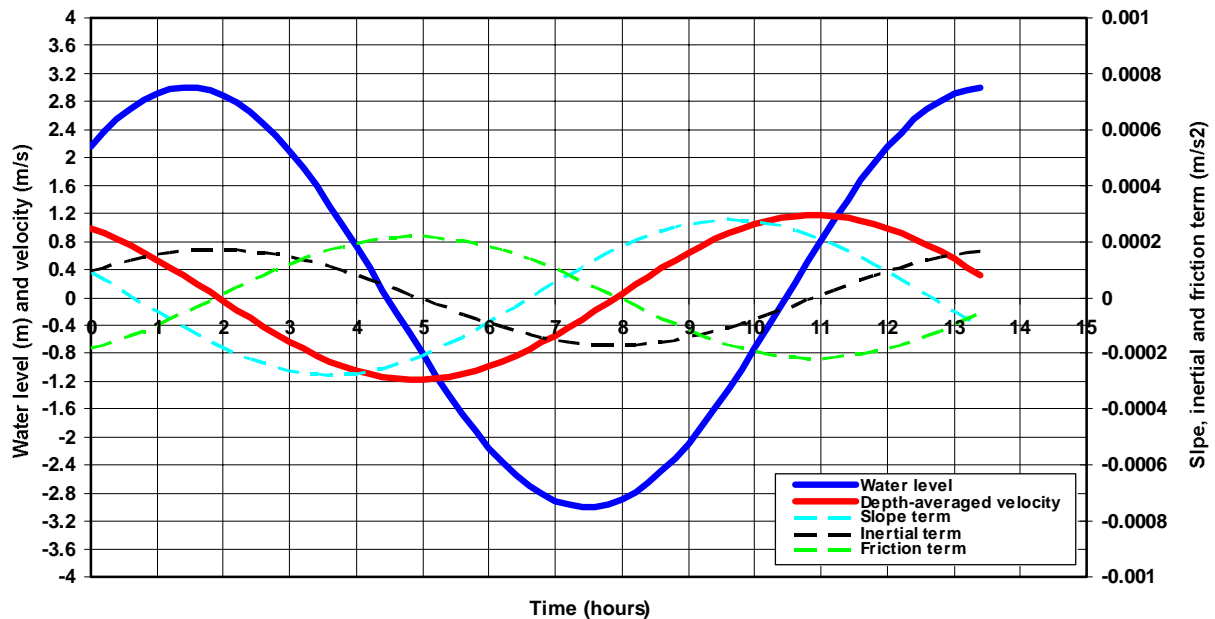


Figure 4.2.5 Water surface and depth-averaged velocity and three force terms of momentum equation over tidal cycle at $x = 90$ km (mid-channel); depth = 10 m

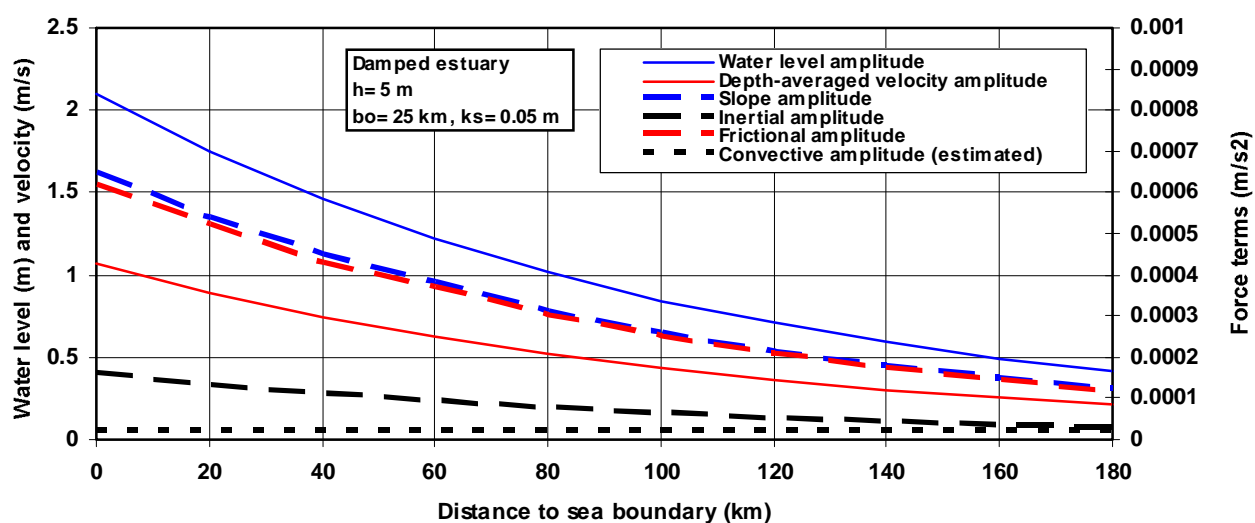
Figures 4.2.6 and **4.2.7** and **Table 4.2.2** show the peak values of the force terms of the momentum equation along the estuary. The peak values of the water level and velocity are also shown. The slope force term always is the dominant (driving) force of the tidal system. The frictional force term is slightly smaller. It is noted that the peak values occur at different times within the tidal cycle. The peak values of the slope and frictional terms occur around maximum flow when the inertial term is almost zero. The peak values of the inertial term occurs at slack tide (zero velocity). The sum of the three terms is approximately zero. In a damped estuary where friction dominates (depth $h = 5$ m), the slope and frictional terms are gradually decreasing. The inertial force term is significantly smaller in a damped estuary. In an amplified estuary where the funnelling effect dominates (depth $h = 10$ m), the slope and frictional terms are gradually increasing. The inertial force term is less important than the other terms, but its contribution is larger than in a damped estuary.

The model results can also be used to estimate the relative importance of the convective acceleration term ($\bar{u} \partial \bar{u} / \partial x$), which is not accounted for by the analytical model. In the mouth of the estuary the velocity \bar{u} is of the order of 1 m/s and the velocity gradient $\partial \bar{u} / \partial x$ is of the order of 0.1 to 0.2 m/s per 10 km resulting in $\bar{u} \partial \bar{u} / \partial x \approx 0.00001$ to 0.00002 m/s², which is much smaller than the other three terms in the mouth of the estuary up to $x = 90$ km, see **Figures 4.2.6** and **4.2.7** and **Table 4.2.1**. Thus, it is correct to neglect this term in the mouth of the estuary.

The convective term cannot be neglected in the landward end of the estuary when the depth is small (order of 5 m). In that case the inertial term reduces to about 0.00003 m/s² (see **Table 4.2.2**), which is comparable to the convective acceleration term. The slope term and the frictional term remain much larger than the convective acceleration term in a shallow estuary. Hence, maximum flow is mainly affected by the water surface slope and bottom friction.

Table 4.2.2 Model results of force terms for converging estuary; depth of 5 and 10 m

x (km)	h = 5m					h = 10 m				
	Tidal ampl. (m)	Peak vel. (m/s)	Slope term (m/s ²)	Inert. term (m/s ²)	Frict. term (m/s ²)	Tidal ampl. (m)	Peak vel. (m/s)	Slope term (m/s ²)	Inert. term (m/s ²)	Frict. term (m/s ²)
0	2.10	1.07	0.00065	0.00016	0.00062	2.10	0.82	0.000194	0.000119	0.000151
20	1.75	0.89	0.00054	0.00013	0.00052	2.27	0.89	0.000210	0.00013	0.000165
40	1.46	0.74	0.00045	0.00011	0.00043	2.46	0.96	0.000226	0.00014	0.000177
60	1.22	0.62	0.00038	0.000092	0.00037	2.67	1.05	0.000245	0.000153	0.000194
80	1.02	0.52	0.00031	0.000075	0.00030	2.88	1.13	0.000266	0.000164	0.000208
100	0.84	0.43	0.00026	0.000065	0.00025	3.12	1.22	0.000289	0.000177	0.000224
120	0.71	0.36	0.00021	0.000052	0.000207	3.38	1.33	0.000311	0.000193	0.000245
140	0.59	0.30	0.000179	0.000043	0.000174	3.65	1.43	0.000337	0.000207	0.000264
160	0.49	0.25	0.000148	0.000034	0.000145	3.96	1.55	0.000363	0.000225	0.000286
180	0.41	0.21	0.000125	0.000029	0.000116	4.28	1.68	0.000394	0.000244	0.000310

**Figure 4.2.6** Amplitude values of water level, depth-averaged velocity, slope term, inertial term and frictional term, depth= 5 m

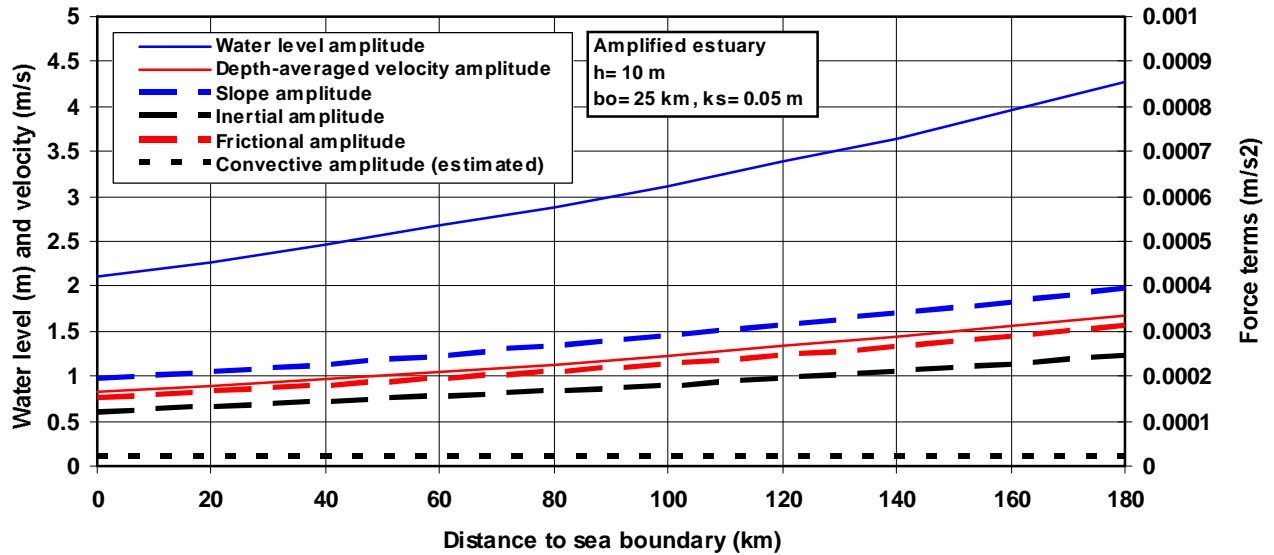


Figure 4.2.7 Amplitude values of water level, depth-averaged velocity, slope term, inertial term and frictional term, depth= 10 m

4.3 Numerical model results

For reasons of simplicity and clarity, the attention here is focussed on the one-dimensional equations for homogeneous flow.

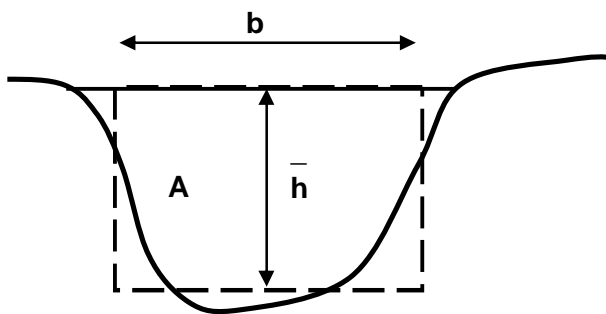


Figure 4.3.1 Channel cross-section

The equations of continuity (mass balance) and motion (momentum balance) for a regular cross-section (Figure 4.3.1) are:

$$\text{continuity: } \frac{b_s \partial \bar{h}}{\partial t} + \frac{\partial Q}{\partial x} = 0 \quad \text{or} \quad \frac{\partial A}{\partial t} + \frac{\partial Q}{\partial x} = 0 \quad (4.9)$$

$$\text{motion: } \frac{\partial Q}{\partial t} + \frac{\partial(\alpha Q^2/A)}{\partial x} + \frac{g A \partial z_s}{\partial x} + \frac{g Q |Q|}{C^2 A R} - \frac{\sum F_x}{\rho R} = 0 \quad (4.10)$$

in which:

b_s = surface width of cross-section (constant in time; $b_s = b$ for rectangular cross-section),

\bar{h} = water depth averaged over the width of the cross-section ($= A/b_s$),

Q = discharge ($= A \bar{u}$),

A = area of cross-section ($= b_s \bar{h}$),

R = hydraulic radius ($= A/O$),

O = wet surface,

C = Chézy-coefficient ($= 18 \log(12h/k_s)$),

\bar{u} = cross-section averaged flow velocity,

z_b = bottom level above a horizontal datum ($l_b = -dz_b/dx$),

z_s = water surface level above a horizontal datum ($= \bar{h} + z_b$),

z_b = bottom level above a horizontal datum ($l_b = -dz_b/dx$),

α = coefficient ($\cong 1$),

F_x = external Force (N) in x-direction (wind force, etc.),

ρ = depth-averaged fluid density,

x = horizontal coordinate,

t = time,

g = acceleration of gravity.

The dimension of the terms of the momentum equation is m^3/s^2 .

In the case of a wide channel ($b \gg h$) with a rectangular cross-section and a constant width, Equations (4.9) and (4.10) reduce to (with $\alpha = 1$):

$$\text{continuity: } \frac{\partial h}{\partial t} + \frac{\partial(\bar{u} h)}{\partial x} = 0 \quad (4.11)$$

$$\text{motion: } \frac{\partial \bar{u}}{\partial t} + \frac{\bar{u} \partial \bar{u}}{\partial x} + \frac{g \partial h}{\partial x} + \frac{g \bar{u} |\bar{u}|}{C^2 h} - g l_b - \frac{\sum F_x}{\rho h} = 0 \quad (4.12)$$

1
2
3
4
5
6

in which:

\bar{u} = depth-averaged flow velocity,

h = water depth,

l_b = bottom slope ($= -dz_b/dx$),

F_x = external force per unit area (A) of cross-section.

The dimension of the terms of the momentum equation is m/s^2 .

The following terms can be distinguished in the equation of motion (Equation 4.12):

- Term 1:** acceleration of the fluid volume by forces that vary in time which is known as the local acceleration term (inertial term),
- Term 2:** acceleration of the fluid volume by forces that vary in x-direction which is known as the advective or convective acceleration term,
- Term 3:** net pressure force related to the water surface gradient in x-direction, pointing in the direction of the lowest water level,
- Term 4:** bottom friction force acting on the fluid volume,
- Term 5:** gravity force acting on the fluid volume,
- Term 6:** additional external fluid forces acting on the fluid volume (wind- and wave-induced forces).

In the case of tidal flow, it is often assumed that:

$$h = h_o + \eta \text{ and thus: } h + z_b = \eta + h_o + z_b$$

with h_o = water depth to mean sea level (horizontal) and η = water level to the horizontal mean sea level.

This yields: $\partial(h + z_b)/\partial x = \partial(\eta + h_o + z_b)/\partial x = \partial\eta/\partial x$ because $\partial h_o/\partial x = -\partial z_b/\partial x$ or $\partial h_o/\partial x = I_b$

Based on this, **Term 3** and **Term 5** can be combined into one term: $g\partial\eta/\partial x$.

Similar terms do appear in the 2DH (two-dimensional horizontal) equations of mass and momentum for depth-averaged flow.

The 1D and 2DH equations of mass and momentum including all terms and quadratic friction can only be solved by applying numerical techniques (DELFT3D-model).

Information of the relative magnitude of the various terms of the equation of motion, Equation (4.12), can be obtained from scale analysis using numerical model results.

4.3.1 Model run conditions Scheldt Estuary

Herein, the 2DH DELFT-model of the Scheldt estuary with bathymetry of 1998 has been used. The tidal conditions (two tides of 12.5 hours) refer to the morphological tide of 1998 which is approximately equal to mean tidal conditions of 1998. The bottom roughness is based on a spatially variable Manning coefficient (n) in the range of 0.013 to 0.043. The Manning coefficient (n) of the main channels is about 0.02 to 0.03. The Nikuradse roughness is about $k_s \cong (n/0.04)^6$. Thus, the k_s -value of the main channels is about 0.02 to 0.2 m.

The computed water levels around NAP (approximately equal to mean sea level MSL) are shown in **Figures 4.3.2** and **4.3.3**. The data of Westkapelle with tidal range of about 3.5 m (mean tide) represent the sea boundary conditions. The tidal range increases to about 4.6 m in Bath (amplification factor of $4.6/3.5 = 1.3$) and to about 5.8 m in Antwerpen. **Figure 4.3.4** shows the computed tidal range values compared to measured values of two periods (1901-1910 and 1991-2000). Measured and computed values up to Liefkenshoek are in reasonable agreement. Landward of this latter station Liefkenshoek the computed tidal range values in the river section are much too large, which may be caused by the landward boundary conditions used (river discharge).

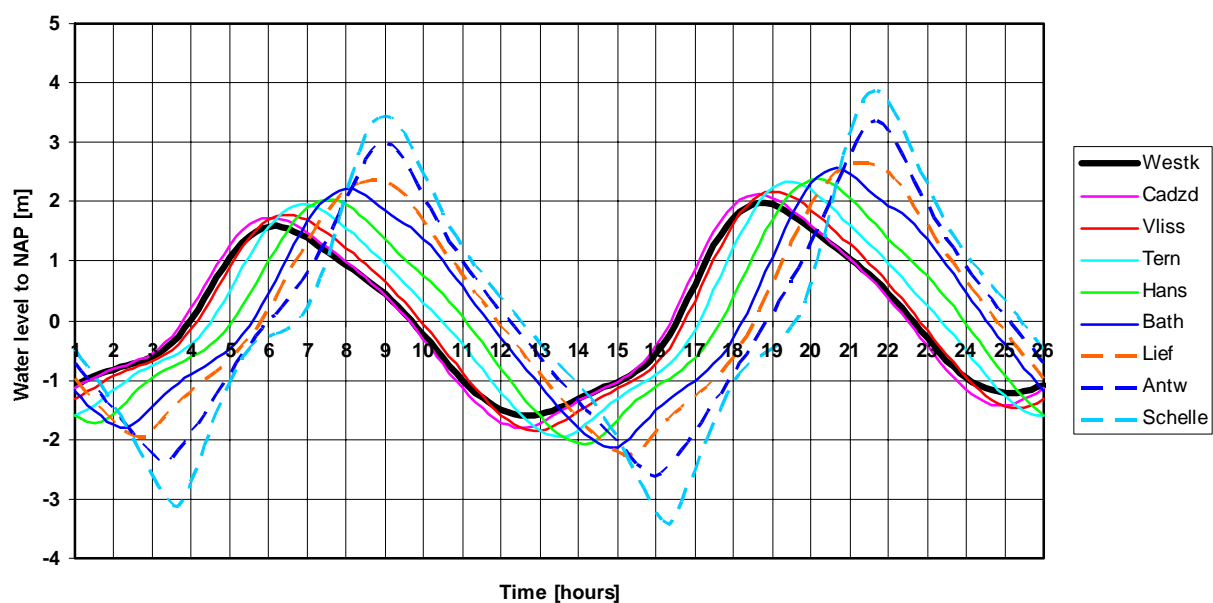


Figure 4.3.2 Water levels in 9 stations between Westkapelle and Schelle of Scheldt estuary (mean tidal conditions 1998)

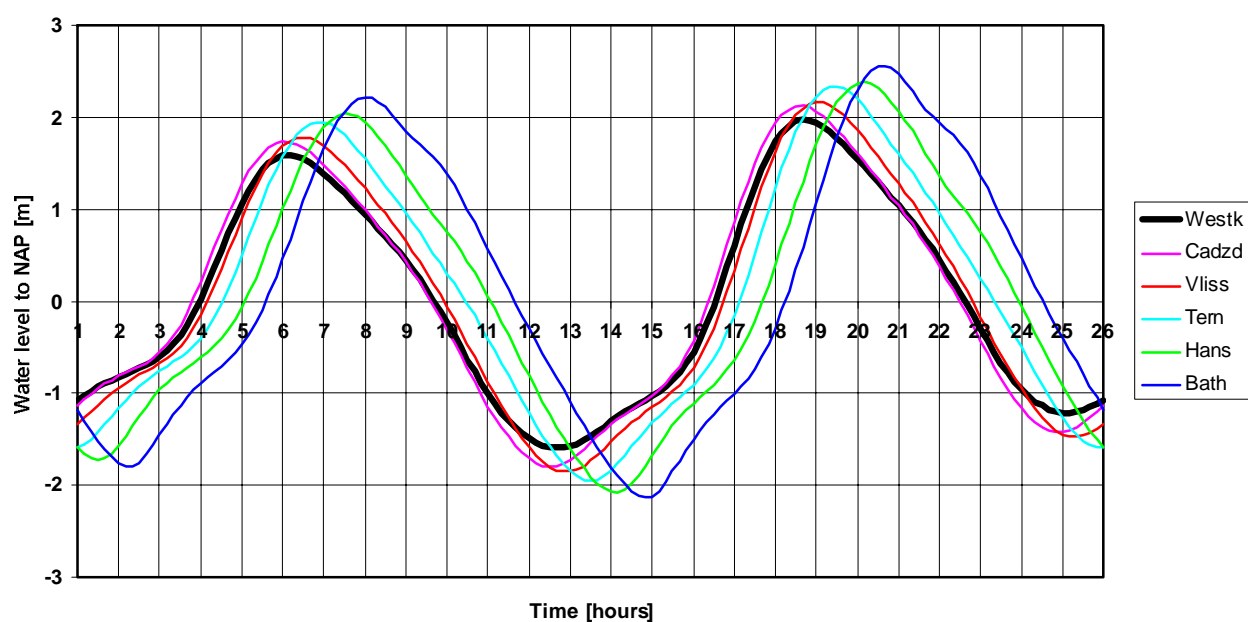


Figure 4.3.3 Water levels in 6 stations between Westkapelle and Bath; western part of Scheldt estuary (mean tidal conditions 1998)

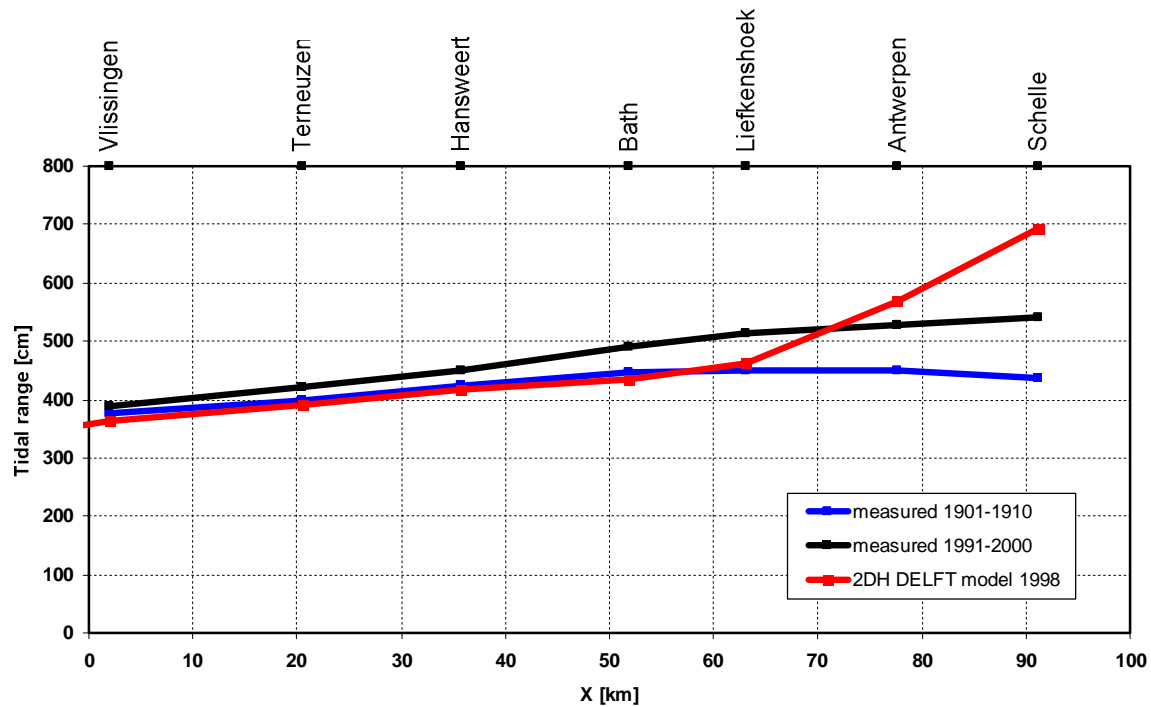


Figure 4.3.4 Measured and computed tidal range values in Scheldt estuary

Some examples of the depth-averaged flow velocity as function of time in three primary channels of the Scheldt estuary are shown in **Figures 4.3.5 to 4.3.7**.

Some examples of the depth-averaged flow velocity along the main channels at maximum flow are shown in **Figures 4.3.8 to 4.3.11**.

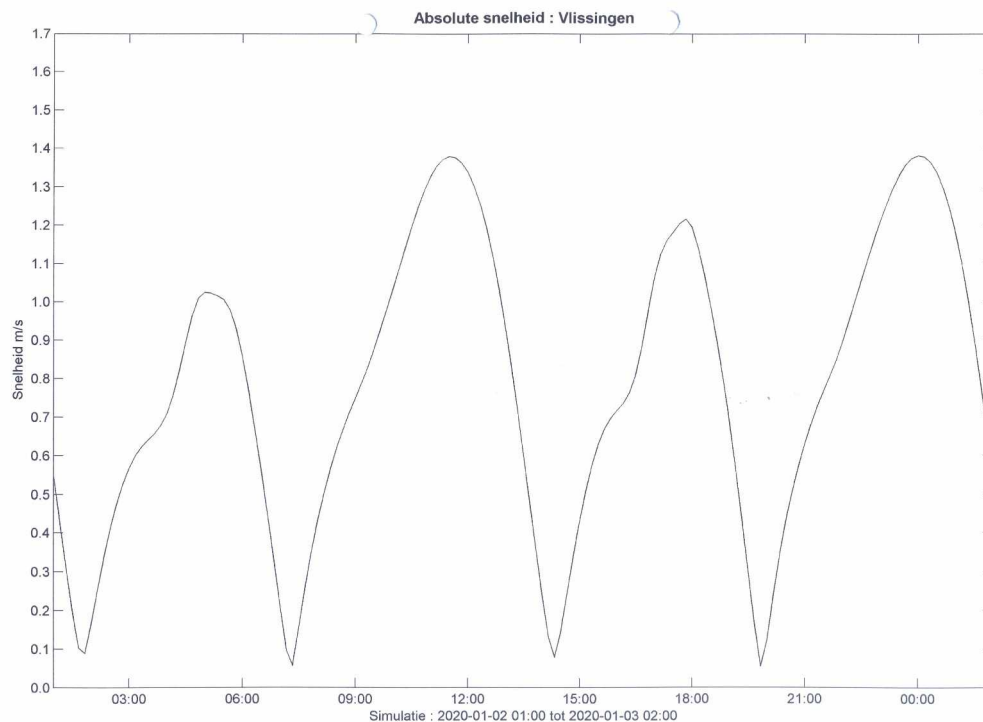


Figure 4.3.5 Velocity as function of time: Honte channel, west of Vlissingen (flood 02-08 hrs)

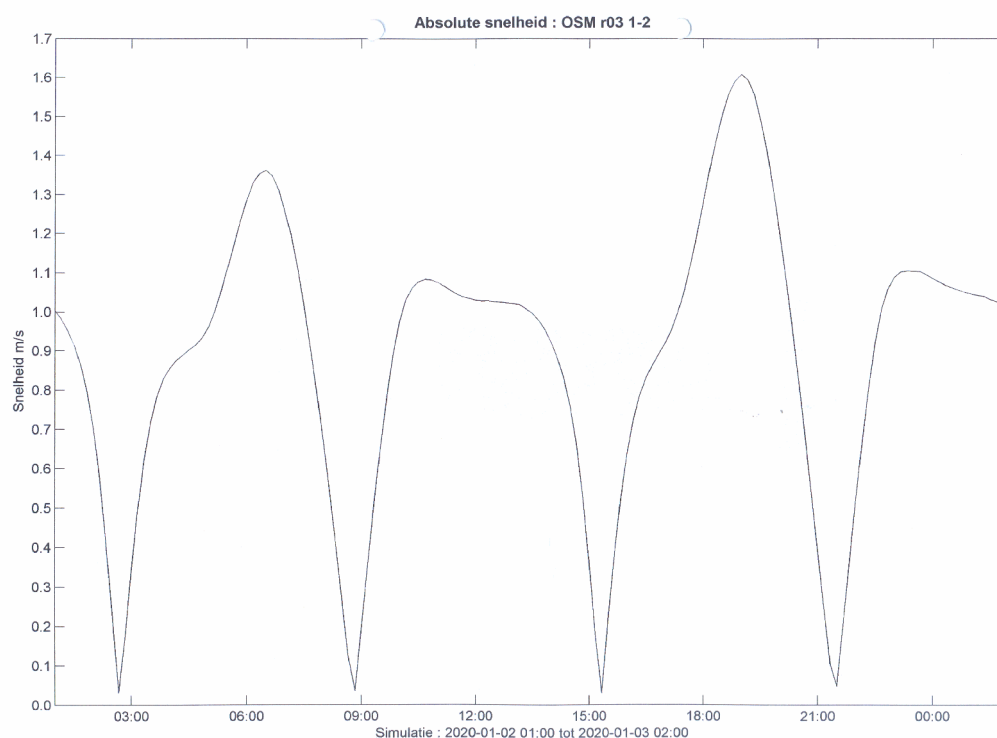


Figure 4.3.6 Velocity as function of time; Pas van Terneuzen, west of Terneuzen (flood 03-09 hrs)

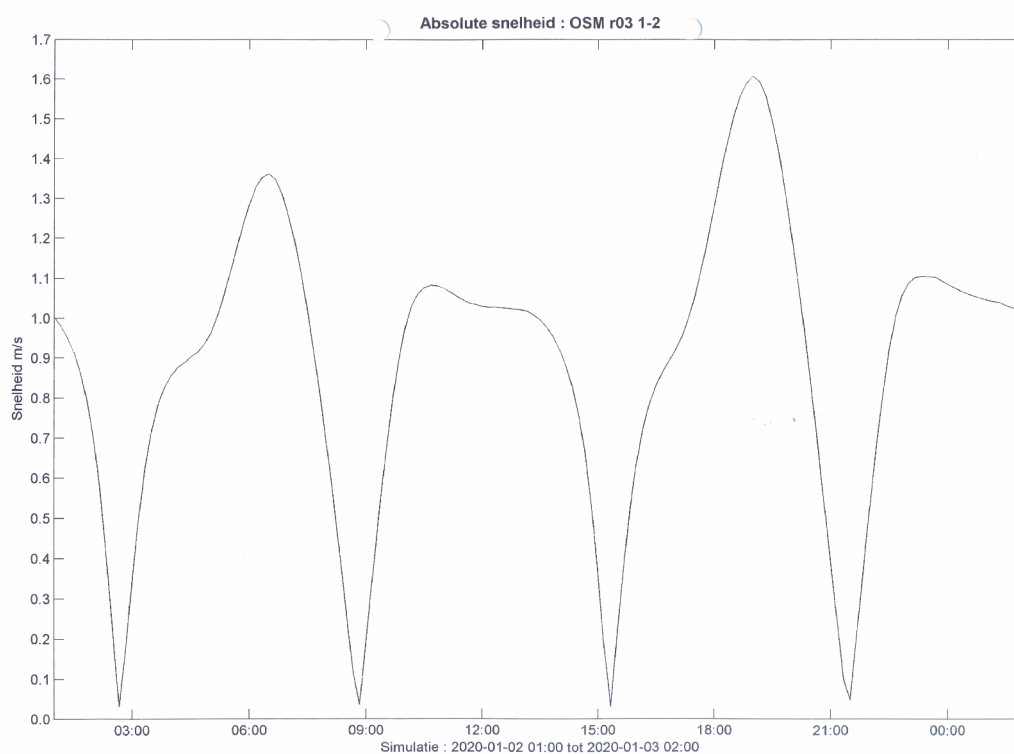


Figure 4.3.7 Velocity as function of time; Overloop van Valkenisse, west of Bath (flood 03-09 hrs)

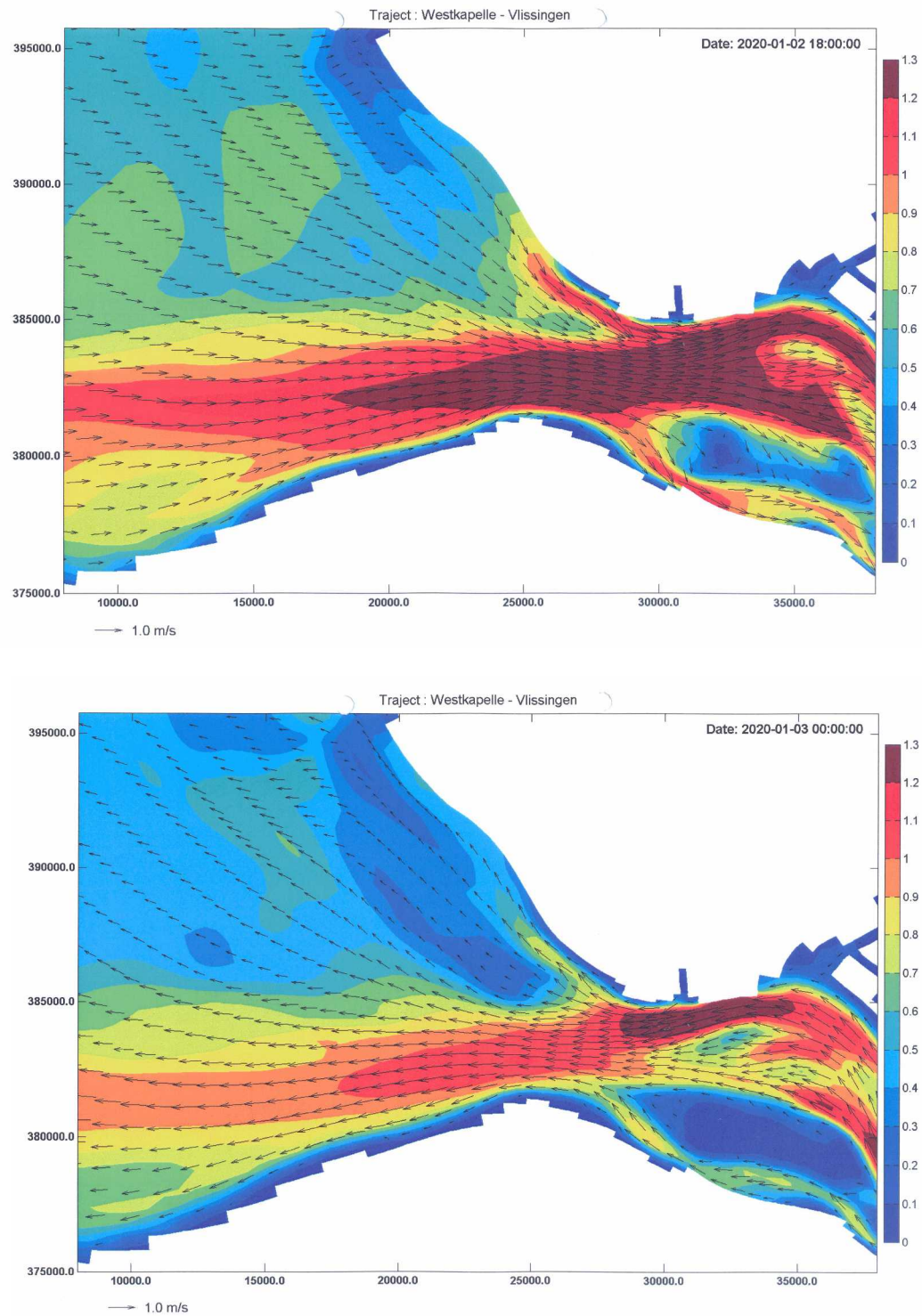


Figure 4.3.8 *Computed depth-averaged flow velocity at maximum flood and ebb flow; Westkapelle-Vlissingen, Scheldt estuary (velocity scale in m/s on right)*

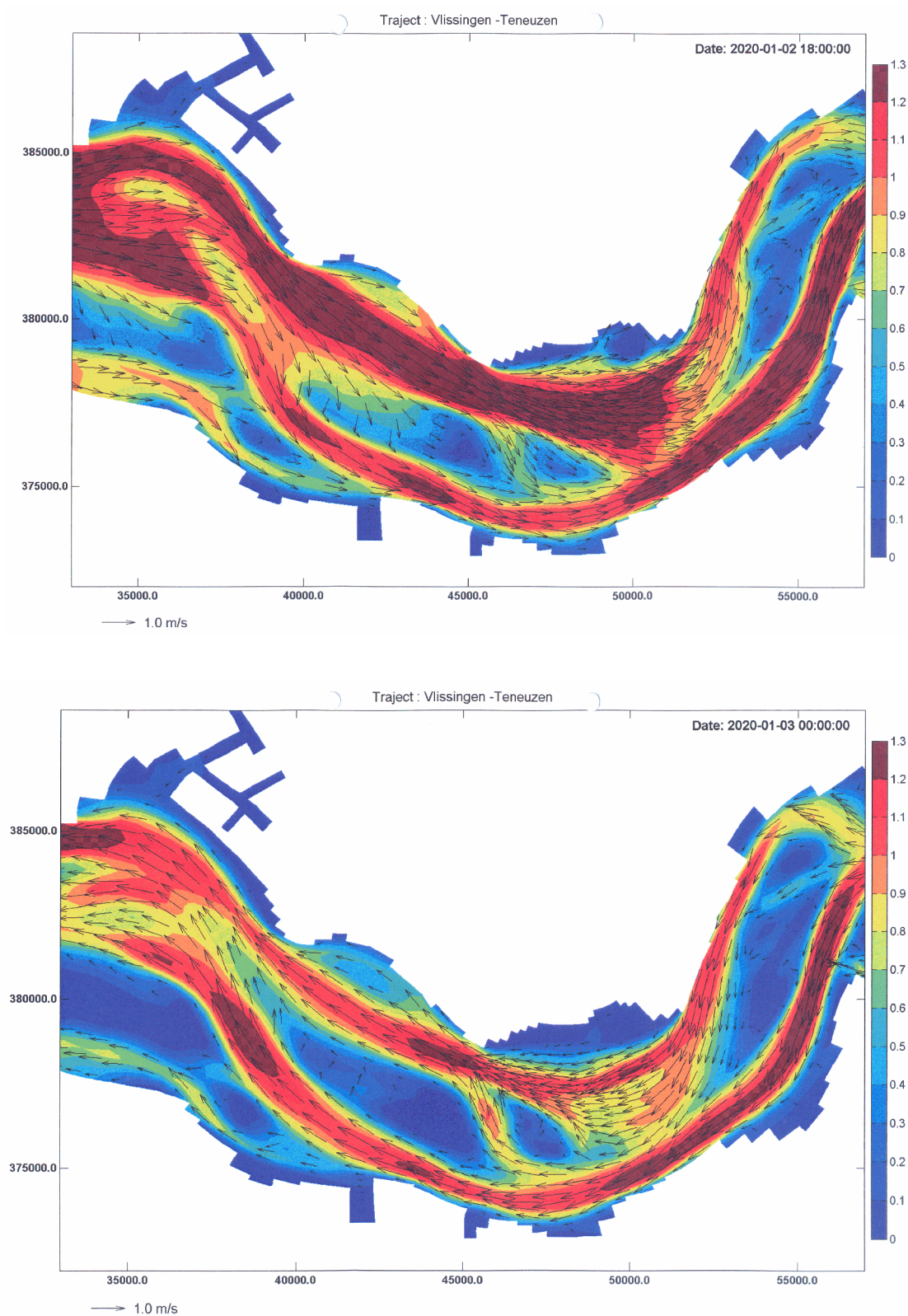


Figure 4.3.9 *Computed depth-averaged flow velocity at maximum flood and ebb flow; Vlissingen-Terneuzen, Scheldt estuary (velocity scale in m/s on right)*

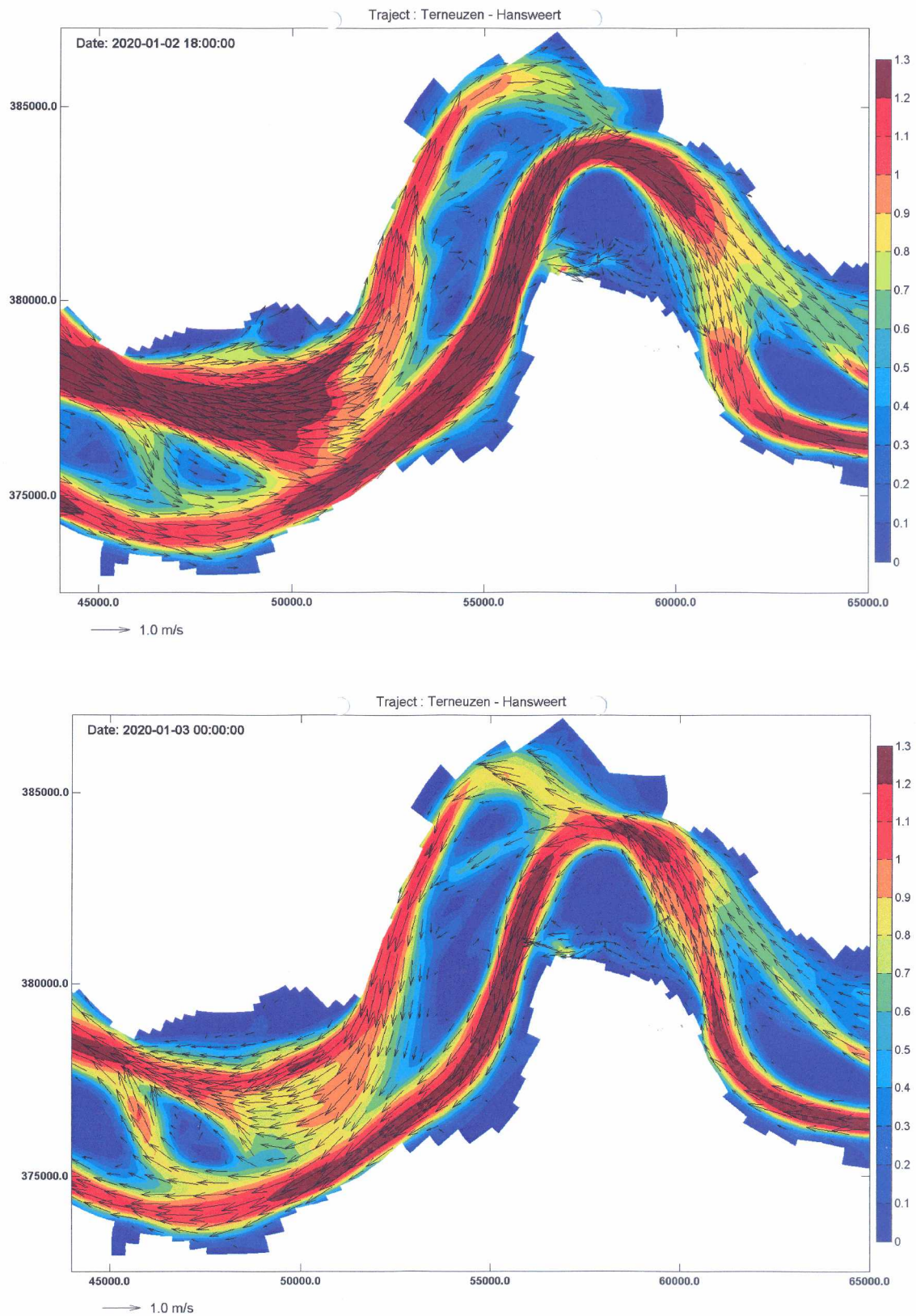


Figure 4.3.10 *Computed depth-averaged flow velocity at maximum flood and ebb flow; Terneuzen-Hansweert, Scheldt estuary (velocity scale in m/s on right)*

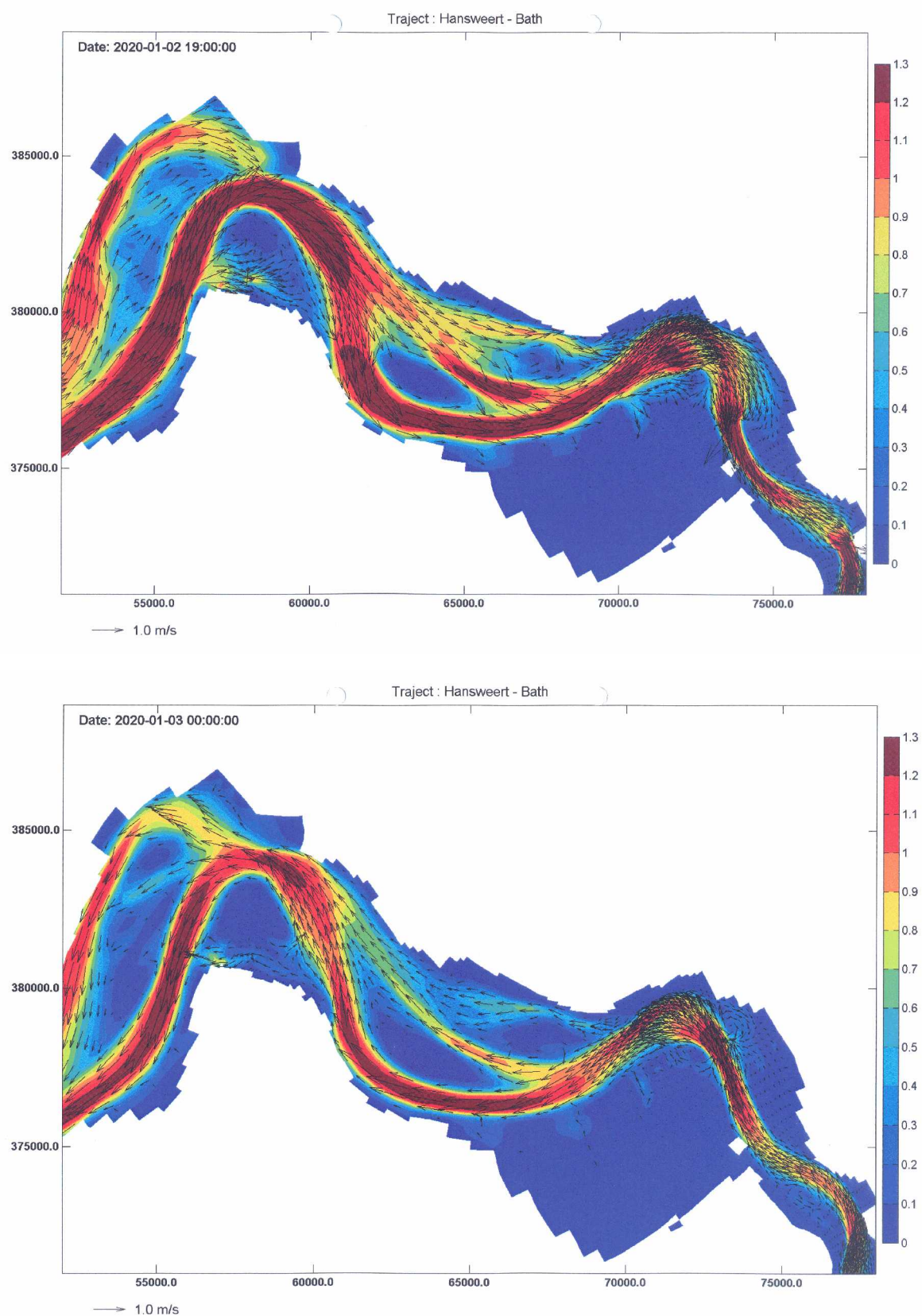


Figure 4.3.11 Computed depth-averaged flow velocity at maximum flood and ebb flow; Hansweert-Bath, Scheldt estuary (velocity scale in m/s on right)

4.3.2 Scale analysis of force terms

Inertial term ($\partial \bar{u} / \partial t$)

The variations of the depth-averaged flow velocity around maximum flow varies roughly 0.05 m/s over 15 minutes (see **Figures 4.3.5 to 4.3.7**), which yields: $\partial \bar{u} / \partial t \cong 0.00005$ ($\pm 30\%$)

Convective acceleration term ($\bar{u} \partial \bar{u} / \partial x$)

The depth-averaged flow velocity in the primary and secondary channels is of the order of 1 m/s around maximum flow. The variation of the flow velocity along these channels is of the order of 0.2 m/s (during maximum flow) over a length of about 5 km resulting in: $\bar{u} \partial \bar{u} / \partial x \cong 0.00004$ ($\pm 30\%$)

Slope term ($g \partial \eta / \partial x$)

The slope term in the sections Westkapelle-Vlissingen, Vlissingen-Terneuzen, Terneuzen-Hansweert and Hansweert-Bath can be estimated from the data of **Figure 4.3.3**. The length of these sections vary in the range of 15 to 20 km. The water level differences around maximum flow in these sections vary in the range of 0.3 to 0.5 m (or 1.5 to 3 cm per km). Based on these values the slope term is: $g \partial \eta / \partial x \cong 0.000225$ ($\pm 30\%$)

Frictional term ($g \bar{u}^2 / (C^2 h)$)

The frictional term can be simplified using the Strickler equation ($C = 25 (h/k_s)^{1/6}$ with h = water depth and k_s = bed roughness of Nikuradse) to represent the C-value, yielding: $g \bar{u}^2 / (C^2 h) = 0.0156 k_s^{1/3} \bar{u}^2 / h^{4/3}$

The k_s -value is assumed to be in the range of 0.05 to 0.1 m, yielding: $k_s^{1/3} \cong 0.4$ (± 0.05). Based on this, the frictional term is: $0.006 \bar{u}^2 / h^{4/3}$

The flow system of the Scheldt estuary during mean tidal conditions can be roughly grouped in three velocity classes, see **Table 4.3.1**.

The frictional term around maximum flood and ebb flow is approximately 0.00025 ($\pm 20\%$) in the primary, secondary and tertiary channels between the mouth at Westkapelle and eastern station Liefkenshoek. Hence, the frictional term is fairly constant over the major part of the estuary.

Table 4.3.1 Frictional term values in channels of Scheldt estuary (mean tidal conditions)

Channel	Mean depth (m)	Maximum velocity (m/s)	Frictional term (m/s ²)
Primary	15-20	1.2-1.4	0.00023-0.00022
Secondary	10-15	1.0-1.2	0.00028-0.00023
Tertiary (Cross/Margin)	7-10	0.7-1.0	0.00022-0.00028

Conclusion

This scale analysis shows that the slope term and the frictional term around maximum flow (during mean tidal conditions) are approximately equal in the range of 0.0002 to 0.00025 m/s². These two terms are fairly constant over the length of the estuary between the mouth Westkapelle and Liefkenshoek (Belgium). The inertial term around maximum flow is much smaller (factor 4 to 5). The inertial term is dominant around slack tide. The convective acceleration term is the smallest term and can be neglected around maximum flow (factor 5 smaller than the slope term and the frictional term).

5 Summary and conclusions

The Scheldt estuary is a large-scale estuary in the south-west part of the Netherlands. The estuary is connected to the Scheldt river, which originates in the north-west of France. The total length of the Scheldt river including the estuary is about 350 km; the tide penetrates up to the city of Gent in Belgium (about 180 km from the mouth). The length of the estuary is about 60 km (up to Bath). The cross-sections of the estuary show two to three deeper channels with shoals in between and tidal flats close to the banks. The width of the mouth at Westkapelle (The Netherlands) is about 20 to 25 km and gradually decreases to about 0.8 km at Antwerp.

The Scheldt estuary has important environmental and commercial qualities. It is the main shipping route to the Port of Antwerp in Belgium. The depth of the navigation channel to the Port of Antwerp in Belgium is a problematic issue between The Netherlands and Belgium because of conflicting interests (commercial versus environmental). Large vessels require a deep tidal channel up to Antwerp, which enhances tidal amplification with negative environmental consequences. Since 1900, the main shipping channel has been deepened (by dredging and dumping activities) by a few metres. Furthermore, sand mining activities have been done regularly. Both types of dredging works may have affected the tidal range along the estuary. The tidal range at the mouth (Westkapelle and Vlissingen) has been approximately constant over the last century, but the tidal range inside the estuary has gone up by about 1 m (**Pieters, 2002**). Particularly, the high water levels have gone up considerably. The low water levels have gone down slightly at some locations (about 0.2 m at Antwerp) despite sea level rise of about 0.2 m per century.

The Scheldt estuary can be subdivided into a series of macro-cells (**Deltares, 2011**). Each cell system consists of meandering tidal channels with decreasing dimensions in landward direction. The tidal channels show a regular pattern of main flood and main ebb channels (primary and secondary channels) with peak tidal velocities in the range of 1 to 1.4 m/s during mean tidal conditions (based on DELFT3D-model results). Generally, the flood tide enters through the more shallow channels (mean depths of 10 to 15 m) and leaves through the deeper channels (mean depths of 15 to 20 m depths with respect to MSL). The main ebb channels are deepest and form the navigation route to the Port of Antwerp. The main flood channels generally are shallower than the main ebb channels. Shallow areas (sills) are found at the seaward side of the ebb channels and at the landward side of the flood channels. Along the banks smaller, tertiary channels can be found (marginal channels). Various connecting (tertiary) channels are present between the parallel main flood and ebb channels.

The sediment in the Scheldt estuary mainly consists of medium fine sand in the channels (0.2 to 0.4 mm sand) and fine sand on the shoals (0.05 to 0.2 mm sand). The percentage of mud (< 0.03 mm) is rather small (< 10%) in the main channels. Alongside the estuarine margins, at the intertidal areas and at the salt marshes, the percentage of mud is much larger.

Substantial dredging at the sill locations is required to maintain the required depth of the main navigation route to Antwerp, Belgium. Mean annual dredging volumes have gradually increased from about 4 to 5 Mm³ per year in the 1960's to about 10 Mm³ per year around 2000 to accommodate the passage of larger vessels to the Port of Antwerp (**Deltares, 2004**).

The sills were deepened again in the period 1997-1998 (second deepening campaign).

Recent morphological changes after the second deepening of the navigation route (1997-1998) have been reported by **Rijswaterstaat 2006** (MOVE final report, RIKZ, Rijkswaterstaat).

Basic tidal processes

The tidal wave in the Scheldt estuary is affected by reflection, amplification, deformation and damping.

Reflection is herein defined as wave propagation opposite to the incoming wave motion due to the presence of a change of the depth and/or width. Full reflection will occur in a closed-end channel.

Partial reflection will occur if the depth and width of the cross-section become smaller abruptly (narrowing of the cross-section). If a local sill (relatively shallow section) and/or a local constriction are present, the water level upstream of this location (seaward during flood and landward during ebb) will build up to overcome the extra flow resistance at this location. This backwater effect will propagate upstream (seaward during flood), which can be interpreted as partial reflection of the tidal wave.

Amplification due to the funnel-type planform of the estuary is herein defined as the increase of the tidal wave height due to the gradual decrease of the width of the system. Amplification due to shoaling is herein defined as the increase of the tidal wave height due to the gradual decrease of the depth of the system. Both processes (funneling and shoaling) lead to landward amplification of the wave height (tidal range) in convergent channels (decreasing width and depth in landward direction) and is an important phenomenon in estuaries where the depth and the width are gradually decreasing. The amplification of the tide due to the funnel-type planform can also be explained in terms of an incoming wave and a reflected wave of almost equal strength generated by the converging planform. Both (frictionless) waves are assumed to travel with wave speed $c_0 = (gh)^{0.5}$. The effect of width convergence can be very well represented by schematizing the estuary in a series of prismatic channels (Pieters, 2002) provided that the phase shift between velocity and water level curve is known (calibration). Using this method, the width convergence is represented by local reflection points (abrupt changes of the cross-section). A reflected wave is required to match the solution at the reflection points. These local reflection points should not be identified as real, local flow constrictions present in the Scheldt estuary. It is just an artificial method of representing the funnel planform by a stepwise planform.

Deformation of the tidal wave occurs because a harmonic wave propagating from deep water to shallow water cannot remain harmonic (sinusoidal) due to the decreasing water depth. Furthermore, the water depth (h) varies along the wave profile. The water depth is largest under the wave crest and smallest under the wave trough. As the propagation velocity is proportional to $h^{0.5}$, the wave crest will propagate faster than the wave trough, and the wave shape will change which is known as deformation. The wave is then no longer a smooth sinusoidal wave; the tidal high water becomes a sharply peaked event and low water is a long flat event.

Damping of the tidal wave occurs due to friction between the flowing water and the bottom causing a loss of energy and as a result the wave height will be reduced (energy $\propto H^2L$). These effects are relatively important in the landward part (river section) of the estuary where the channels are smaller and less deep. Small changes of the channel width and depth may have relatively large effects on the tidal wave propagation in this part of the estuary. Generally, frictional losses are quadratically related to the mean velocity. Using quadratic (non-linear) friction, the equations of motion and continuity can only be solved numerically. Using linear friction, analytical solutions can be obtained. According to the energy principle of **Lorentz**, the total energy dissipation in a tidal cycle is the same for both linearized and quadratic friction.

Analytical model for converging estuary

Analytical models can be derived by neglecting the convective acceleration and assuming linear properties of the momentum equation, linear friction, constant depth (to MSL) and a prismatic or exponential planform of the estuary.

Application of the analytical model to the funnel-type Scheldt estuary shows that tidal damping occurs for water depth values smaller than about 7 m due to the dominant effect of friction. Tidal amplification occurs for water depths larger than about 7 m due to dominant funneling effect (decrease of width). The amplification effect is maximum for a water depth of about 12 m. The tidal amplification reduces again for water depths larger than 12 m. Tidal amplification approaches 1 for very large depths (> 50 m). In that case the wave speed is very large and the length of the tidal wave is much larger ($L=cT$) than the channel length resulting in an almost horizontal water surface moving up and down. The results of the analytical model (based on linear friction) are in good agreement with those of the 1D numerical DELFT-model (including convective acceleration, reflection and quadratic friction). The tidal range values of the numerical 1D model are systematically smaller (10% to 15%) as this model is based on quadratic friction, whereas the analytical model is based on linear friction. Measured tidal range values (springtide) up to Antwerp are in reasonable agreement (within 5% to 10%) with the results of both models.

The tidal range of the Scheldt estuary can be simulated quite well by the analytical model using the dimensions of the primary navigation channel only. This demonstrates that the amplification of the tide in the Scheldt estuary is largely caused by the gradual reduction of the effective flow width of the main tidal channels, as the minimum depth (about 15 m) of the main tidal channels is fairly constant up to Antwerp through dredging activities.

Effect of planform and abrupt changes of cross-section

The numerical 1D-model has been used to study the effects of the planform and the presence of local flow constrictions (sills and narrows) on the tidal range.

The model results with various planform changes in the landward part of the estuary clearly show the importance of the width convergence effect resulting in a significant increase of the tidal range if the flow width is reduced. A constant width landward of the converging section leads to decrease of the tidal range in the constant-width section but also in the more seaward converging section.

Abrupt local changes of the cross-section in a **prismatic** estuary have a significant effect on the tidal range on both sides of the modified cross-section. A 50% reduction of the cross-section yields a 15% to 20% increase/decrease of the tidal range. A 75% reduction of the cross-section yields a 35% to 45% increase/decrease of the tidal range.

In the case of a **converging** estuary the effect of abrupt local changes of the cross-section on the tidal range on both sides of the modified cross-sections is rather insignificant for relatively small changes of the cross-section. The amplification effect due to the converging planform seems to be dominant over the effects of abrupt changes of the cross-section. Only, very extreme changes ($>75\%$) of the cross-section have a pronounced effect in a converging estuary. The reduction of the local depth from 20 m to 7.5 m (local sill; 62.5% reduction of cross-section) yields a very small reduction of the tidal range on the landward side of the sill locations. Similarly, the reduction of the local width by about 75% (local narrows) yields a very slight reduction of the tidal range on the landward side. The increase of the tidal range on the seaward side of the modified cross-section is very marginal (<0.1 m) for all cases studied.

Tidal wave propagation appears to be more sensitive to depth changes (sills) than to width changes (narrows), because the depth affects both the wave speed and the flow resistance. Abrupt depth changes also influence the tidal asymmetry. The tidal curve becomes more peaked with a higher HW and a less low LW.

It is remarked that abrupt changes of the cross-section larger than about 50% are extreme schematizations. In reality, very abrupt changes of the total cross-sections of the Scheldt estuary do not occur. Cross-sectional data show a very gradual reduction of the total cross-section. However, the tidal flow system of the Scheldt estuary has local flow constrictions due to the presence of narrow sills. For example, the flood flow from the Honte-channel (cell 1+2) near Vlissingen to the Pas van Terneuzen-channel (cell 3) is severely constricted by the Borssele sill where the flow area is relatively small. The tidal flow system with two parallel channels deals with this by creating lateral flows around the sill location (flow diversion) into the less deep Everingen-channel which reduces partial flow reflection effects.

Based on the results of the 1D numerical model runs, it is concluded that local widening and deepening of the navigation channel to Antwerp by dredging will lead to a smaller tidal range on the seaward side and to a larger tidal range on the landward side of the dredging locations. As the increases of the depth and width due to dredging of the navigation channel of the Scheldt estuary are rather small (<10%), the effects on the tidal range will be marginal (<0.1 m).

Effect of tidal flats

The effect of tidal flats on the tidal range has been studied by using the 1D numerical model and the linearized analytical model for a compound cross-section.

The analytical model has been applied to an exponentially converging compound channel with open end (length of 180 km, width at mouth of 25000 m and depth of 10 m, $k_s = 0.05$ m). The effect of the cross-section is taken into account by using the hydraulic radius in the friction term. Two methods have been used to compute the wave speed c_0 : based on the hydraulic radius and based on the effective wave propagation depth. The results have been compared to those for a converging channel with a rectangular cross-section. The compound cross-section is assumed to consist of one main channel and tidal flats. The total width of the tidal flats at the mouth is about 60% of the total width, which is an extreme situation and does not really apply to the Scheldt estuary. The real contribution of the tidal flats to the total storage is between 5% (mouth) to 20% (landward end of estuary). The analytical results of the linearized model show that significant amplification only occurs in a compound channel when the depth of the main channel is relatively large ($h_0 > 15$ m). The effect is largest for a relatively large contribution of the tidal flats (60%). The effect is relatively small for a small contribution of the tidal flats (20%). Based on this, the effect of the tidal flats on the amplification of the tidal range is found to be marginal for the Scheldt estuary and thus the cross-section can be reasonably well represented by a rectangular cross-section.

Effect of tidal storage

To evaluate the effect of a local tidal storage variation on the computed tidal range values, various computations (using numerical model for compound cross-section only) have been made for a converging-prismatic channel. The width of the tidal flats has been increased/decreased over a length of about 5 km between $x = 20$ and $x = 25$ km from the mouth. This simulates a local variation of the storage (local inundation) by increasing/decreasing the local surface area and hence the local storage volume (storage volume is surface area times tidal range). Three runs have been made: decrease of the surface area of about 15 km^2 and an increase of 30 km^2 and 90 km^2 between $x=20$ and $x=25$ km. The total surface area of the converging tidal channel between the mouth (Westkapelle) and the end of the Scheldt estuary (Bath) is about 450 km^2 . A reduction of the surface area by about 15 km^2 (3%) results in computed tidal range values, which are slightly larger (within 0.05 m). An increase of the surface area leads to smaller tidal range values by about 0.1 m for an increase of 30 km^2 (7%) and by about 0.3 to 0.4 m for an increase of about 90 km^2 (20%).

Relative contribution of basic processes (water surface slope, bottom friction, inertial forces)

Analysis of the force terms (inertial force term, surface slope force term and frictional force term) of the analytical model shows that the surface slope term and the frictional term have opposing values which are of almost equal magnitude during maximum flow. The sum of the three terms is approximately zero. The maximum values of the slope term and the frictional term are much larger in a damped estuary than in an amplified estuary. The maximum value of the inertial term is much smaller than the other terms in a damped estuary and slightly smaller in an amplified estuary. The water surface slope is maximum just before maximum flow (velocity lags behind). The inertial term is maximum around slack tide; the inertial term is minimum around maximum flow, when the surface slope term and the frictional term are dominant.

The force terms of the momentum equations have very similar values (in range of 0.0001 to 0.0003 m/s²) in the middle of the estuary for both cases, (damped and amplified) although the local tidal range and peak velocity values are quite different. Model results for larger depth values of 10 m (amplified cases) show smaller values of the three terms of the momentum equation than for a depth of 5 m (damped cases).

The analytical model results can also be used to estimate the relative importance of the convective acceleration term, which is not accounted for by the analytical model. In the major part of the estuary this term is much smaller than the other three terms. The convective term cannot be neglected in the landward end (river section) of the estuary when the depth is small (order of 5 m).

Scale analysis of the 2DH DELFT-model results shows that the slope term and the frictional term around maximum flow (during mean tidal conditions) are approximately equal in the range of 0.0002 to 0.00025 m/s². These two terms are fairly constant over the length of the estuary between the mouth Westkapelle and Liefkenshoek (Belgium). The inertial term around maximum flow is much smaller (factor 4 to 5). The inertial term is dominant around slack tide. The convective acceleration term is the smallest term and can be neglected around maximum flow (factor 5 smaller than the slope term and the frictional term).

6 References

- Deltares, 2004.** *Morphological modelling of the Western Scheldt. Final Report Z3648/A1198, Delft, The Netherlands*
- Deltares, 2004.** *Morphological modelling of the Western Scheldt. Intermediate Report Z3648/A1198, Delft, The Netherlands*
- Deltares, 2010.** *LTV O & M Safety: Data analysis and hypothesis Western Scheldt, Project 1202019, Delft, The Netherlands*
- Deltares, 2011.** *Restoration Scheldt estuary through improvement of large-scale physical processes. Report 1204087, Delft, The Netherlands (in Dutch)*
- Green, G., 1837.** *On the motion of waves in a variable canal of small depth and width. Trans. Cambridge Philos. Soc., 6, p. 457-462*
- Jay, D.A. 1991.** *Greens's law revisited: tidal long-wave propagation in channels with strong topography. Journal of Geophysical Research, Vol. 96, No. C11, p. 20585-20598*
- Pieters, T., 2002.** *The tide in the Western Scheldt Estuary (in Dutch). Document BGW-0102. Consultancy Tidal Waters, Vlissingen, The Netherlands*
- Rijkswaterstaat, 2006.** *Monitoring of the effects of navigation channel dredging 48'/43', MOVE final report, RIKZ/2008.003, The Netherlands (in dutch)*
- Savenije, H.H.G, 2005.** *Salinity and tides in alluvial estuaries. Elsevier*
- Van Rijn, L.C., 2010.** *Tidal phenomena in Scheldt Estuary, Report 1202016, Deltares, Delft, The Netherlands*
- Van Rijn, L.C., 1993, 2011a.** *Principles of fluid flow in rivers, estuaries and coastal seas. Aqua Publications, The Netherlands (www.aquapublications.nl)*
- Van Rijn, L.C., 2011b.** *Analytical and numerical analysis of tides and salinities in estuaries, Part I: tidal wave propagation in convergent estuaries. Ocean Dynamics, DOI 10.1007/S10236-011-0453-0*
- Verspuy, C., 1985.** *Lecture notes: Long waves (in Dutch). Delft University of Technology, Delft, The Netherlands*

A Cross-sections of Scheldt Estuary

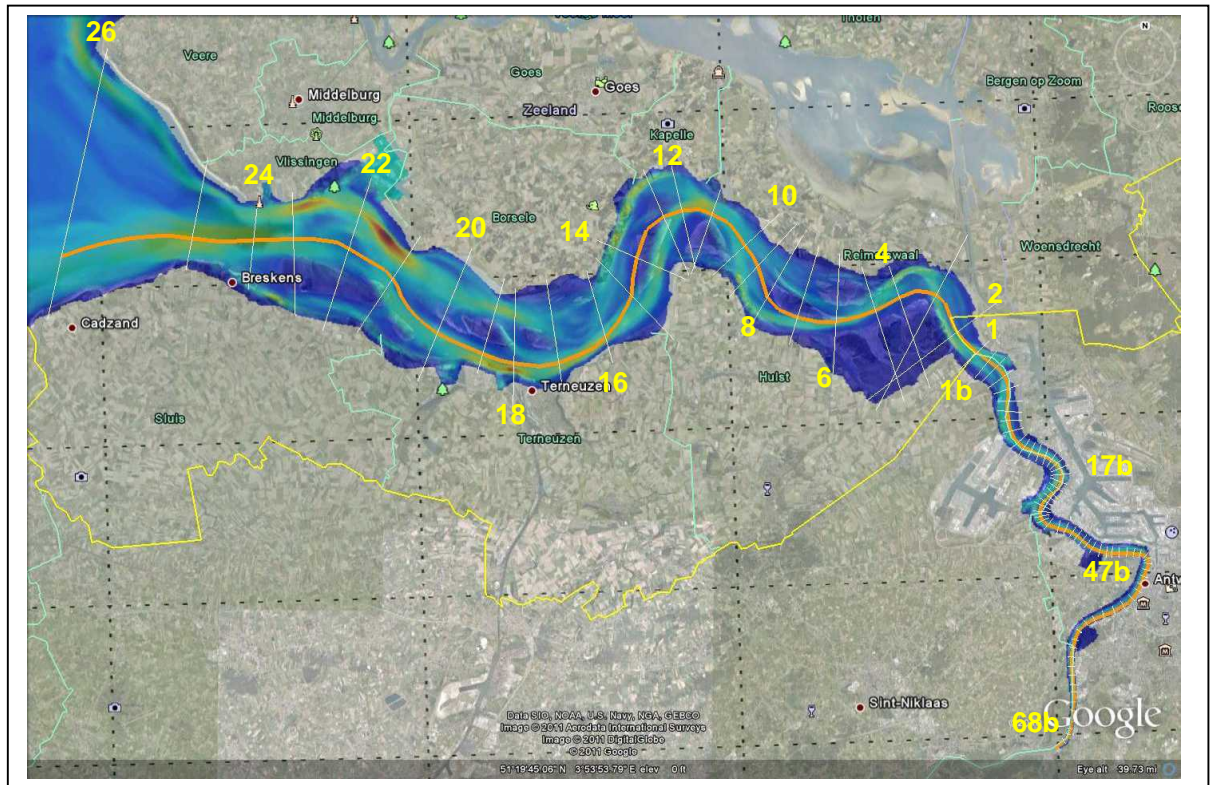


Figure A1 *Locations of cross-sections in the Scheldt estuary (1-26) and in the Lower Scheldt (1b-68b). Location 1 is at the Dutch-Belgium border. Left bank is bank on the left side facing the sea; left bank is south bank in Scheldt estuary*

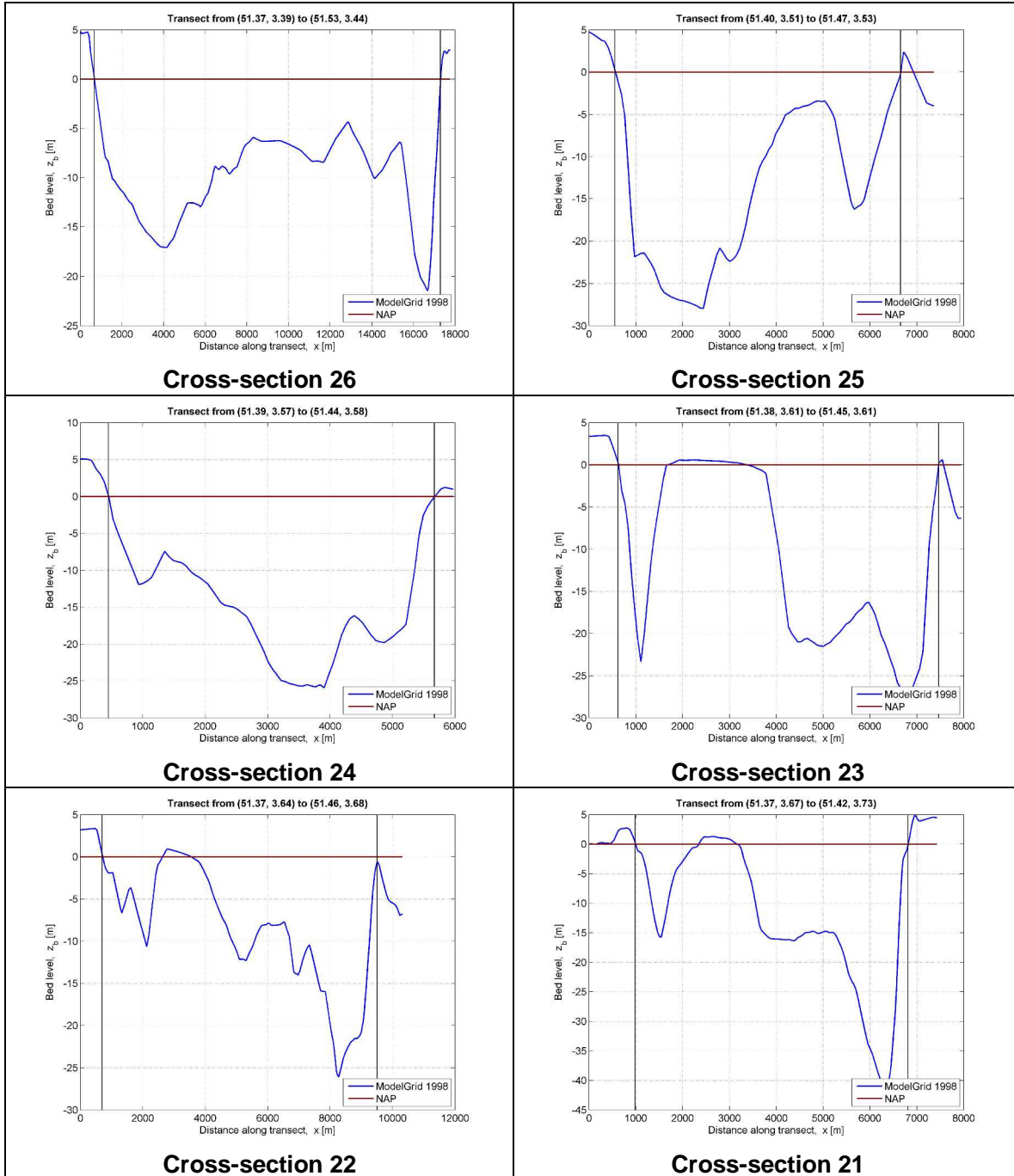


Figure A2 Cross-sections in the Scheldt estuary for the Delft3D model bathymetry of 1998 (distances are relative to the left bank on left side of plots).

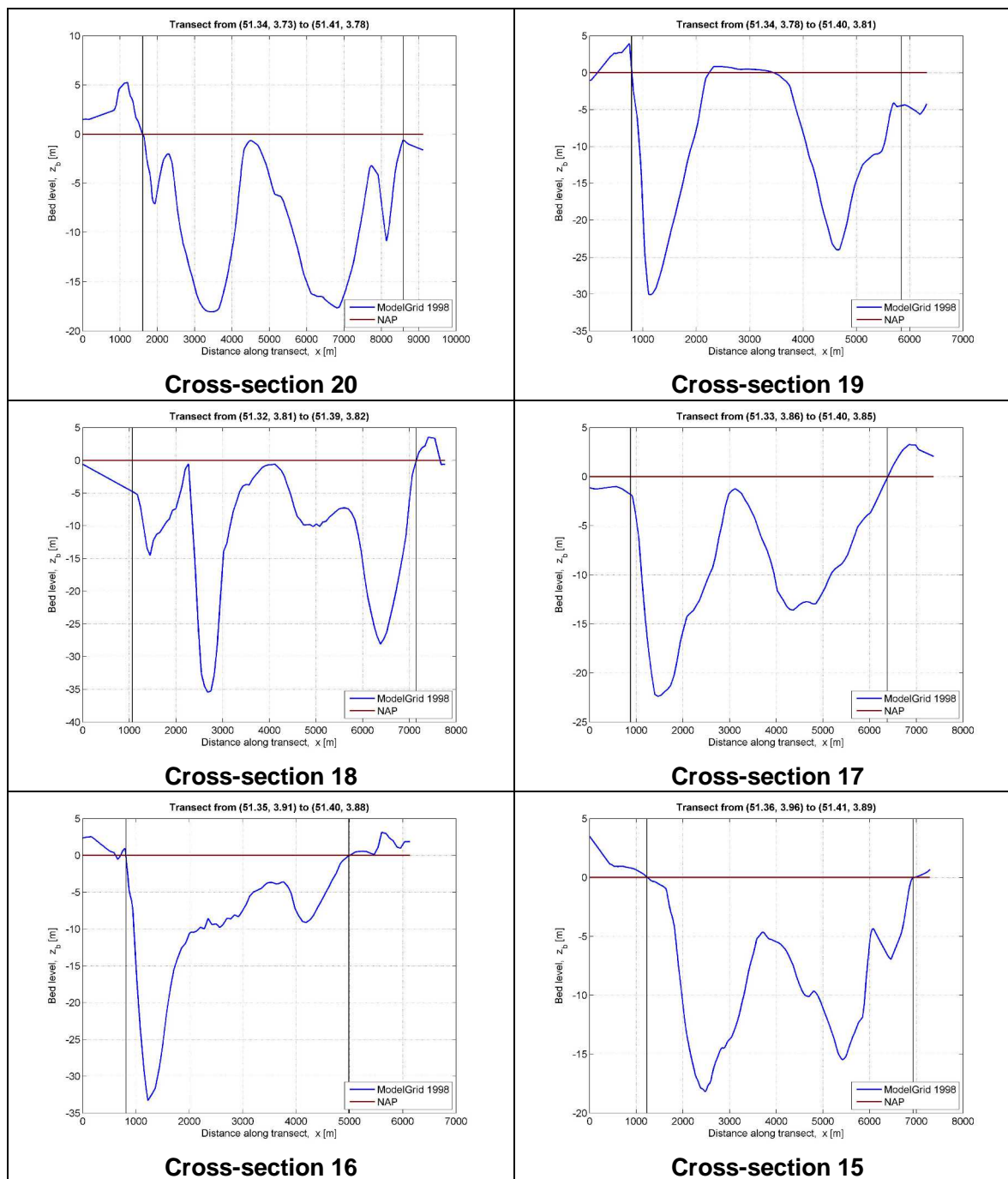


Figure A2 Cross-sections in the Scheldt estuary for the Delft3D model bathymetry of 1998 (distances are relative to the left bank on left side of plots).

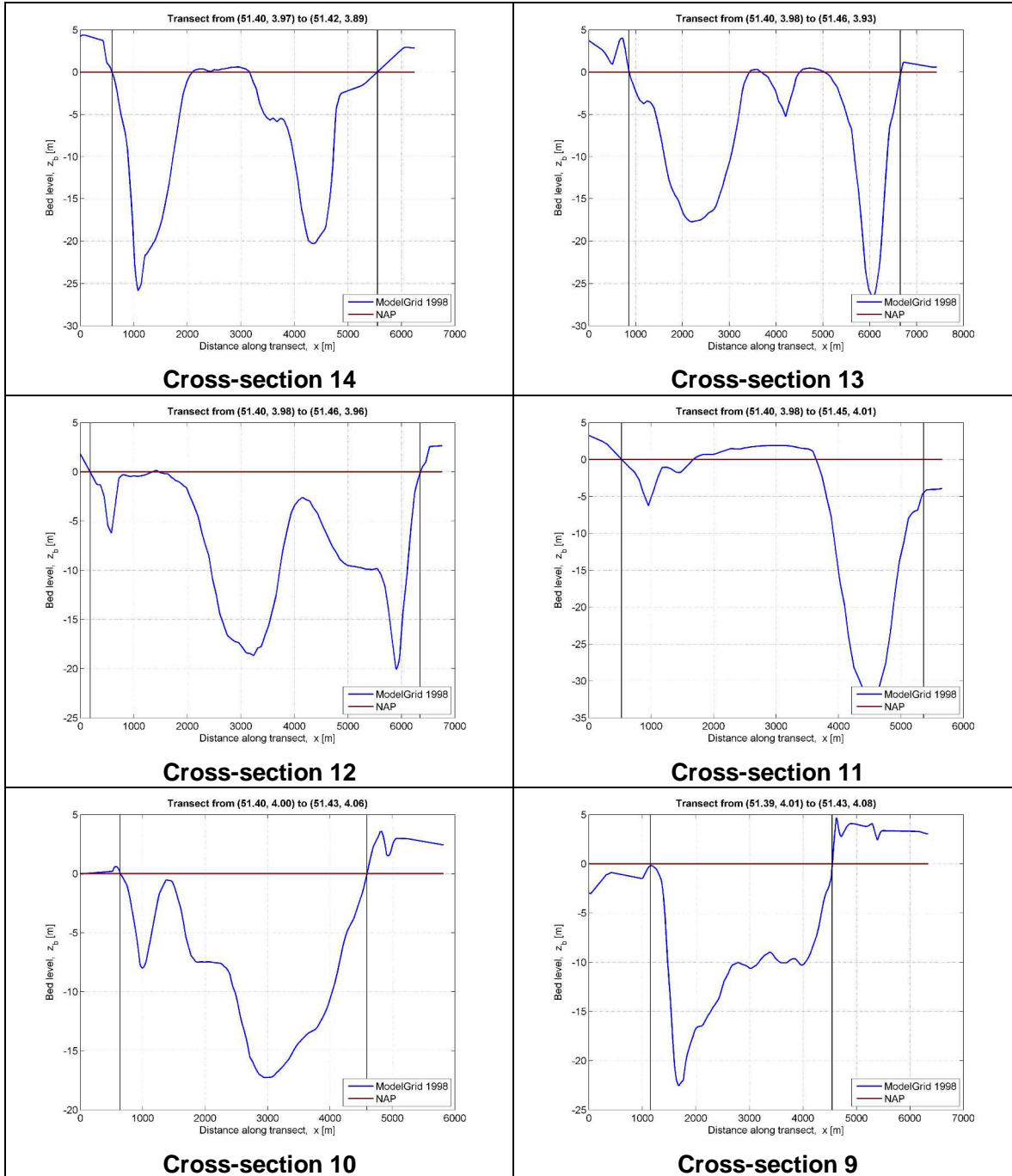


Figure A2 Cross-sections in the Scheldt estuary for the Delft3D model bathymetry of 1998 (distances are relative to the left bank on left side of plots).

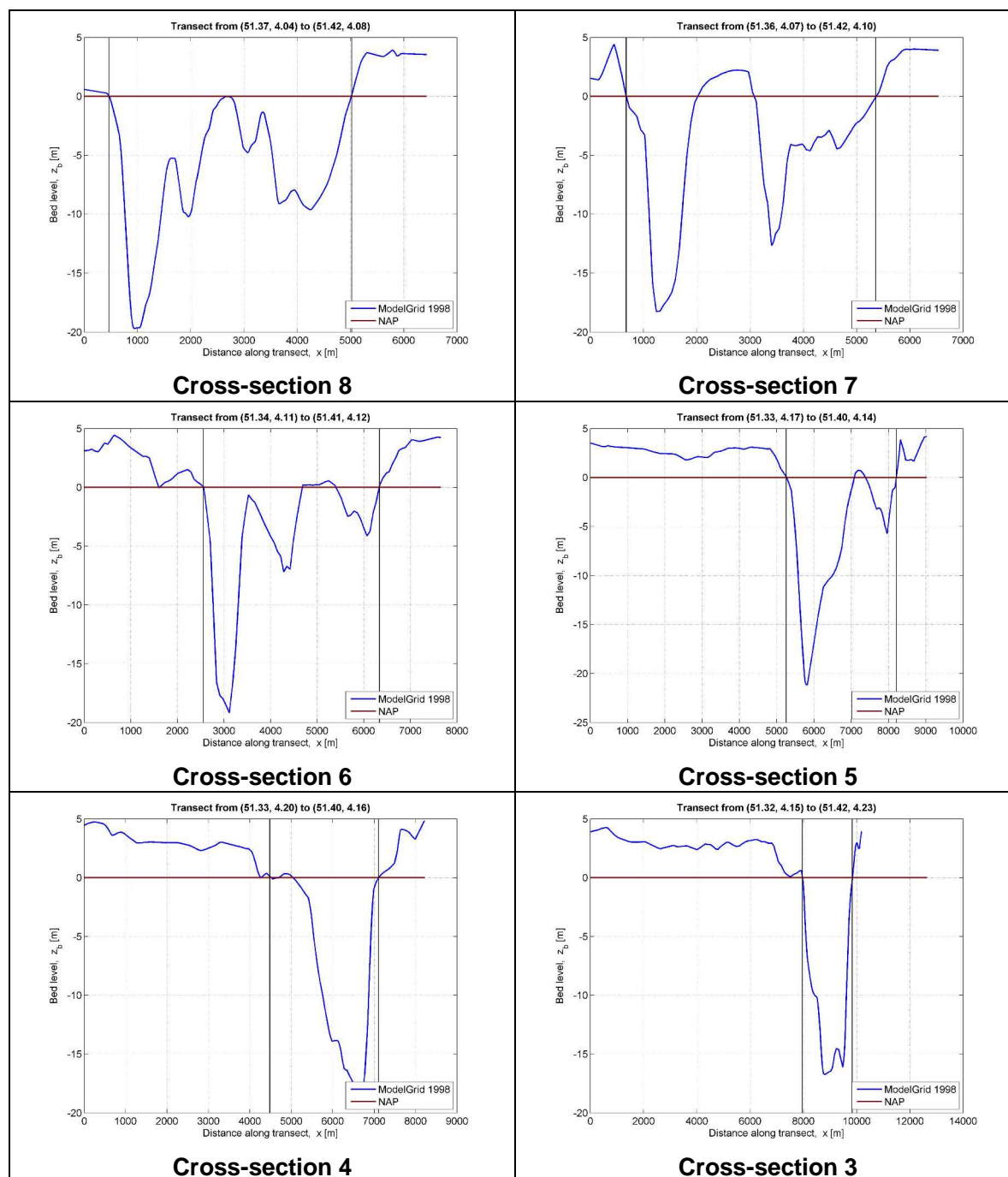


Figure A2 Cross-sections in the Scheldt estuary for the Delft3D model bathymetry of 1998 (distances are relative to the left bank).

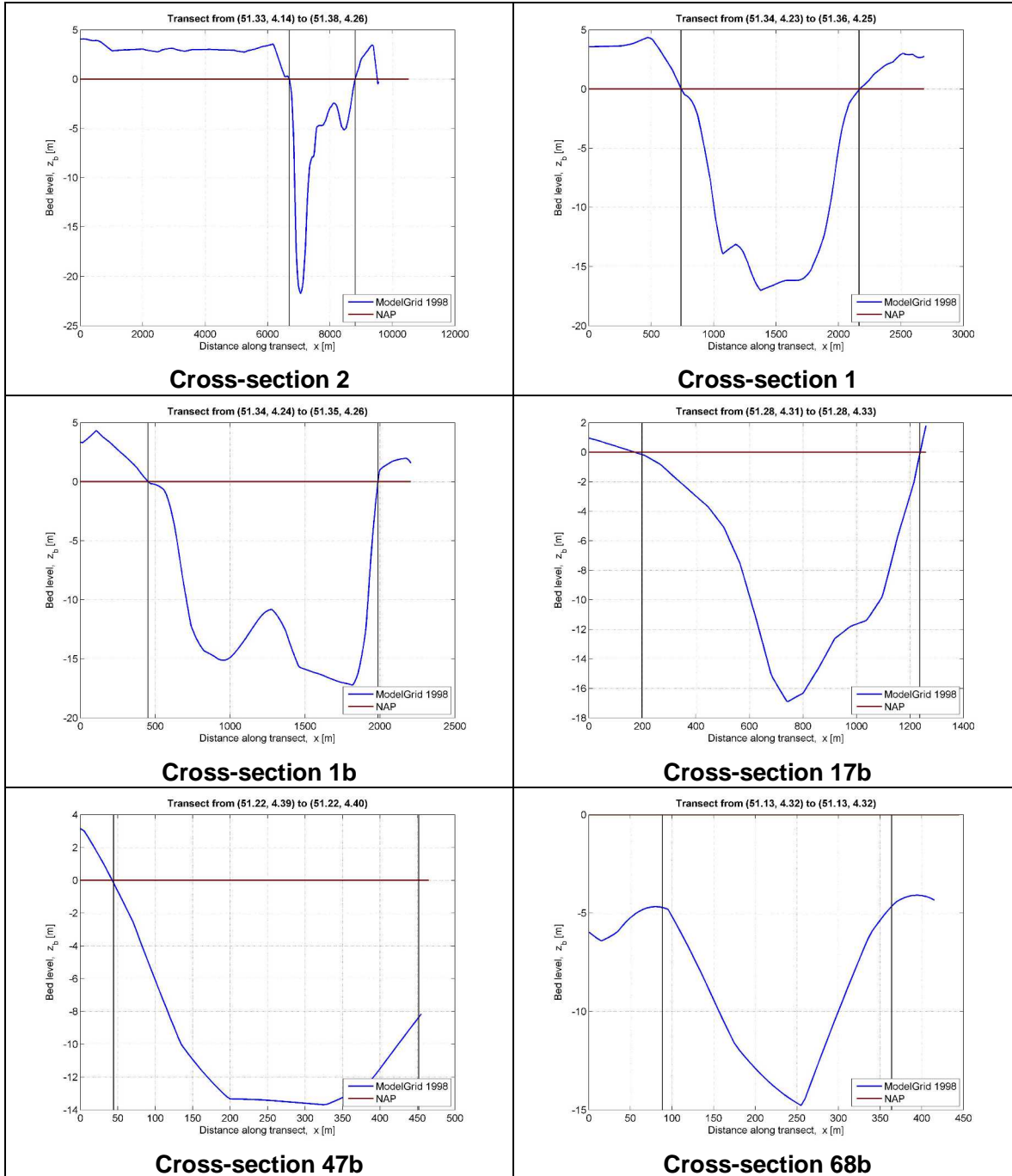


Figure A2 Cross-sections in the Scheldt estuary for the Delft3D model bathymetry of 1998 (distances are relative to the left bank on left side of plots).